Materials Horizons

ROYAL SOCIETY OF CHEMISTRY

REVIEW

View Article Online
View Journal | View Issue

Cite this: *Mater. Horiz.*, 2021, **8**, 758

Engineered two-dimensional nanomaterials: an emerging paradigm for water purification and monitoring

Minxiang Zeng,*[a] Mingfeng Chen,[a] Dali Huang,[b] Shijun Lei,[a] Xuan Zhang,[c] Ling Wang*[c] and Zhengdong Cheng*[abde]

Water scarcity has become an increasingly complex challenge with the growth of the global population, economic expansion, and climate change, highlighting the demand for advanced water treatment technologies that can provide clean water in a scalable, reliable, affordable, and sustainable manner. Recent advancements on 2D nanomaterials (2DM) open a new pathway for addressing the grand challenge of water treatment owing to their unique structures and superior properties. Emerging 2D nanostructures such as graphene, MoS_2, MXene, h-BN, g-C_3N_4, and black phosphorus have demonstrated an unprecedented surface-to-volume ratio, which promises ultralow material use, ultrafast processing time, and ultrahigh treatment efficiency for water cleaning/monitoring. In this review, we provide a state-of-the-art account on engineered 2D nanomaterials and their applications in emerging water technologies, involving separation, adsorption, photocatalysis, and pollutant detection. The fundamental design strategies of 2DM are discussed with emphasis on their physicochemical properties, underlying mechanism and targeted applications in different scenarios. This review concludes with a perspective on the pressing challenges and emerging opportunities in 2DM-enabled wastewater treatment and water-quality monitoring. This review can help to elaborate the structure–processing–property relationship of 2DM, and aims to guide the design of next-generation 2DM systems for the development of selective, multifunctional, programmable, and even intelligent water technologies. The global significance of clean water for future generations sheds new light and much inspiration in this rising field to enhance the efficiency and affordability of water treatment and secure a global water supply in a growing portion of the world.

Received 21st August 2020,
Accepted 4th November 2020

DOI: 10.1039/d0mh01358g

rsc.li/materials-horizons

[a] *Artie McFerrin Department of Chemical Engineering, Texas A&M University, College Station, TX 77843, USA. E-mail: glennzeng@tamu.edu, zcheng@tamu.edu*
[b] *Department of Materials Science & Engineering, Texas A&M University, College Station, TX 77843, USA*
[c] *School of Materials Science & Engineering, Tianjin University, Tianjin 300350, China. E-mail: lwang17@tju.edu.cn*
[d] *Mary Kay O'Connor Process Safety Center, Texas A&M University, College Station, TX, 77843-3122, USA*
[e] *Department of Chemical Engineering, Texas A&M University at Qatar, PO Box 23874, Education City, Doha, Qatar*

Minxiang Zeng

Minxiang Zeng received his BS Degree from the University of Science and Technology of China in 2014. He completed his PhD in Chemical Engineering from Texas A&M University in 2018. He is currently a Postdoctoral Researcher at the University of Notre Dame. His research interests include the self-assembly of two-dimensional materials, additive manufacturing of functional devices, and development of sustainable water technologies.

Mingfeng Chen

Mingfeng Chen is a PhD student in Guangdong University of Technology and was a visiting student in Zhengdong Cheng's group at Texas A&M University. His research focuses on the phase transition of 2D nanoplatelets, orientation control of liquid crystals, ferronematic structure of magnetic nanoplatelets, and 2D material-based functional hydrogels.

1. Introduction

Water is of paramount significance for all known forms of life, and plays an important role in human civilization, social development, and even space exploration.[1–4] On Earth, water mainly exists in form of salty seawater, where fresh water only accounts for around 3% of the total water resources with mostly groundwater, icecaps, and glaciers (Fig. 1a and b).[5–7] As the fresh water demand rockets with the growth of the global population, it has long been a grand challenge to provide clean water affordably and sustainably.[8] Freshwater scarcity has been intensified by water pollution, which is either from naturally occurring contaminants or human activities. Various types of diseases and even lethal effects have been reported from common contaminants such as pesticides,[9] pharmaceuticals,[10] volatile organic compounds (VOCs),[11] pathogenic microorganisms,[12] and heavy metals and metalloids (Fig. 1c).[13,14] In 2015, 29% of the global population lived without a safe freshwater system, and contaminated water causes nearly half a million diarrheal deaths annually.[15,16] Moreover, water pollution not only prevails in underdeveloped water-stressed areas, but also has been increasingly witnessed in developed countries such as the United States. Thus, to address this grand challenge, many wastewater treatment technologies, such as coagulation, flocculation, screening, electrolysis, centrifugation, aerobic and anaerobic treatments, have been

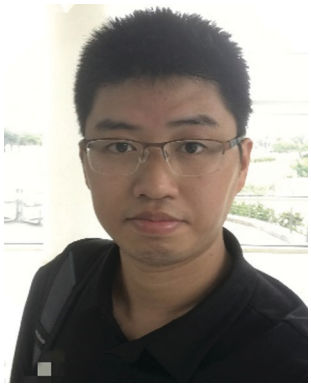

Dali Huang

Dali Huang is currently a PhD student in the Department of Materials Science & Engineering and Mary Kay O'Connor Process Safety Center at Texas A&M University. His research interests include 2D colloidal nanoparticles in photonic crystals, liquid crystals, and advanced functional materials.

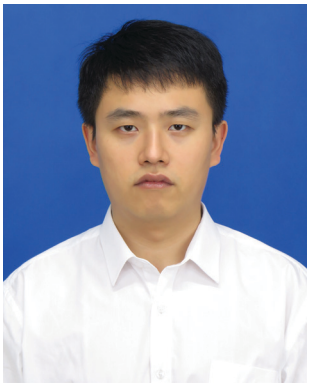

Shijun Lei

Shijun Lei completed his PhD at Tianjin University, under the supervision of Dr Beidou Xi from the Chinese Research Academy of Environmental Science and Dr Guanyi Chen from Tianjin University in 2020. He served as a visiting PhD student in the group of Dr Zhengdong Cheng at Texas A&M University from 2017 to 2019. He is currently a Postdoctoral Researcher in the group of Dr Yuan Hu at State Key Laboratory of Fire Science, University of Science and Technology of China. His research interests include carbon-based nanomaterials for oil–water separation, solar-powered water vapor generation, and solar distillation for seawater desalination/wastewater treatment.

Ling Wang

Ling Wang is a full Professor at the School of Materials Science and Engineering of Tianjin University. He received his PhD degree in Materials Science from the University of Science and Technology Beijing in 2013. Prior to joining Tianjin University, he worked as a Postdoctoral Research Fellow at the Advanced Materials and Liquid Crystal Institute of Kent State University (USA), and Senior Research Fellow at the Artie McFerrin Department of Chemical Engineering of Texas A&M University (USA). His research interests focus on the design, synthesis and properties of smart soft materials, bioinspired materials and functional nanomaterials, and their emerging applications in diverse fields ranging from soft robotics, adaptive camouflage, and additive manufacturing to energy and safety issues.

Zhengdong Cheng

Zhengdong Cheng is a Professor at the Artie McFerrin Department of Chemical Engineering at Texas A&M University. He received his PhD Degree in Physics from Princeton University, followed by Postdoctoral Fellowships at Harvard University, ExxonMobil Research & Engineering, and the Princeton Materials Institute. His research focuses on the self-organization of anisotropic particles, water treatment/monitoring, clean and sustainable energy systems, and the application of microfluidics in bio-encapsulation.

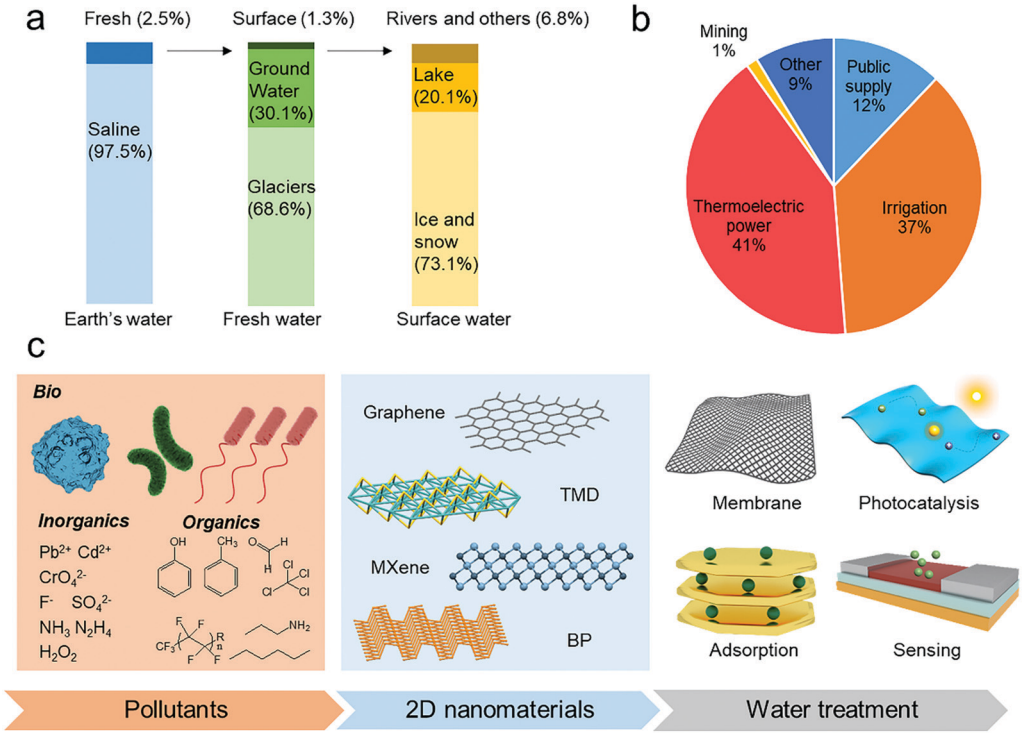

Fig. 1 Challenges of freshwater scarcity and emerging water treatment technologies. (a) Water distribution on Earth. Credit: U.S. Geological Survey.[47] (b) Estimated use of water in the USA (2015). Credit: U.S. Geological Survey.[7] (c) Schematic illustration of water treatment processes leveraging the versatile behavior of 2D nanomaterials in membrane separation, adsorption, photocatalysis, and pollutant sensing.

traditionally employed. However, most of these processes involve bulky/expensive systems or labour-intensive operation.[17] Thus, there is a huge demand for innovations in conventional water processes globally, such as banning the use of Cl_2 for water disinfection because of the potential generation of carcinogens.[18]

The 21st century has brought to the field of water treatment exciting new opportunities in nanoscience and nanotechnology. Various nanosystems, including zero-dimensional (0D) nanoparticles,[19,20] one-dimensional (1D) nanowires/nanorods,[21–24] two-dimensional (2D) nanoplates/nanosheets,[25–27] three-dimensional (3D) nanostructures,[28] and their functional composites,[29–34] have garnered research interest in water treatment and monitoring. Among them, 2D nanomaterials (2DM) are arguably the thinnest materials and may possess the largest surface-to-volume ratio,[35] which promises ultralow material use, ultrafast processing time, and ultrahigh treatment efficiency.[36,37] In addition, the unique shape of 2D nanomaterials also enables highly anisotropic physical and chemical properties compared to 1D and 3D nanosystems.[35] Through control of their size, thickness, and nanostructure, 2D nanomaterials have led to innovations in multiple water treatment systems with exceptional catalytic, adsorptive, and separation performances. These systems include atomic-thin graphene membranes,[38,39] high-efficiency oil adsorbents,[40] ultrafast visible light photocatalysts,[41,42] and other smart/self-healing structures.[43,44] Thus far, numerous 2D nanomaterials have been designed and developed through the bottom-up method from small-molecule precursors or top-down exfoliation method from bulk crystals.[45] Fig. 2 presents several prominent examples of 2D nanomaterials that have emerged in the field of water purification/monitoring, such as graphene (Gr), graphitic carbon nitride (g-C_3N_4), hexagonal boron nitride (h-BN), metal carbides/carbonitrides/nitrides (MXene), transition metal dichalcogenides (TMDs), transition metal oxides (TMOs), black phosphorus (BP), metal organic frameworks (MOFs), covalent organic frameworks (COFs), 2D nanoclays, and many other 2D nanostructures. Graphene is a single-layer graphite, where the sp^2 C atoms are arranged in a "honeycomb" lattice. Similar to graphene, h-BN and g-C_3N_4 can be viewed as doped graphene by B and N atoms, though much more defective sites are commonly found in g-C_3N_4. MXene and TMDs have an ultrathin nanostructure with the chemical formula of $M_{n+1}X_nT_x$ (n = 1–3) and MY_2, respectively, where M is a transition metal (*e.g.*, Ti, Mo, W, and Zr); X is C and/or N atom; T is the surface termination element (O, OH, and F); Y is a chalcogen (S, Se, Te, *etc.*). TMOs, similar to TMDs, are transition metal-based 2D nanomaterials, although TMOs possess larger bandgaps. 2D MOFs are hybrid materials with metal ions or clusters interconnected by molecular linkers to form two-dimensional crystals. 2D COFs, known as "organic zeolites", are porous crystalline polymer nanosheets, in which their organic molecular building units are covalently bonded. Clay nanoplates such as kaolinite, montmorillonite and layered double hydroxides (LDHs) are naturally occurring 2D nanomaterials with layers of octahedral hydroxide and/or tetrahedral silicate.[46]

Despite the tremendous advancements in the literature regarding 2DM-based water treatment technology, to date, very

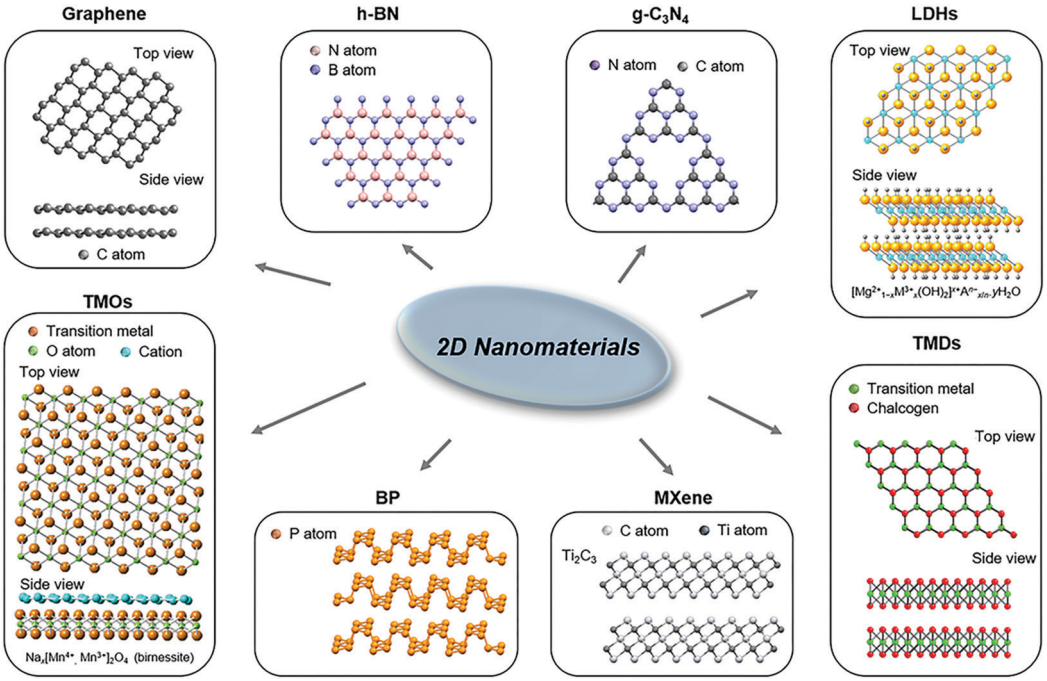

Fig. 2 Different 2D nanomaterials and their schematic nanostructures. Reproduced with permission.[51] Copyright 2019, The Royal Society of Chemistry.

few have made it to market, and thus the social benefit of 2DM in the water sector has yet to meet its initial promise.[37,48–50] A question that this review seeks to answer is what are the practical barriers preventing 2D nanomaterials from large-scale applications, and more importantly, what are the next directions needed to be prioritized. In addition, the rich chemical diversity of 2D nanomaterials offers numerous opportunities, but also presents a great challenge for comprehensively understanding and predicting their performance in water cleaning, particularly considering their complicated physicochemical response to the aqueous environment in the colloidal state. Therefore, we aim to provide a framework to better understand how the fundamental structures of 2D nanomaterials affect their collective behaviour, material properties, and corresponding applications in water treatment. This review will elaborate these connections in various application-targeted scenarios and discuss the chemical properties and molecular interaction of 2DM at the colloidal level (interaction radius between approximately 1 and 1000 nm). Initially, the state-of-the-art advances in functional membrane-based water treatment technologies including ultrathin monolayer membranes, stacked multilayer membranes, and solar desalination membranes are discussed. The discussion on 2DM-based adsorbents is sequentially presented, highlighting recent developments in the adsorption of oil spills, organic pollutants, heavy metal ions, and other contaminants. Then, various types of 2DM-based photocatalytic systems leveraging light in water decontamination are introduced. Since sensors are used to quantitatively determine the effectiveness of water decontamination, we expand our discussion to the 2DM-related detection of pollutants. Finally, promising directions and emerging trends of 2DM technologies are considered together with their possible negative implications. This review aims to summarize the typical scenarios of targeted applications, help to elaborate the structure-to-property relationship of 2DM systems, and provide an impetus toward the fast development of this highly interdisciplinary research field involving chemistry, physics, hydrology, biology, microbiology, materials science, chemical engineering, civil engineering, ocean engineering, and others.

2. Functional membranes with 2D nanomaterials

Since the primary objective of water treatment is the removal of undesired components from water, functional membranes offer a physical barrier to separate these components from water based on their size or permeability.[52–55] Also, since there is a typical trade-off between water permeability and selectivity, the development of functional membranes that maintain high permeability and high selectivity simultaneously is particularly challenging based on traditional membrane materials. It is well-known that the permeability is inversely proportional to the membrane thickness. Therefore, 2D nanomaterials with a thickness of one to a few atoms have emerged as promising building units for the development of next-generation separation membranes. In particular, introducing 2D nanomaterials into functional membrane design allows the realization of atomic-thin separation structures, which can selectively facilitate water molecules to pass through. These 2DM-based functional membranes can maintain relatively high permeation without serious sacrifice of the separation selectivity.[56] Based on the phase of water that permeates the membranes (*i.e.*, either gas phase or liquid phase), separation membranes can be categorized into

membrane filtration (liquid phase of water) and solar membrane distillation (gas phase of water). Filtration membranes primarily rely on the design of the hydrodynamic size of their pores for size-selective separation (adsorption selective separation will be discussed in detail in the next section),[57,58] while the design of solar desalination membrane involves several factors such as water evaporation enthalpy, hydrodynamic water transport, and light–matter interaction.[59,60] In this part, we mainly introduce filtration membranes and solar desalination membranes based on engineered two-dimensional nanomaterials.

2.1. Filtration membrane

In size-selective separation, the purification of water by membranes relies on the effect of the excluded volume repulsion between the membrane pores and undesired pollutant molecules. Therefore, two main strategies (*i.e.*, monolayer membranes and stacked multilayer membranes) have been studied to fabricate 2DM-based filtration membranes with a controlled pore size. Since the membrane permeation rate is inversely proportional to membrane thickness, the atomic thickness of 2D nanomaterials (*e.g.*, $t_{graphene} \approx 0.34$ nm) helps to achieve higher water permeability and less energy consumption than the commercial polyamide membranes ($d \approx 100$ nm).[61] Furthermore, since the structural voids of many 2D nanosheets (*e.g.*, graphene or graphene oxide (GO)) are too small for water molecules to permeate, additional modifications are commonly required. By introducing nanopores with a controlled size by electron beam irradiation, ion/plasma etching, and electrochemical oxidation (as shown in Fig. 3a), membranes with a 2DM monolayer are promising alternatives to conventional separation membranes. Several examples of 2DM-based functional membranes are listed in Table 1.

Theoretical works have predicted that nanoporous monolayers are highly efficient in water treatment.[76] Driven by a pressure difference, the nanoporous graphene monolayer forms a physical "mesh", which selectively allows water molecules to pass through the membrane (Fig. 3g). Molecular dynamics calculations showed that nanoporous graphene may achieve an excellent water flux of 66 L cm^{-2} day^{-1} MPa^{-1} and salt removal efficiency of up to 99%.[78] In these simulations, the nanopores of graphene monolayer play an essential role in water desalination, enabling H_2O molecules to selectively pass through. By controlling the size and functional groups of the pores on 2D nanomaterials, some porous monolayers may achieve a water permeation rate several orders of magnitude higher than that of the current RO membranes (Fig. 3i).[77,79]

Experimentally, early studies on graphene have suggested that an electron beam (e-beam) may be used to generate nanopores on its 2D sheets with nanometer precision (Fig. 3b and c).[73] Nanopores with a controlled size have been realized on graphene using the focused e-beam technique.[80] O'Hern *et al.* fabricated nanoporous graphene monolayers *via* the transfer of CVD graphene on porous polycarbonate.[81] Scanning transmission electron microscopy (STEM) showed that ~83% of the pores were relatively small with a diameter of less than 10 nm. These nanopores on graphene enabled the selective transport of several molecules, including potassium chloride, tetramethylammonium chloride, and tetramethylrhodamine dextran (70 000 Da).

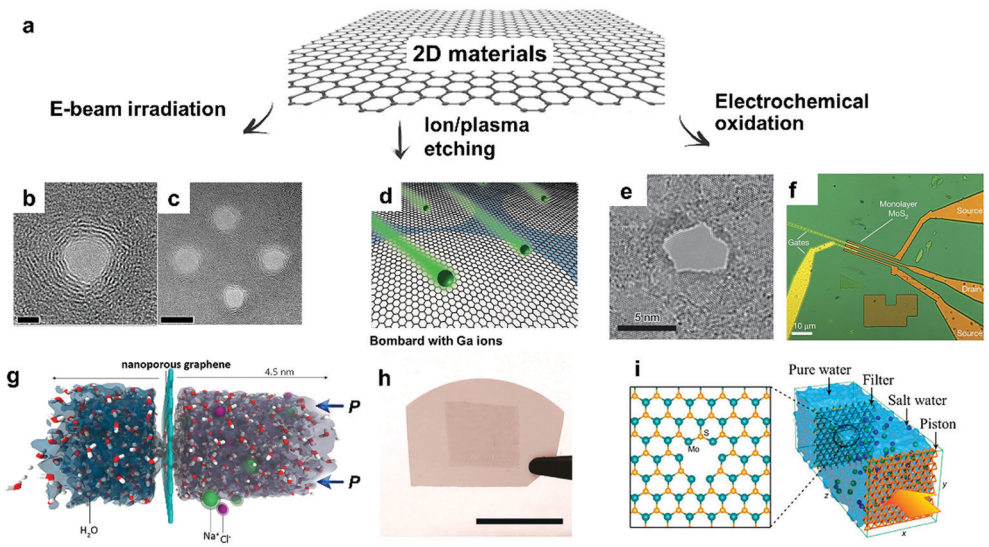

Fig. 3 Single-layer filtration membrane from 2D nanomaterials. (a) Popular strategies for the fabrication of single-layer nanoporous membranes. (b) Transmission electron microscopy (TEM) image of a nanopore on graphene. (c) TEM image of multiple graphene nanopores forming a porous structure. Scale bars in (b) and (c) are 2 and 10 nm, respectively. Reproduced with permission.[73] Copyright 2008, the American Institute of Physics. (d) Nanopores in graphene by ion bombardment. Reproduced with permission.[74] Copyright 2014, the American Chemical Society. (e) TEM image of MoS_2 nanopore with a diameter of 5 nm. (f) Optical microscopic image of the single-layer nanoporous MoS_2 device. (e and f) Reproduced with permission.[75] Copyright 2016, Springer Nature. (g) Schematic illustration of water purification by nanoporous graphene. Reproduced with permission.[76] Copyright 2012, the American Chemical Society. (h) Photo of nanoporous graphene membrane prepared by ion bombardment and oxidative etching. Reproduced with permission.[74] Copyright 2014, the American Chemical Society. (i) Modeled MoS_2 nanopore for membrane desalination. Reproduced with permission.[77] Copyright 2016, the American Chemical Society.

Table 1 Examples of 2DM-based functional membranes for water treatment

2DM	Pollutant	Flux/permeance	Efficiency	Comments	Ref.
Gr	KCl	10^6 g m^{-2} s^{-1}	~100%	Nanometer-sized pores in a graphene monolayer.	39
GO	Congo red	8.4 kg m^{-2} h^{-1}	99.5%	Separates ions and organics.	62
GO	RB5[a]	37.5 kg m^{-2} h^{-1}	99.2%	Surface zwitterionic-functionalized graphene oxide.	63
GO	$MgCl_2$	4.2 L m^{-2} h^{-1}	93.9%	LbL assembly of graphene oxide and polyethylenimine.[a]	64
GO	$MgSO_4$	2 L h^{-1} m^{-2} bar^{-1}	91.1%	Moderate salt rejection of NaCl (60%).	65
rGO	Na_2SO_4	60.6 L m^{-2} h^{-1}	93.57%	Low salt rejection of NaCl (36.6%).	66
MoS_2	Ag^+	160 L h^{-1} m^{-2} bar^{-1}	~99% (0.2 ppm)	High removal capacity of ~4000 mg g^{-1}.	67
MoS_2	Evans blue	245 L h^{-1} m^{-2} bar^{-1}	89%	High structural stability up to 1.0 MPa.	68
WS_2	Evans blue	730 L m^{-2} h^{-1} bar^{-1}	90%	Nanostrands forming fluidic channels in the WS_2 membrane.	69
MXene	Evans blue	1084 L m^{-2} h^{-1} bar^{-1}	90%	Colloidal $Fe(OH)_3$ used as a distance holder.	70
h-BN	CH_2Cl_2	2.65 L m^{-2} s^{-1}	—	Effective treatment of oil-polluted water.	71
g-C_3N_4	RhB[a]	957 L m^{-2} h^{-1} bar^{-1}	60%	Integration of filtration and visible light photocatalysis.	72

[a] RB5 stands for reactive black 5; RhB stands for rhodamine B and LbL stands for layer-by-layer.

The graphene composite membrane enabled KCl and tetramethylammonium chloride to pass through, while rejecting tetramethylrhodamine dextran. To fabricate dense pores on graphene with controlled sizes, Surwade *et al.* developed a single-layer membrane *via* ambient pressure CVD (APCVD) on copper.[39] During the fabrication process, nanopores were introduced on graphene and tuned *via* the oxygen plasma etching technique. The size-controlled nanopores improved the membrane selectivity and allowed water to pass through, while rejecting other species such as Li^+, Na^+, and K^+. In particular, this monolayer membrane achieved excellent salt rejection (~100%) with high water permeability. It is worth mentioning that the selectivity of the low-porosity membrane exceeded five orders of magnitude; however, it decreased at high porosities, possibly because of the size change of the nanopores. Under an external pressure, a flux of 10^6 g m^{-2} s^{-1} at 40 °C was achieved. Based on the estimated hole density of approximately 1/100 nm^2, the permeation rate at one nanopore could reach a value of three molecules per picosecond.

The ion bombardment technique has also been applied for the fabrication of nanoporous graphene membranes (Fig. 3).[82] Compared with conventional pore generation strategies, which mainly rely on direct oxidative processes,[83–85] ion-bombardment-based techniques (for example, argon ion irradiation) can generate pores with a controlled size and density.[82] For example, O'Hern *et al.* fabricated a monolayer graphene membrane with high-density nanopores *via* a two-step method (Fig. 3d).[74] In the first step, gallium ion bombardment was used to generate isolated reactive defects. In the second step, these defects were enlarged using oxidative etching into permeable nanopores (0.40 ± 0.24 nm). After the two-step treatment, a nanoporous graphene membrane with a pore density of over 10^{12} cm^{-2} was prepared, as shown in Fig. 3h. Interestingly, the authors found that the nanopores by short-time etching were cation selective, which is likely due to the formation of negatively charged groups (*e.g.*, –COOH). However, a longer oxidation time led to a larger pore size, and thus the electrostatic effect determining the K^+/Cl^- selectivity weakened. Owing to the size exclusion effect of the graphene membrane, the authors also observed that the membrane pores allowed small-sized salt to pass through, while hampering the transport of larger organic species.

As an economic alternative, electrochemical oxidation has also been reported for the formation of nanopores on 2D nanosheets (Fig. 3). For example, Feng *et al.* established a facile approach to generate nanoholes on MoS_2 nanosheets by applying electrochemical reaction (ECR).[86] The formation of a nanopore starts at the lattice defects of MoS_2 by the ECR process, which subsequently enlarges these defects into nanoscale holes by removing atoms or unit cells from single-layer MoS_2. The step-like feature in the ionic current gives direct feedback on the pore dimensions, which can be calculated from a conductance vs nanopore size model.[86] Interestingly, Feng *et al.* took advantage of the superior transport property of porous MoS_2 and prepared single-layer MoS_2 nanopower generators (Fig. 3e and f). The authors observed an osmotically driven current generated from a salt gradient with an estimated power density of up to 10^6 watts per m^2, which is likely due to the high efficiency of the atomically thin membrane of MoS_2.[75]

Although monolayer 2DM membranes possess several unique advantages including high water permeability, one practical barrier preventing their application is the difficulty of fabricating leak-free, large-area monolayer membranes with precise pores on an industrial scale.[74,87,88] By contrast, commercial nanofiltration membranes made from polymers or polymer composites often have low production cost and high scalability. Thus, to reduce the fabrication cost and improve the scalability, novel separation membranes based on stacked nanosheets have been proposed (Fig. 4). Owing to their highly anisotropic feature, 2D nanosheets have been readily assembled into lamellar structures by external assembly methods (*e.g.*, vacuum filtration and layer-by-layer (LbL) assembly), as shown in Fig. 4a.[89] Owing to their solution processable feature, these fabrication methods are compatible with low-cost nanosheets, which can be synthesized in large quantities *via* liquid-phase exfoliation strategies. Therefore, the layered stacking of 2DM promises the low-cost and industrial-scale manufacturing of high-performance separation membranes.[90,91]

During vacuum-assisted filtration, the nanosheet concentration increases continuously, and thus they tend to assemble into an ordered lamellar structure. Li *et al.* developed a lamellar MXene-based membrane using vacuum filtration (Fig. 4b).[70] The MXene membrane exhibited a high water flux

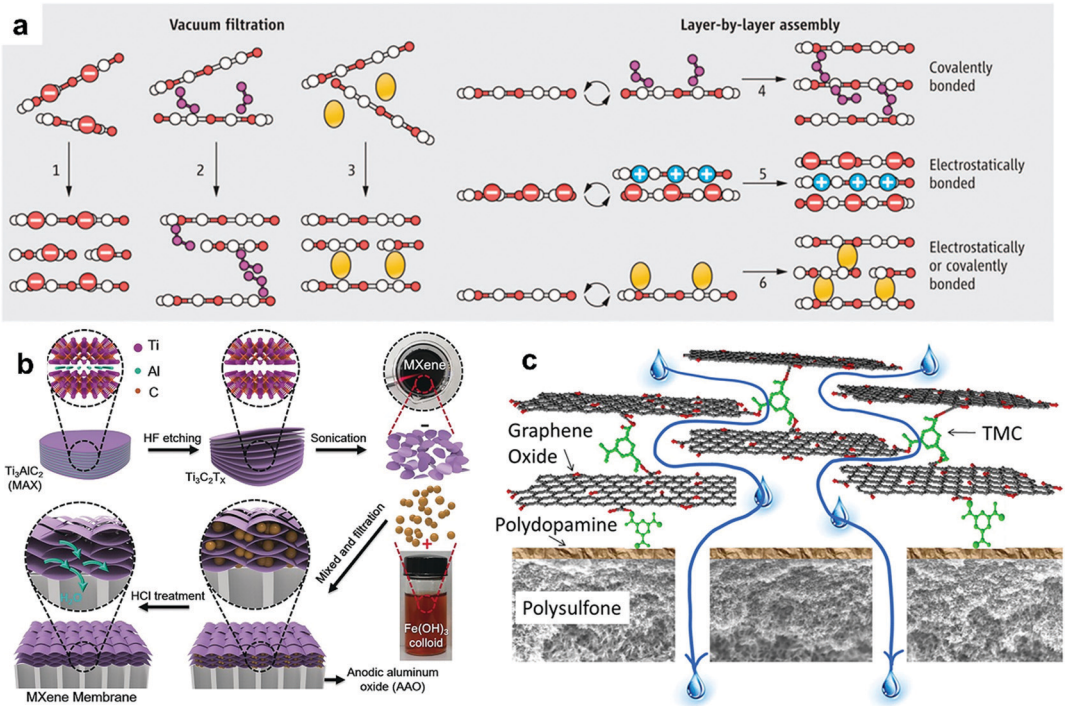

Fig. 4 Common methods for the fabrication of multilayer filtration membranes from 2D nanomaterials. (a) Schematic illustration of nanoporous membranes based on stacked nanosheets. Reproduced with permission.[89] Copyright 2014, AAAS. (b) MXene membrane fabricated by vacuum filtration. Reproduced with permission.[70] Copyright 2017, Wiley-VCH. (c) GO-based separation membranes by LbL assembly. Reproduced with permission.[79] Copyright 2013, the American Chemical Society.

(>1000 L m^{-2} h^{-1} bar^{-1}) and good rejection efficiency ($>90\%$) for pollutants bigger than 2.5 nm. Han *et al.* reported a graphene-based nanofiltration membrane by filtering chemically converted graphene (CCG) on porous substrates.[92] This graphene-based membrane demonstrated an excellent rejection efficiency ($>99\%$) for dye molecules and inferior efficiency (20–60%) for salts. The authors attributed the separation performance to the effect of electrostatic interaction and size sieving. Tsou *et al.* showed that the type of deposition method can change the morphology of layered GO membranes.[93] They compared the effect of the vacuum-, pressure-, and evaporation-assisted self-assembly techniques on the prepared GO membrane. Under the tested conditions, the authors found that pressure-assisted filtration techniques help to induce an ordered laminate structure of GO, leading to an excellent separation performance. In addition to the deposition methods, the deposition rate of GO through vacuum filtration is another crucial factor in the membrane performance.[94] Specifically, it was found that a slow deposition of GO nanosheets can adjust the separation efficiency and water flux of GO-based separation membranes. The authors suggested that the interlayer spacing of GO laminates can be engineered by changing the deposition rate.

Since GO nanosheets are intrinsically hydrophilic, GO membranes that are solely vacuum-filtered may lack sufficient bonding between GO nanosheets, and thus may suffer from structural damage under the cross-flow conditions commonly encountered in industrial membrane operations.[89] Thus, to improve the structural stability of 2DM stacked membranes, tremendous efforts have been made in LbL assembly strategy to introduce an interlayer bonding by electrostatic attraction or/and covalent linkage during membrane fabrication. Multiple molecular interactions, including coordination interactions, covalent bonding, charge-transfer interactions, and biologically specific interactions, have been increasingly investigated to facilitate LbL assembly for the stabilization of the functional multilayers.[89,95] During the LbL process, 2D nanosheets are first dispersed in a stable colloidal dispersion, followed by dip, spin, or spray assembly. 2D graphene oxide nanosheets[43,96,97] with rich charged groups have been widely reported for the fabrication of 2DM-based stacked membranes *via* LbL assembly techniques. For example, Hu *et al.* developed a separation membrane *via* the LbL assembly of graphene oxide, where 1,3,5-benzenetricarbonyl trichloride was used as the cross-linker (Fig. 4c).[79] The authors found that the cross-linkers considerably improved the structural stability of the stacked GO monolayers. This GO membrane showed a water flux in the range of 80 to 276 LMH per MPa (depending on the number of GO layers), which is roughly 4–10 times better than that of many conventional nanofiltration systems.[79]

For most multilayer membranes, the interlayer spacing of stacked nanosheets has been regarded as one of the most crucial factors in determining their performance.[89,99,100] Taking GO nanosheets as an example, the average interlayer spacing can reach $\sim$0.9 nm in an ionic solution due to the hydration effect, allowing ions with a hydrodynamic radius of 0.45 nm or smaller to

permeate, while rejecting larger-sized molecules.[101] Therefore, desalination requires that the interlayer distance of nanosheets to be <0.7 nm for the separation of hydrated Na^+ (with a hydrodynamic radius of 0.36 nm) from water (Fig. 5a).[89] This small spacing can be achieved by covalently bonding GO with small molecules to overcome the hydration force in an aqueous environment. By contrast, a medium-sized GO spacing (0.7 to 2 nm) can be useful for the separation of pollutants and fuel purification. If even larger-sized particles were adopted as spacers, GO membranes with an interlay distance of >2 nm can be obtained for possible application in biomedical processes (*e.g.*, artificial kidneys and dialysis), in which the separation of large biomolecules is important. Long *et al.* investigated the transport properties of a metal-ion-decorated GO membrane.[102] By using LiCl, NaCl, KCl, $MgCl_2$, $CaCl_2$, $SrCl_2$, $Ca(NO_3)_2$, $MnCl_2$, and YCl_3 to functionalize the surface of GO, the authors systematically evaluated the effect of different salts on the permeation rate of organic molecules on the metal-ion-decorated GO membrane. They observed that the Ca^{2+}–/Mg^{2+}–GO membranes showed high selectivity for organic solvents, such as acetone, acetonitrile, and benzene. They attributed the selective permeability of the metal-ion-decorated GO membrane to the relative strength of the cation–π interaction, electrostatic force, and hydrogen bonding. In addition to the use of interlayer spacing, Wang *et al.* reported a 2D multilayer membrane with both artificial nanopores and self-supporting spacers (Fig. 5b).[98] The authors used porous g-C_3N_4 nanosheets as building blocks and unstripped fragments as self-supporting spacers to fabricate a separation membrane, providing a water transport pathway that tolerates pH and pressure changes during the water treatment. A porous g-C_3N_4 membrane with a thickness of 190 nm showed a salt rejection of 90% with a decent water flux of 11.6 L m^{-2} h^{-1} bar^{-1}. Recently, to suppress the swelling effect of 2D nanomaterials, which adversely changes their ion sieving performance, Ding *et al.* leveraged the intercalation of Al^{3+} ions for the fabrication of non-swelling MXene membranes. As shown in Fig. 5c, the as-prepared MXene membrane could effectively reject NaCl from seawater, while maintaining strong structural stability with high water fluxes ($\sim$1.1–8.5 L m^{-2} h^{-1}).[99]

However, despite the significant advances in 2DM membranes, major challenges, *e.g.* large-scale fabrication of these membranes with long-term stability, still exist.[103] Fouling is a common issue that prevents the long-term operation of many membranes since it increases the energy consumption and reduces the water recovery of desalination processes.[58,104] Thus, to mitigate fouling/biofouling, several nanostructure-based materials have been proposed, such as effectively inactivating bacteria on direct contact.[105,106] Combining GO nanosheets with other antibacterial nanomaterials (such as silver nanoparticles) appears to be a promising approach to ensure the inactivation of bacteria.[107] In addition, self-cleaning and self-repair design may further facilitate the practical use of 2DM membranes in water treatment.[108]

2.2. Solar desalination membrane

The ability to generate desalinated water directly using sunlight, solar steam desalination has emerged as an encouraging solution toward addressing the increasingly pressing global freshwater shortage.[109] Different from separation membranes,

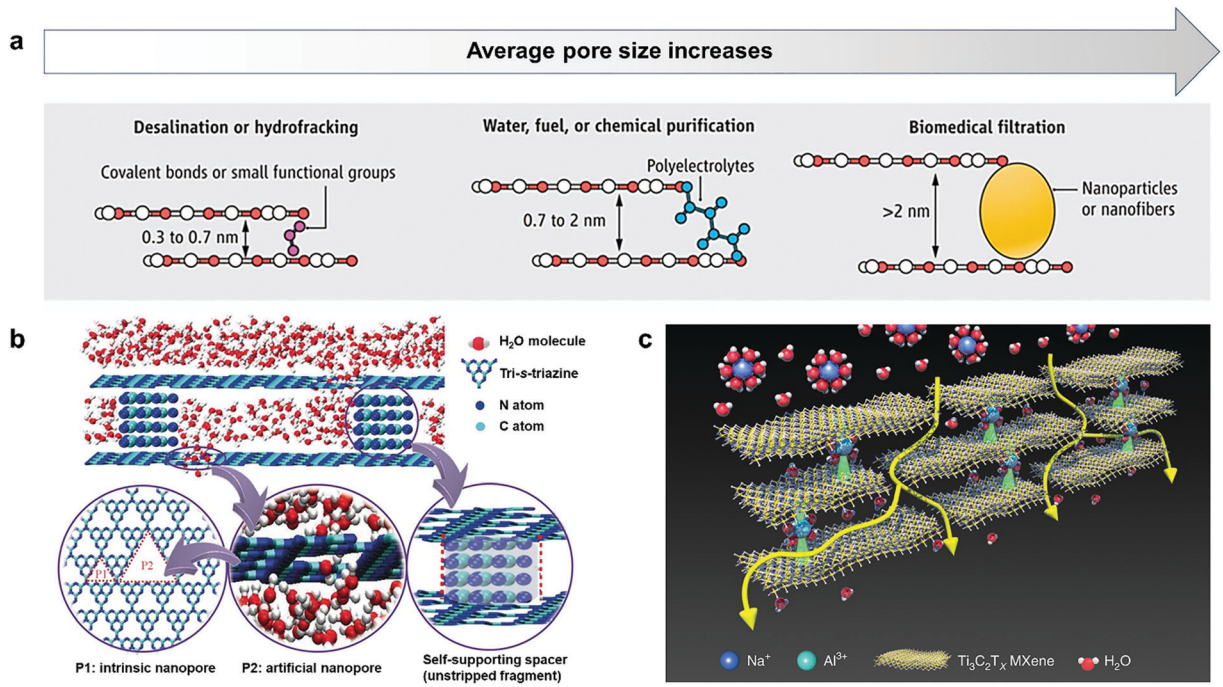

Fig. 5 Pore size engineering for the separation of different compounds. (a) Tunable separation capability of 2D multilayer membrane by tailoring the interlayer spacing. Reproduced with permission.[89] Copyright 2014, AAAS. (b) Diagram showing water transport through g-C_3N_4 nanosheets *via* water nanochannels including intrinsic nanopores (P1), artificial nanopores (P2), and self-supporting spacers. Reproduced with permission.[98] Copyright 2017, Wiley-VCH. (c) Schematic illustration of ion sieving with multilayer MXene membrane. Reproduced with permission.[99] Copyright 2020, Springer Nature.

which are primarily based on size selective separation, desalination membranes leverage the difference in evaporation enthalpy between water and pollutants. Fig. 6a presents a typical solar desalination device, consisting of four components, including a seawater reservoir, solar desalination membrane, condenser, and freshwater collector. Among these components, the solar desalination membrane plays a key role in converting solar energy into heat for steam generation. Black 2D nanomaterials, such as graphene and MXene, have been investigated for solar water evaporation applications due to their outstanding photon-harvesting ability, low molar specific heat, and tunable thermal conductivity by chemical doping.[60] In contrast to the popular lamellar design in filtration membranes, high porosity and even vertically aligned structure of 2D sheets have been proposed to promote the water transport. For example, a vertically aligned graphene sheet membrane (VA-GSM) was fabricated to convert solar energy into heat for desalinated water production.[110] Compared to graphene with a lamellar alignment (Fig. 6b) and random structure (Fig. 6c), the VA-GSM (Fig. 6d) demonstrated unique advantages for water transport, and thus showed a higher solar desalination performance. The VA-GSM showed a high vapour generation rate of 1.6 and 6.3 kg m^{-2} h^{-1} under 1 and 4 sun illumination with an excellent efficiency of up to 86.5% and 94.2%, respectively.[110] To maximize the use of solar energy and reduce thermal loss, efficient solar absorption and effective heat management have been regarded as the two essential factors for solar desalination.[111–121] Efficient solar absorption has been achieved in a variety of advanced functional materials,[116,119,120] and an ideal sunlight absorber will minimize the effect of reflectance or transmittance in a broad wavelength range. To date, several strategies have been investigated to develop highly efficient absorbers, including effective antireflection,[120,121] strong light coupling for efficient absorption,[122] and high density of optical modes.[115,123] Due to the low-cost and environment-friendly feature of carbon-based nanomaterials, they are increasingly studied for membrane desalination and solar steam desalination.[124–130] However, despite their ability to absorbing light by the π-band optical transitions, conventional graphitic materials suffer from roughly 5–10% reflection at the air–dielectric interface.[131] Thus, to overcome this limitation, the design of nanostructured carbon materials appears to be an effective approach, *e.g.*, porous graphene.[132–136] These nanostructures can on-demand confine sunlight to small regions by resonant recirculation, increasing the interaction of light within the materials.[137] Moreover, plasmon resonance techniques have also been studied to increase the absorption bandwidth.[138–144] On the surface of a metal, light can trigger the collective excitation of electrons if its frequency matches the oscillation frequency of delocalized electrons. As shown in Fig. 6e–h,[145] these excited hot electrons interact coherently with the incident electromagnetic field, leading to heat generation in materials.[146–148]

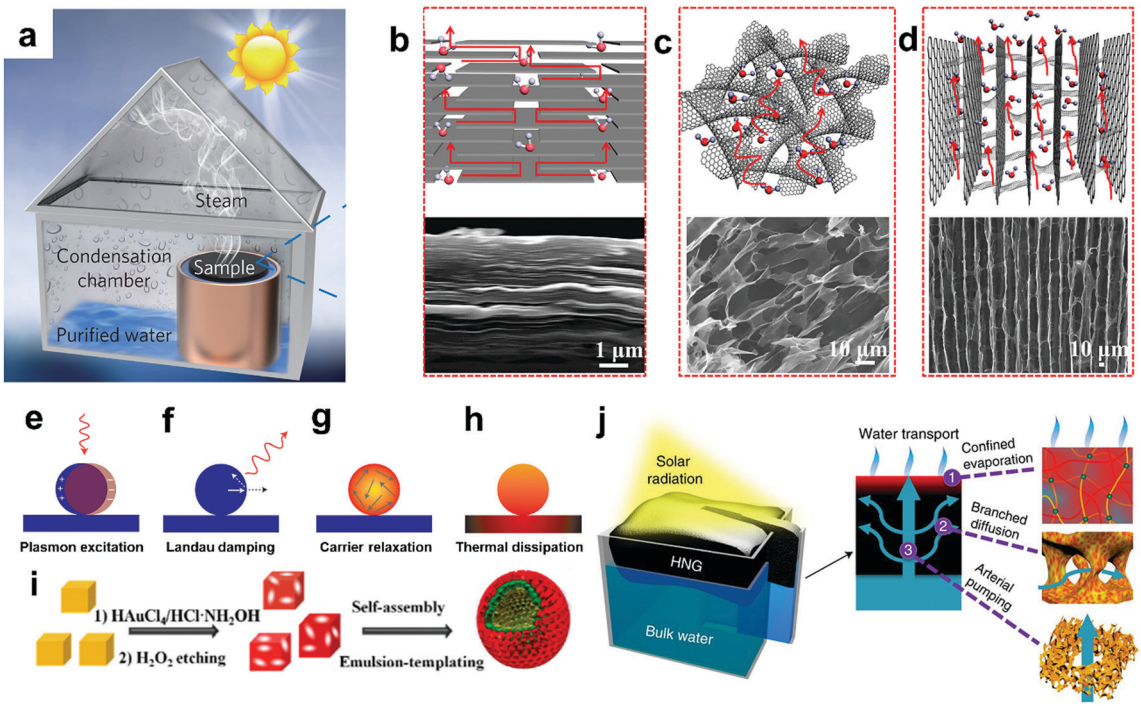

Fig. 6 Solar desalination membranes from 2D nanomaterials. (a) Schematic demonstration of a solar desalination device. Reproduced with permission.[109] Copyright 2016, Springer Nature. Water transport channels based on lamellar (b), random (c), and vertically aligned structures (d). Reproduced with permission.[110] Copyright 2017, the American Chemical Society. Plasmon-induced hot carrier phenomena of metallic nanoparticles involving photoexcitation (e), Landau damping (f), carrier relaxation (g), and subsequent thermal dissipation processes (h). Reproduced with permission.[145] Copyright 2015, Springer Nature. (i) Schematic of plasmonic colloidosomes prepared from metal precursors. Reproduced with permission.[150] Copyright 2018, Elsevier B.V. (j) Schematic of solar steam production in hierarchically nanostructured gel (HNG). Reproduced with permission.[151] Copyright 2018, Springer Nature.

During this process, the hot carriers complete the energy redistribution through electron–electron scattering processes, generating a considerable amount of heat, which can be further transferred to surrounding materials by thermal conduction.[149]

Experimentally, various plasmonic components integrated with 2D nanomaterials have been realized on membrane substrates. As presented in Fig. 6i, Wang *et al.* designed a solar desalination membrane using graphene oxide and a multiscale plasmonic nanostructure, in which Ag/Au nanocubes were used as assembly blocks to build plasmonic colloidosomes.[150] Owing to the plasmonic coupling of the metal nanoparticles, the authors reported an excellent efficiency of 92% at 10 kW m^{-2} and steam generation rate of 12.96 kg m^{-2} h^{-1} for the solar desalination membrane.

Since the average solar energy on Earth is commonly around or even less than 1 kW m^{-2} (1 sun condition), effective heat management can be equally important. Although a higher efficiency can be achieved by applying a concentrated solar flux,[113,152,153] it will be advantageous if high efficiency can be achieved under 1 kW m^{-2} or even weaker light intensity. Thus, to suppress undesirable heating loss such as water heating and parasitic thermal loss during solar steam generation,[154] heat localization is an efficient strategy for solar energy utilization since it can restrict heat to small quantity of water for effective evaporation.[112,155,156] In addition, from dispersed particles,[157,158] to porous carbon films,[154,159] and thin metallic absorbers,[160–162] an increasing trend of using a confined region for localized heating has been observed for reducing heat loss to the bulk water and surrounding environment. Zhao *et al.* developed an energy confinement approach by hierarchical water pathways in a hydrogel (Fig. 6j).[151] This hierarchically nanostructured gel (HNG) showed an excellent evaporation rate of 3.2 kg m^{-2} h^{-1}, producing 18–23 litres of H_2O per square metre of HNG per day from brine water. Li *et al.* reported a GO-based solar desalination device and found that an efficient water supply and suppressed heat loss could be achieved simultaneously by confining the water path to a 2D geometry (Fig. 7a and b). Due to the suppressed heat loss, the authors demonstrated that the exceptional performance of solar desalination can be independent of the amount of water and effective water evaporation can be achieved even in the absence of thermal insulation in the container.[156]

For 2DM-based solar desalination membranes, graphene, TMDs, and MXene have been demonstrated as advantageous photothermal materials. Since TMDs contain active sulphide bonds and can adsorb heavy metal ions, Li *et al.* showed that MoS_2-based photothermal devices not only produce a high

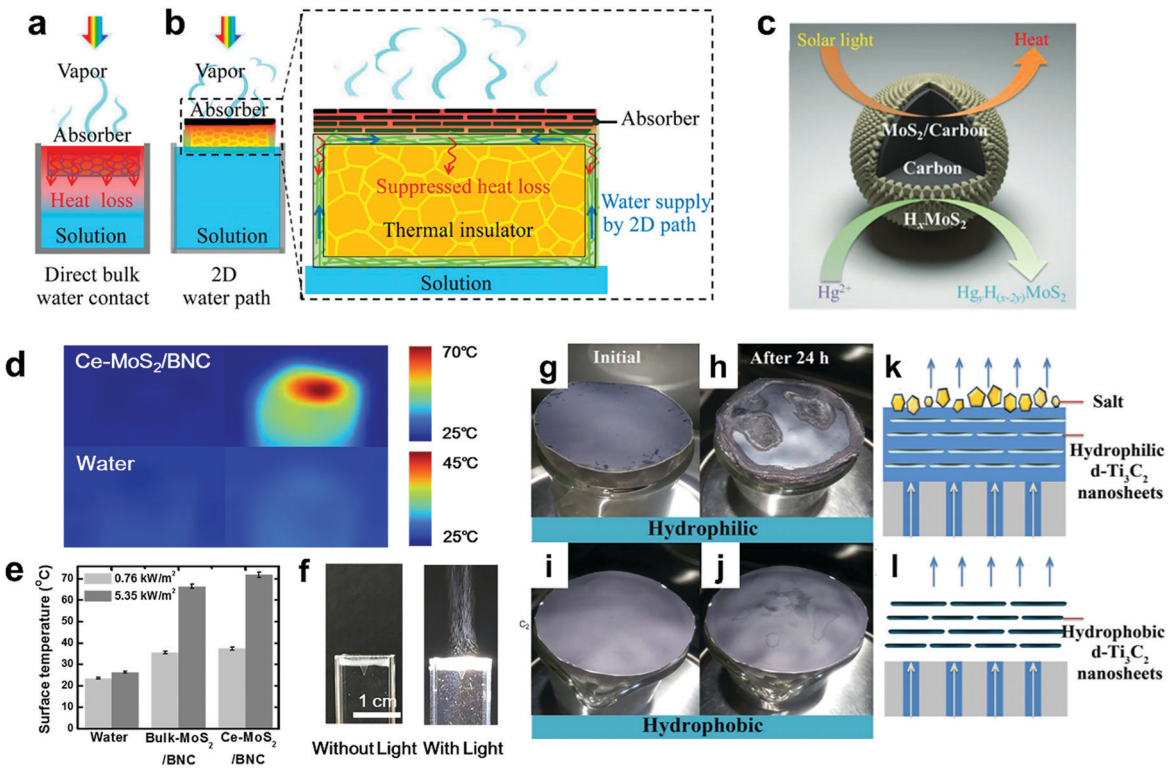

Fig. 7 Strategies to improve the efficiency of solar desalination systems using 2D nanomaterials. (a and b) Enhanced thermal management by 2D path of water supply. Reproduced with permission.[156] Copyright 2016, the National Academy of Sciences. (c) Schematic of bifunctional MoS_2/C microbeads. Reproduced with permission.[163] Copyright 2018, Wiley-VCH. (d) Infrared thermal images of chemically exfoliated MoS_2/bacterial nanocellulose (Ce-MoS_2/BNC) and reference samples. Surface temperature of bare water, Ce-MoS_2/BNC, and bulk-MoS_2/BNC aerogels (e) and camera image showing the water steam at the surface of Ce-MoS_2/BNC bilayer aerogel under light irradiation (f). Reproduced with permission.[166] Copyright 2018, Elsevier B.V. Photographic images and solar steam generation of the hydrophilic and hydrophobic 2D MXene membranes before (g and i) and after 24 h (h and j). Schematic showing the solar desalination process with (k) and without salt formation (l). Reproduced with permission.[170] Copyright 2018, The Royal Society of Chemistry.

evaporation rate (1.95 kg m^{-2} h^{-1}) at 1 sun, but also can reduce Hg from 200 to 1 ppb (Fig. 7c).[163] In addition, chemical exfoliation of MoS_2 enables a partial phase transition from the 2H phase to the 1T phase, leading to a higher visible light absorption of MoS_2.[164,165] Ghim *et al.* proposed chemically exfoliated MoS_2 (Ce-MoS_2) as a photothermal material for solar desalination (Fig. 7d–f).[166] The authors used bacterial nanocellulose (BNC) as the support material for heat localization and demonstrated that the chemically exfoliated MoS_2/BNC bilayer aerogel (96%) outperformed the unexfoliated MoS_2/BNC (~90%) and bare BNC (~10%).[166] In addition to TMDs, MXene has also been suggested as a promising photothermal material because of its high light-to-heat conversion efficiency.[167] An MXene-based solar desalination membrane was developed by vacuum filtration on a porous substrate, exhibiting a decent solar conversion efficiency of 84% under 1 sun condition.[168] However, despite the tremendous efforts in designing and developing 2DM-based desalination membranes, some technical challenges still exist. For instance, the long-term stability of many solar desalination membranes is limited in highly saline water because salt continuously accumulates on the top of the membrane, and thus decreases the light absorption and water supply, leading to a decrease in the water evaporation performance.[109,156,169] To address this issue, Zhao *et al.* reported an MXene-based solar desalination membrane with a hydrophobic surface (Fig. 7g–l).[170] Using trimethoxy(1*H*,1*H*,2*H*,2*H*-perfluorodecyl)silane as the surface modifier, this membrane showed strong hydrophobicity under high salinity conditions, and thus demonstrated good stability under one sun over 200 h.[170] Another technical challenge comes from the generated water vapour, which can interfere with the light collection of solar desalination membranes. This issue may be circumvented by integrating solar steam generation with the conventional membrane distillation process using advanced design of distillation geometries.[171] In conventional membrane distillation, a temperature difference is established between the input fluid and distilled water for generating a vapour pressure difference, which enables water vapour to pass through the membrane from the input side to the distilled side. By modifying the membrane with light-absorbing nanoparticles, solar energy can be used to replace conventional heating of the input fluid for the distillation process. This process integration of solar-driven steam generation with membrane distillation may profoundly improve the conventional membrane distillation process. Therefore, in addition to the material aspect, judicious system design and innovation, such as introducing Janus membranes or enhanced convection,[172–177] will be highly desirable for off-grid, large-scale applications.

3. Functional adsorbents with 2D nanomaterials

Although functional membranes can be readily adapted into the workflow of wastewater treatment, adsorption-based technology, due to its low capital expense and simple procedure, is another promising option for wastewater treatment, particularly for oil spill mitigation and heavy metal collection. In particular, 2D nanomaterials have received broad interest for contaminant adsorption applications. Since the adsorption of pollutants is essentially an interfacial process, 2D nanomaterials with a large surface area that enables high levels of surface/interface interactions may possess exceptional adsorption efficiency. The plausible adsorption or interaction mechanisms and selective adsorptions are summarized in Fig. 8, including hydrophobic interaction, π–π stacking, H-bonding, ion/ligand exchange, Lewis acid/base and electrostatic interactions. In this section, the recent developments in 2DM-based adsorbents are discussed to address the challenges of oil spills, heavy metals, anions, and hydrophilic organic pollutants.

3.1. Oil spill adsorbents

Frequent oil spills have resulted in serious harm to the marine ecosystems and huge loss of valuable resources.[178,179] Thus, to quickly eliminate oil contaminants, efficient and environmentally friendly oil adsorbents are needed. There are several desirable features for an ideal oil spill adsorbent as follows: (1) high-speed clean-up of oil spills to reduce the oil diffusion; (2) the ability to restore the oil spill at a high oil water separation efficiency; (3) negligible impacts to ocean creatures; (4) applicable in a large area and easy to operate; and (5) work effectively under severe ocean conditions. However, conventional oil recovery processes, such as the use of chemical dispersants,[180] emulsifiers,[181–183] solidifiers,[184] *in situ* burning[185] and skimmers,[186] have their own shortcomings, and thus new materials toward oil spill mitigation are desirable.

2DM-based advanced sorbents with oleophilicity and hydrophobicity have become promising candidates for fast oil spill mitigation. Taking advantage of conductive reduced graphene oxide (rGO) nanosheets, Ge *et al.* reported that a graphene-wrapped sponge (GWS) was designed for viscous crude clean-up (Fig. 9a and b).[40] After applying a current, the Joule-heated graphene-wrapped sponge showed hydrophobic characteristics and oleophilic features (Fig. 9c and d). As shown in Fig. 9d, the highly viscous crude oil easily spread over the surface of the heated GWS. This can be explained by the fact that the Joule heating of GWS reduced the oil viscosity, which considerably increased the oil-diffusion rate in the GWS pores, speeding up the oil adsorption. It was observed that the adsorption time was shortened by 5.4% of the original time. In addition, compared with the unheated sponge, the heated one showed a much higher oil recovery rate due to the reduced viscosity of the crude oil.

Compared with hydrophobic structures, superhydrophobic materials with even higher contact angles (CA > 150°) have shown further improvement in adsorbing oil pollutants from water due to their exceptional water/oil selectivity. The functional groups and geometric morphology of a surface directly affect the wetting behavior of the testing liquids on it.[188,189] In general, pristine nanosheets require surface functionalization to become superhydrophobic. Jayaramulu *et al.* reported a highly fluorinated graphene oxide, which exhibited a low oil CA of 0° and large water CA of 162°. Thus, this fluorinated graphene oxide showed high sorption selectivity and good

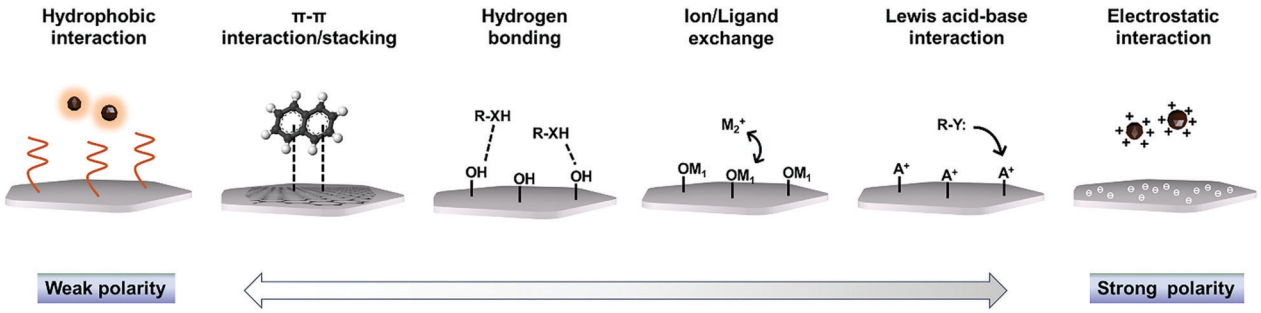

Fig. 8 Main mechanisms of pollutant adsorption on 2D functional nanomaterials.

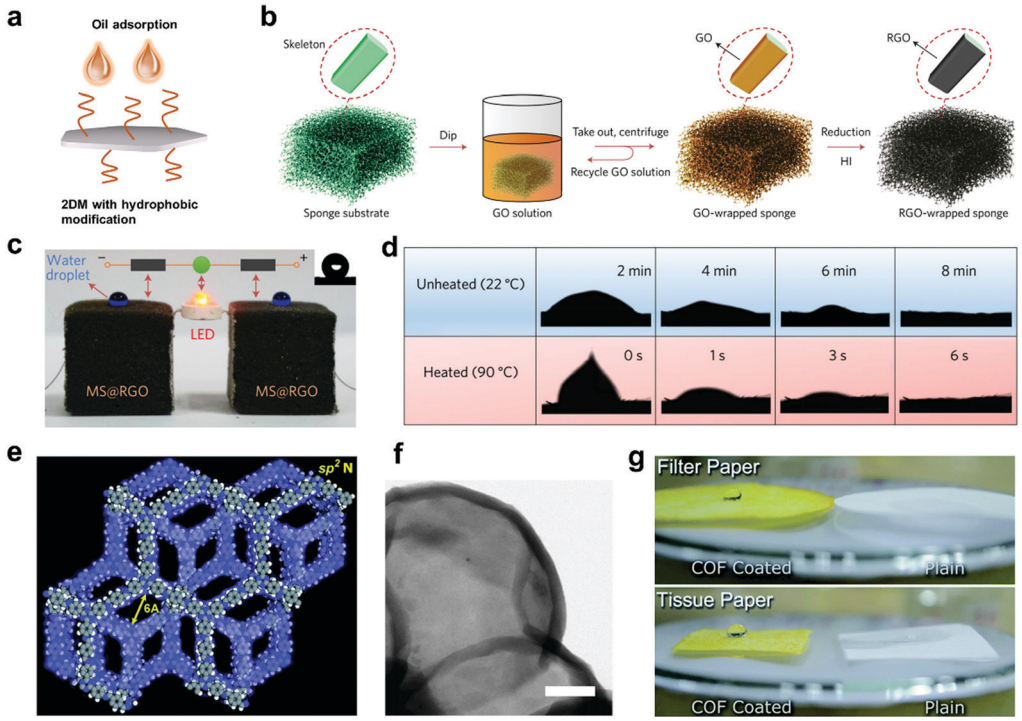

Fig. 9 Removal of oil pollutant by hydrophobic 2D nanomaterials. (a) Hydrophobic modification of 2DM, enabling effective oil adsorption. (b) Demonstration of the GWS fabrication process. (c) GWS device showing both hydrophobic and conductive features. The inset image demonstrates the water contact angle of GWS. (d) Oil droplet permeating behavior on GWS with (lower row) or without (upper row) external voltage. (b–d) Reproduced with permission.[40] Copyright 2017, Springer Nature. (e) Structure of functional hydrophobic 2D COFs. (f) TEM image of COF nanosheets. Scale bar is of 200 nm. (g) COF-based composites showing strong hydrophobicity. (e–g) Reproduced with permission.[187] Copyright 2017, The Royal Society of Chemistry.

absorbencies.[190] Taking advantage of the versatile chemistry of 2D COFs (Fig. 9e–g), superhydrophobic COFs were used as coatings with excellent water repellency (water CA of 163°).[187] It was found that the coatings still retained superhydrophobicity under harsh conditions from pH = 1 to pH = 14, and temperature from 0 °C to 80 °C. In addition to the low energy surface by chemical modification, high surface roughness also plays a role in improving the superhydrophobicity. According to Wenzel's model,[189] the apparent contact angle, θ^*, at the stable equilibrium state can be estimated by the equation: $\cos\theta^* = R \times \cos\theta$, where θ is the contact angle, which corresponds to an ideal flat surface. R is the surface roughness ratio of the sample.

Since most flat surfaces do not exhibit sufficient hydrophobicity by only low energy coatings,[191,192] controlled manufacturing of the microstructures is critical to enhance surface roughness and achieve superhydrophobicity. For instance, Jiang *et al.* developed microstructures on plain surfaces by introducing polymers/carbon nanotubes.[193,194] Yu *et al.* synthesized hydrophobic aerogels with 1D carbonaceous fibers[195,196] and 2D graphene sheets[197] as building blocks. Besides graphene oxides, superhydrophobic and superoleophilic h-BN composite materials have also been realized *via* the self-assembly of exfoliated h-BN nanosheets.[71] The as-prepared composite material can be used to effectively separate various water/oil emulsions, in which droplets can be between 10^{-6} m to 10^{-9} m in size

with exceptional separation efficiency, even under severe high flux rate.

To investigate the correlation between surface roughness and nanoscale building blocks, Du *et al.* designed several microstructures of various dimensions including zero, one, two dimensions and 1D–2D and 0D–1D composites on commercial melamine foams (Fig. 10a–g).[198] Experiments and simulations were performed to explain the dimension-to-wettability relation. Among these composites, the authors found the highest surface roughness in the hierarchical structure of the 1D/2D nanomaterials, in which CNTs were conformally deposited on $Co(OH)_2$ sheets. Indeed, the hierarchical structure allows larger surface interaction, and thus amplifies the intrinsic hydrophobicity. Since 2D nanomaterials possess a large surface area and tunable surface chemistry that enable facile co-assembly or post-functionalization with other building blocks, numerous hierarchical nanostructures made from 2D nanomaterials have been extensively demonstrated in the recent success in energy storage,[199] high-performance catalysts,[200] and bio-inspired structures.[201–203] Taking advantage of the barrier properties of 2D zirconium phosphate nanoplates (ZrP), Cheng's group proposed a hierarchical structure with self-healing and superhydrophobic features (Fig. 10h and i).[204] With the hierarchical porous platform textile fibers, the 2D ZrP nanoplatelets with a superhydrophobic coating could remove oil from an oil–water mixture with high separation efficiency (99.9%). After chemical etching, the hybrid film was capable of autonomously and repeatedly recovering its hydrophobicity since the layered structure protected the healing agent, which could gradually diffuse to the surface to reduce the surface energy.

3.2. Hydrophilic organic pollutant adsorbents

Hydrophilic organic molecules, such as detergents, biphenyls, fertilizers, pesticides, and pharmaceuticals, are common water contaminants.[205] Thus, to effectively remove these hydrophilic species from water, judicious design of 2DM with electrostatic attraction, van der Waals force, and hydrogen bonding are important approaches for developing 2DM-based adsorbents. In particular, water-soluble dyes have been extensively studied as model pollutants for investigating the decontamination behavior of adsorbents for the following two reasons: (1) dye pollution exists in the textile, rubber, plastic, printing and other industries, which easily results in water body contamination and (2) importantly, the ability of dyes to absorb a certain wavelength of light allows the pollutant concentration to be monitored in a simple, straightforward, and accurate manner. Therefore, the removal of dyes by 2DM-based adsorbents is highlighted herein.

Li *et al.* reported a water-stable graphene-like MOF (**BUC-17**) for the adsorption of dyes from simulated wastewater, showing excellent adsorption properties at room temperature.[207] Ahmad *et al.* reported a 2D MOF material for the removal of rhodamine

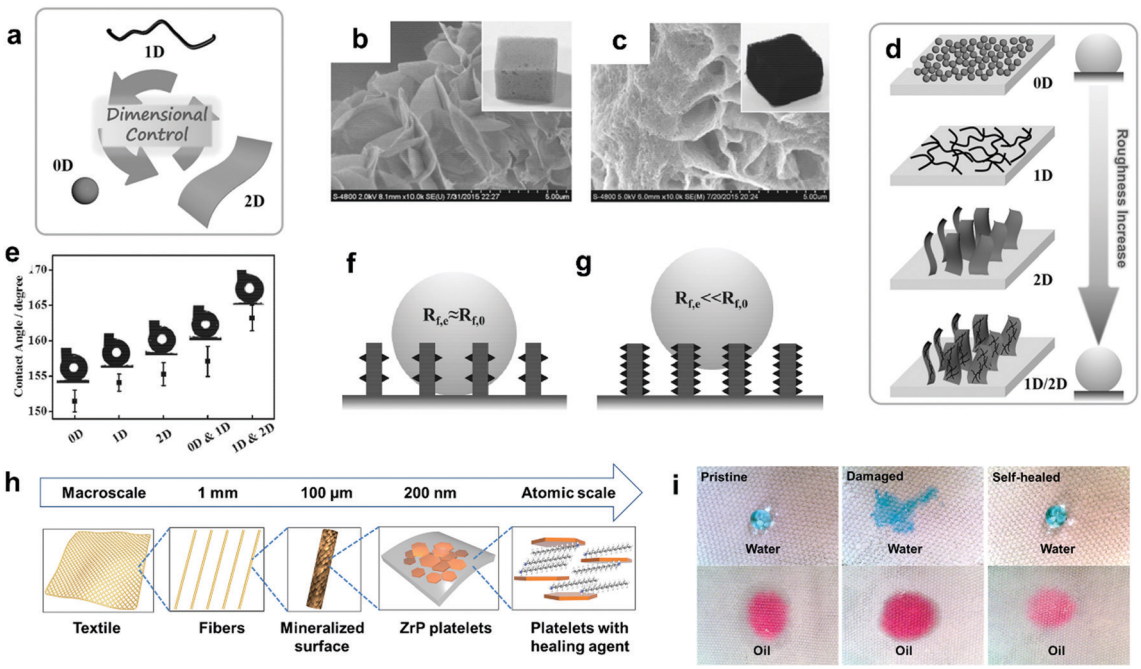

Fig. 10 Removal of oil pollutants based on hierarchical structure of 2D nanomaterials. (a) Schematic illustration of dimension control on microstructures. (b) Scanning electron microscopy (SEM) images of melamine foams with 2D particle coating. The inset shows the optical image of the coated foam. (c) SEM images and camera image (inset) of melamine foams with 1D/2D particle coating. (d) Stepwise modulation of the wettability of materials by engineering the dimension of the microstructures. (e) Water contact angles of various coated foams. (f) Water droplet possesses an effective roughness ($R_{f,e}$) close to the intrinsic surface roughness ($R_{f,0}$) on a less rough surface. (g) Effective roughness $R_{f,e}$ much smaller than $R_{f,0}$ on an extremely rough surface. Reproduced with permission.[198] Copyright 2016, Wiley-VCH. (h) Schematic illustration of hierarchical structure in ZrP-coated membrane. (i) Contact of various liquid droplets on membrane surface before and after the healing process, demonstrating self-healing behavior. Reproduced with permission.[204] Copyright 2018, the American Chemical Society.

B (RhB), methyl orange (MO), methylene blue (MB), and Congo red (CR), as shown in Fig. 11.[206] Adsorption was selective for the size, shape, and ionic strength of the dye. In addition, MoS_2 nanosheets have also been developed into adsorbent materials, which have a good adsorption capacity for various organic dyes, including MB, MG, RhB, CR and fuchsin acid.[208,209] Similar dye-adsorption behavior has been observed for other 2D nanomaterials, such as graphene-based adsorbents.[210] The dye adsorption efficiency of 2D nanomaterials typically originates from van der Waals interaction, covalent bonding, or electrostatic attraction.[208,209] Since colloidal MoS_2 typically shows a negative charge, the adsorption of cationic species on MoS_2 is much more effective than that of anionic molecules, which demonstrates the important role of electrostatic attractions.[209]

One popular strategy to preserve the high surface area of 2D sheets in devices is to integrate 2DM on a 3D framework. A 3D sponge skeleton can adhere exfoliated 2D nanoplates by van der Waals interactions.[211] Besides, a three-dimensional flower-like nanostructure of 2D MoS_2 nanosheet was successfully fabricated using a hydrothermal process.[209,212] The specific surface area of MoS_2 nanoflowers could reach above 100 $m^2\ g^{-1}$.[209] The flower structure of molybdenum selenide with a good adsorption performance could be achieved by a self-assembly hydrothermal method.[212] Hydrothermal strategies based on combining 2D nanomaterials and other functional materials are popular to prepare novel composite adsorbents. Magnetic Fe_3O_4 can be integrated with 2D nanomaterials to form heterostructures with strong adsorption capability, in which the composite can be easily recovered using a magnetic field.[213]

3.3. Heavy metal ion adsorbents

Heavy metals are toxic pollutants commonly found in industry wastewater and poorly managed water resources.[214] Some of the heavy metal ions that are known to be harmful to humans include Cd, Cr, Hg, and Pb.[215–220] Above the allowable limit,[221] cobalt will result in vomiting, nausea, asthma, and carcinoma. Thus, to remove heavy metal ions, several strategies (including optimizing surface area and enhancing bonding strength with metal ions) have been proposed to fabricate efficient 2DM-based adsorbents.

Single-layer and few-layer 2D nanomaterials have exceedingly high surface areas, which can facilitate the adsorption of heavy metals. For example, 2D TMDs (*e.g.*, MoS_2) can be utilized as high-performance adsorbents for removing several heavy metal ions such as Hg^{2+} and Ag^{+}.[49] This adsorption process often involves the Lewis soft acid and soft base interaction. For example, MoS_2 functions as an adsorbent for the removal of Hg vapour or Pb^{2+}, Cd^{2+}, Zn^{2+}, and Co^{2+} ions.[49] Non-chalcogenide 2D nanosheets can also function as effective adsorbents for the removal of heavy metals. Chengchun *et al.* prepared h-BN-based structures, including porous BN whiskers,[222] activated BN sheets,[223] and three-dimensional carbon/BN structure, for the removal of heavy metals.[224] The 2D fluorinated boron nitride nanoplates with high absorbency were demonstrated to be a capable adsorbents for heavy metal removal, and their water-cleaning capability was attributed to the surface defects and hydroxyl groups of BN.

Since many 2D nanomaterials are weakly bonded layered compounds by short range forces such as van der Waals forces, one of their unique characteristics is the possibility of fine-tuning their properties through tailoring their interlayer distance.[225] Consequently, size-selective adsorption on the interlayer porosity of 2D nanomaterials is often achievable during the decontamination process. Wang *et al.* reported the synthesis of intercalated MXenes with a controlled interlayer distance.[226] Their work showed that the larger interlayer space of hydrated $Ti_3C_2T_x$ can enhance the adsorption performance with higher selectivity of radioactive U over other elements including Co, Ni, and Zn (Fig. 12a).[226] This intercalation process of $Ti_3C_2T_x$ was confirmed by SEM analysis (Fig. 12b–d). As an example of designed framework structure, Chen *et al.* fabricated two-dimensional silicate RUB-15, which exhibited a high adsorption energy and efficient regeneration of heavy metal ions such as UO_2^{2+} ions (Fig. 12e–g).[227] Very recently, Ping's group

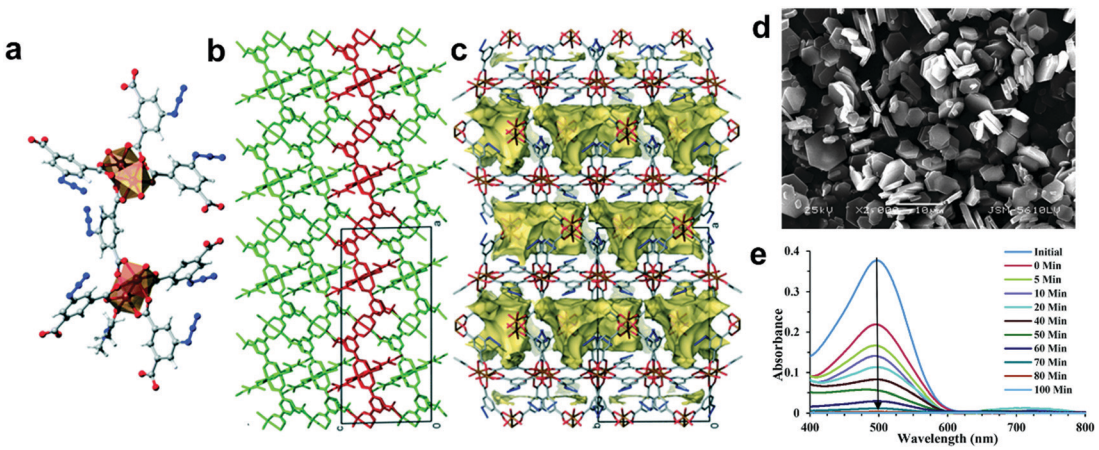

Fig. 11 Removal of hydrophilic organic pollutants by 2D nanomaterials. (a) Crystal structure of 2D MOF (Cu(II)-5N3IP). (b) 2D MOF sheets in the (001) plane. One sheet is shown in red. (c) Solvent-accessible voids in the Kagomé-type structure. (d) SEM of 2D Cu(II)-5N3IP. (e) Adsorption of Congo red (CR) using Cu(II)-5N3IP. Reproduced with permission.[206] Copyright 2018, The Royal Society of Chemistry.

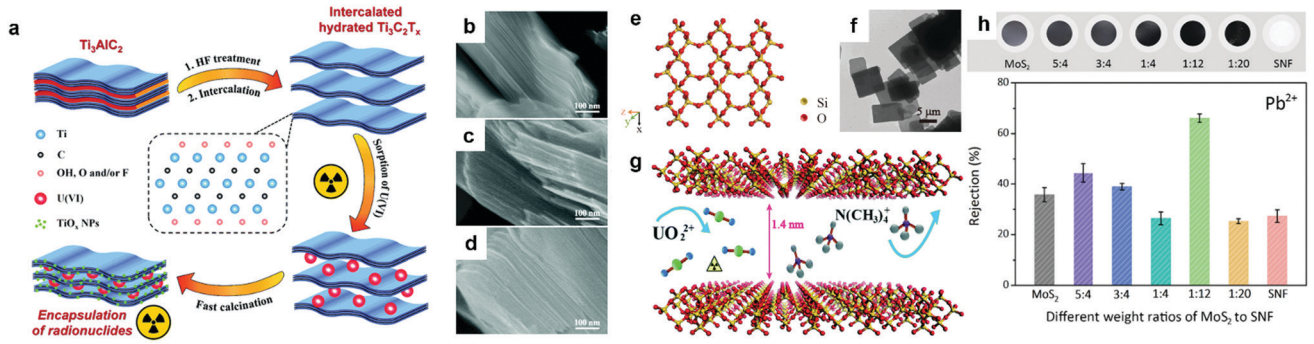

Fig. 12 Heavy metal removal by 2D nanomaterials. (a) Hydrated intercalation synthesis of $Ti_3C_2T_x$ MXene for the efficient adsorption of U(VI). SEM images of $Ti_3C_2T_x$ (b), $Ti_3C_2T_x$–NaOH (c), and $Ti_3C_2T_x$–DMSO (d). Reproduced with permission.[226] Copyright 2017, The Royal Society of Chemistry. (e) Schematic illustration of the 2D silicate RUB-15 at a plane view (110). (f) TEM image of RUB-15. (g) Capture of UO_2^{2+} ions by RUB15 through ion exchange with TMA cations. Reproduced with permission.[227] Copyright 2017, The Royal Society of Chemistry. (h) Pb^{2+} rejection efficiency of MoS_2/silk nanofibril membranes. Copyright 2017, the American Chemical Society.[228]

successfully integrated MoS_2 nanosheets with one-dimensional silk nanofibrils for the removal of heavy metal ions and dyes (Fig. 12h).[228]

In addition, natural multilayer clay-based 2D nanomaterials have exchangeable interlayer cations such as vermiculite and montmorillonite (MMT), which can be used as low-cost adsorbents for large-scale heavy metal ion removal.[230–233] In addition to vermiculite, titanate nanoplates[234] and vanadate-based layered 2D nanomaterials[235] have been demonstrated to remove toxic heavy metals. After the adsorption/intercalation process, a structural change in the thin layers due to the sorption of metal ions was observed.[234,235] To accelerate the interaction of the adsorbent and heavy metals, surfactants are commonly applied to treat 2D clays.[236] Montmorillonite was functionalized with the anionic surfactant sodium dodecyl sulfate (SDS), resulting in excellent heavy metal adsorption. During this process, MMT was first intercalated with SDS surfactant, which enables 2D nanoclays with a larger negative ζ for better heavy metal adsorption.[237]

Owing to their unique structure of pore walls and skeletons, two-dimensional COFs provide a porous framework for adsorbing heavy metal ions from the aqueous phase. Huang *et al.* synthesized an Hg^{2+} adsorbent TAPB–BMTTPA–COF using 1,3,5-tris(4-aminophenyl)benzene (TAPB) and 2,5-bis(methylthio)terephthalaldehyde (BMTTPA) (Fig. 13).[229] This framework structure includes bigger pores than many MOF systems. The methyl sulfide terminal groups have active sites to adsorb the Hg^{2+} element. This COF material could tolerate strong acids or bases, while maintaining its capability, reusability, and selectivity. Thus, these results demonstrate the huge research opportunities of COFs and other framework materials for heavy metal adsorption.

3.4. Anion and oxyanion adsorbents

Many toxic elements, including some heavy metals, exist as an oxyanion in aqueous solution, forming negative charges, and thus the electrostatic attraction of some 2DM-based adsorbents should be redesigned. Arsenic has long been regarded as a deadly poison because of its lethality, and the toxicity of As derivatives decreases from left to right in the order of (1) arsenite, (2) arsenate, (3) monomethyl arsenic acid, and (4) dimethyl arsenic acid.[205] In addition, NO_2^-/NO_3^-, F^-, and $C_2O_4^{2-}$ also have some detrimental effects at high concentration. For example, high concentrations of nitrate (NO_3^-) can cause children to develop blue infant disease.[238] Some anions such as SO_4^{2-}, PO_4^{3-}, and Cl^- in high concentrations can change the taste of water and have adverse effects. Thus, to eliminate anions and oxyanions, ion exchange, anion intercalation, and other mechanisms have been adopted for the design and development of 2DM-based adsorbents.

The large surface areas of thin 2D nanomaterials not only accelerate the adsorption kinetics, but also result in higher adsorption capacity and chemical reactivity compared to many other traditional nanomaterials. Another characteristic of layered 2D nanomaterials (such as 2D clays) is their ion exchange properties, which are related with their interlayer space. For instance, a layered double hydroxide (LDH) is a 2D clay consisting of brucite-like layers with positive charges. It has been reported that LDHs were utilized for the removal of contaminants such as PO_4^{3-},[241] F^-,[242] and an anionic herbicide.[243] The adsorption of LDHs toward anions mainly relies on their cations, and thus a high content of trivalent cations in LDHs typically leads to a good adsorption ability.[241] On the other hand, some molecules such as sodium dodecyl sulfate can also be incorporated into the LDH gap by ion exchange.[244] It has been reported that chloride ions can be embedded in LDHs to effectively remove As(v) from polluted groundwater.[245] The As(v) adsorption capacity of LDHs was about 90 mg g^{-1}, while >98% of As was eliminated from contaminated water. It was shown that the MoS_4^{2-} intercalated LDH (MoS_4-LDH) has excellent removal efficiency (>93%) of As(v) in 60 s.[246] This adsorption/intercalation of $HAsO_4^{2-}$ into LDH induced a decrease in the interlayer distance of MoS_4-LDH.

Furthermore, the efficient removal of As(III) on Fe(III) modified montmorillonite was reported for anion removal.[239] As shown in Fig. 14a, the authors employed a low-temperature clay intercalation approach using $FeCl_3$ followed

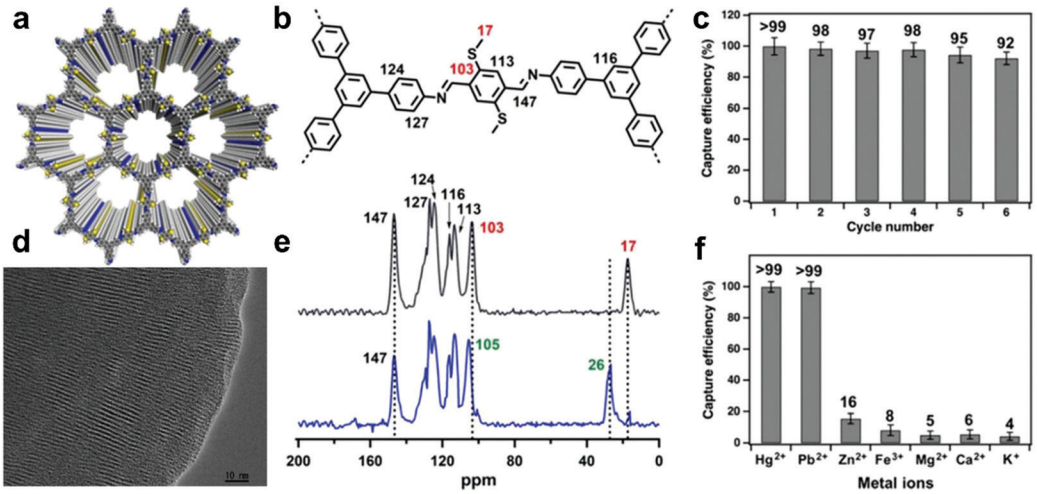

Fig. 13 2D COF for heavy metal removal. (a) Top side views of 1,3,5-tris(4-aminophenyl)benzene (TAPB)–2,5-bis(methylthio)terephthalaldehyde (BMTTPA) COF with mesoporous channels. (b) Chemical structure of TAPB–BMTTPA–COF. (c) Cycle performance of COF on Hg^{2+} removal. (d) TEM image of TAPB–BMTTPA–COF. (e) ^{13}C NMR spectra of pristine (black curve) and Hg^{2+}-adsorbed TAPB–BMTTPA–COF (blue curve). (f) Capture efficiency of various metals. Reproduced with permission.[229] Copyright 2017, the American Chemical Society.

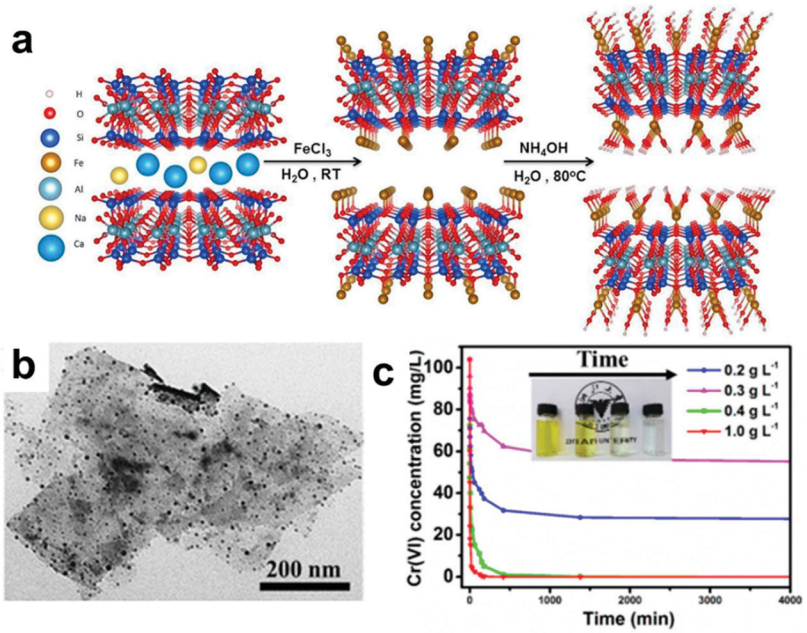

Fig. 14 2D nanoadsorbents for inorganic anion removal. (a) Schematic illustration of the modification of MMT with iron(III) species. Reproduced with permission.[239] Copyright 2018, Elsevier B.V. (b) TEM image of functionalized $Ti_3C_2T_x$ nanosheets after exfoliation. (c) Dosage effect of functionalized $Ti_3C_2T_x$ nanosheets on the removal of Cr(VI) (pH = 5). Inset is a photograph showing the change in colour in the case of 0.4 g L^{-1} MXene nanosheets. Reproduced with permission.[240] Copyright 2015, the American Chemical Society.

by treatment of NH_4OH solution. This nanoclay adsorbent showed a fast arsenite removal with 55% of As(III) removed within 30 s. Recently, two-dimensional MOFs (*e.g.*, FIR-53) with abundant nanotubular channels were used for the removal of $Cr_2O_7^{2-}$, in which FIR-53 presented quick adsorption kinetics, high regeneration ability, and high selectivity for $Cr_2O_7^{2-}$ over Cl^-, Br^-, and NO_3^- ions.[247] However, the selectivity showed a decrease upon the introduction of coexisting ions. It is noteworthy that some 2DM adsorbents were found to be effective to remove same-charged ions. For example, in addition to their good adsorption performance for cations, 2D MXene ($Ti_3C_2T_x$) nanosheets also exhibited excellent removal capacity for anions $Cr_2O_7^{2-}$ (Fig. 14b and c).[240] The XPS study demonstrated that Cr(VI) ions were reduced when adsorbed on the surface of $Ti_3C_2T_x$. This is likely due to the metallic property of MXene and high oxidative capability of $Cr_2O_7^{2-}$. Additional examples of 2DM-based adsorbents can be found in Table 2.

Table 2 Various 2DM-based adsorbents for water treatment

Pollutant	Composite	Synthesis	Time	Removing capability	Ref.
Pb(II)	GO/poly(*N*-vinylcarbazole)	Sonication mixing	24 h	887.98 mg g^{-1}	248
Pb(II)	MXene ($Ti_3C_2T_x$)	Chemical etching	2 h	~30 mg g^{-1}	249
Pb(II)	GO/modified silica	Multi-step method	24 h	333 mg g^{-1}	250
Pb(II)	MoS_2/CeO_2/biochar	Pyrolysis	24 h	263.6 mg g^{-1}	251
Cd(II)	GO/polyamidoamine	Grafting method	360 min	253.81 mg g^{-1}	252
Cu(II)	GO/chitosan	Electrostatic self-assembly	90 min	425 mg g^{-1}	253
As(III)	GO/$MnFe_2O_4$	*In situ* growth	120 min	146 mg g^{-1}	254
U(VI)	GO/amino siloxane oligomer	Cross-linking reaction	30 min	310.6 mg g^{-1}	255
Cr(VI)	rGO/NiO	*In situ* growth	—	198 mg g^{-1}	256
RhB	MoS_2-glue sponge	Dip-coating method	60 min	127.39 mg g^{-1}	257
Rh6G	MoS_2/CuS	Hydrothermal method	240 min	211.18 mg g^{-1}	258
Methylene blue	1T-WS_2	Hydrothermal method	2 min	210.2 mg g^{-1}	259
Pump oil	Polyimide/MXene	Freeze dry	30 min	5.8 g g^{-1}	260

In addition to the judicious design of surface interactions within the aqueous phase, the colloidal stability of 2DM-based adsorbents is important to prevent the aggregation of 2D nanomaterials, which inevitably will reduce their effective surface area for adsorption. When colloidal 2D nanomaterials are dispersed in water, the Derjaguin–Landau–Verwey–Overbeek (DLVO) theory can provide useful information on the trend of nanoparticle aggregation.[51] According to the DLVO theory, the design of electrostatic repulsion and van der Waals attraction may lead to excellent colloidal stability of 2D nanomaterials in water, maintaining the effective adsorption of aqueous pollutants during the contact time. Similar to aggregation, gravity can also negatively impact the colloidal stability of 2DM nano-adsorbents due to the sedimentation ($\rho_{particle} > \rho_{water}$) or creaming effect ($\rho_{particle} < \rho_{water}$). For a spherical particle, the terminal sedimentation (creaming) velocity, U_0, can be estimated using Stokes' law, in which U_0 is related to the particle size, density, gravity force, and solvent viscosity.[51,261]

$$U_0 = \frac{D^2 \cdot \Delta\rho \cdot g}{18\mu}$$

where D is the particle diameter, and μ, g, and $\Delta\rho$ represent the viscosity, gravity constant, and density difference between the solution and particles, respectively.

In pursuit of developing high-performance 2DM adsorbents, the terminal sedimentation rate needs to be prudently considered since fast sedimentation leads to the removal of adsorbents before effective decontamination, while ultra-slow sedimentation may increase the recovery cost in separating used adsorbents from water. More importantly, the judicious design of the dimensions of nano-adsorbents and comprehensive understanding of their nanosheet behaviour in colloidal dispersions can be crucial for the practical application of pollutant adsorbents in lakes and offshore conditions, where homogeneous stirring is often inaccessible. Overall, considering the broad chemical and physical diversity of 2D nanomaterials, more research is needed for the understanding of their molecular levels and adjustment of their surface chemistry to precisely control their adsorption behaviour.

4. Photocatalytic wastewater treatment with 2D nanomaterials

To solve environmental issues with minimal energy input, photocatalysis using solar energy to clean water has been researched broadly and considered as one of the most sustainable approaches.[262–264] Generally, photocatalysis involves one or several photo-reaction processes catalysed by a photocatalyst, where free electrons are excited to the conduction band (CB) and holes are left in the valence band (VB). These electron–hole pairs play an important role in photocatalytic applications, including water splitting, pollutant degradation, and carbon dioxide reduction.[265,266] However, the excited photogenerated charge carriers are not stable and easily recombine, which reduces the conversion efficiency of photocatalysis.[264] Due to the unique structures of 2D nanomaterials and their nanocomposites, 2DM-based photocatalysts are encouraging candidates to provide signature features such as diverse host–guest species, abundant surface-active sites, and high specific surface areas.[267] Recently, several 2DM-based photocatalysts, including graphene, carbon nitride, metal oxide and chalcogenide nanosheets, have been investigated for various applications. According to the pollutant type, the application of 2DM-based photocatalysts can be mainly divided into three main categories: biological disinfection, organic decontamination, and inorganic pollutant removal. The nanosheet size/thickness, chemical structure, and edge morphologies of 2D nanomaterials are important for applying these materials in photocatalytic processes. Here, we consider the synthetic strategies of 2DM-based photocatalysts and critically evaluate their performance in the above categories. Other efficient catalyst systems (*e.g.*, electrocatalysts) have been developed for water treatment, and details can be found in recent topical reviews.[268–274] Table 3 presents several recent examples of 2DM-based photocatalysts for water treatment.

4.1. Photocatalysts for bio-disinfection

Virus and bacteria are pathogens that can cause diseases and threaten human life. Water pollution due to these pathogens is a common phenomenon in some developing countries, and thus the decontamination of water is paramount. By using

Table 3 Various 2DM-based photocatalysts for water treatment

Pollutant	Photocatalyst	Synthesis	Design	Photocatalytic conditions
Formaldehyde	TiO_2/graphene composites	Solvothermal method	0D/2D	UV light in air[275]
Methylene blue	ZnO/rGO	Ultrasonic treatment	0D/2D	UV light irradiation[276]
Methylene blue	CdSe/TiO_2	Hydrothermal method	0D/2D	Visible light irradiation[277]
Rhodamine B	Carbon quantum dots/TiO_2 nanosheet	Assembly method	0D/2D	Visible light irradiation[278]
Rhodamine B	TiO_2 nanorod/SnS_2 nanosheet	Hydrothermal method	1D/2D	UV and visible light irradiation[279]
Methyl orange	Ag_2CO_3/g-C_3N_4 nanosheets	*Ex situ* assembly	0D/2D	visible light irradiation[280]
Methyl orange	$Bi_4Ti_3O_{12}$ nanofiber/BiOCl nanosheet	Electrospinning and solvothermal	1D/2D	Xenon lamp Irradiation[281]
Methyl orange	Copper doped SnS_2 nanosheet/rGO	Cysteine-assisted hydrothermal	2D/2D	Visible light irradiation[282]
Cr(VI)	CdS/rGO	Microwave	0D/2D	Visible light irradiation[283]
Cr(VI)	g-C_3N_4/N-doped graphene/MoS_2	Multi-step method	2D/2D	Visible light irradiation[284]
NH_3	WS_2/MoS_2	Liquid exfoliation	2D/2D	Visible light irradiation[285]
CO_2	TiO_2 nanosheets and graphene	Layer-by-layer assembly	2D/2D	Xenon lamp Irradiation[286]
Bacteria (*E. coli*)	AgBr/g-C_3N_4	Adsorption–deposition method	0D/2D	Visible light irradiation[287]
Bacteria (*E. coli*)	Ag/ZnO/g-C_3N_4	Adsorption–deposition method	0D/2D	Visible light irradiation[288]
Bacteria (*S. aureus*)	MnO_2/g-C_3N_4	Multi-step method	2D/2D	Visible light irradiation[289]
Virus (bacteriophage MS2)	Ag/MoS_2	Multi-step method	0D/2D	Low-power LED[290]

strategies such as bandgap engineering and nanocompositing, several 2D nanosystems have been investigated and developed for the removal of these contaminants from water.[287–290] During a typical photocatalytic process, the photo-exited charge carriers help to generate reactive oxygen species (ROS), which can deactivate bacteria (Fig. 15a and b).[291] For example, as an extension of conventional TiO_2 photocatalysts, TiO_2–Bi_2WO_6 nanosheets (TBWO) were synthesized by Jia *et al.* using a two-step hydrothermal method. Bi_2WO_6 was grafted on the surfaces of TiO_2, which has the ability to absorb visible light. Therefore, TBWO could induce the cell rupture and inactivate *E. coli* due to visible-light-driven photocatalysis.[292] Liu *et al.* fabricated a novel MoS_2 (FLV-MoS_2) film by vertically aligning several layers of 2D platelets, which could absorb the whole spectrum range of visible light (which contains about 50% of solar energy) in the water disinfection process (Fig. 15c–e).[42] To increase the bandgap of MoS_2, the domain size was decreased. The results showed that the bandgap increased from 1.3 to 1.5 eV, which enabled FLV-MoS_2 to inactivate bacteria in water by generating reactive oxygen species (ROS), enabling the deactivation of >99.999% bacteria in 20 min. In addition to metal oxides and dichalcogenides, a metal-free 2D g-C_3N_4 nanosheet photocatalyst was developed *via* a two-step template-free method (Fig. 15f–k).[293] This porous g-C_3N_4 nanosheet possessed

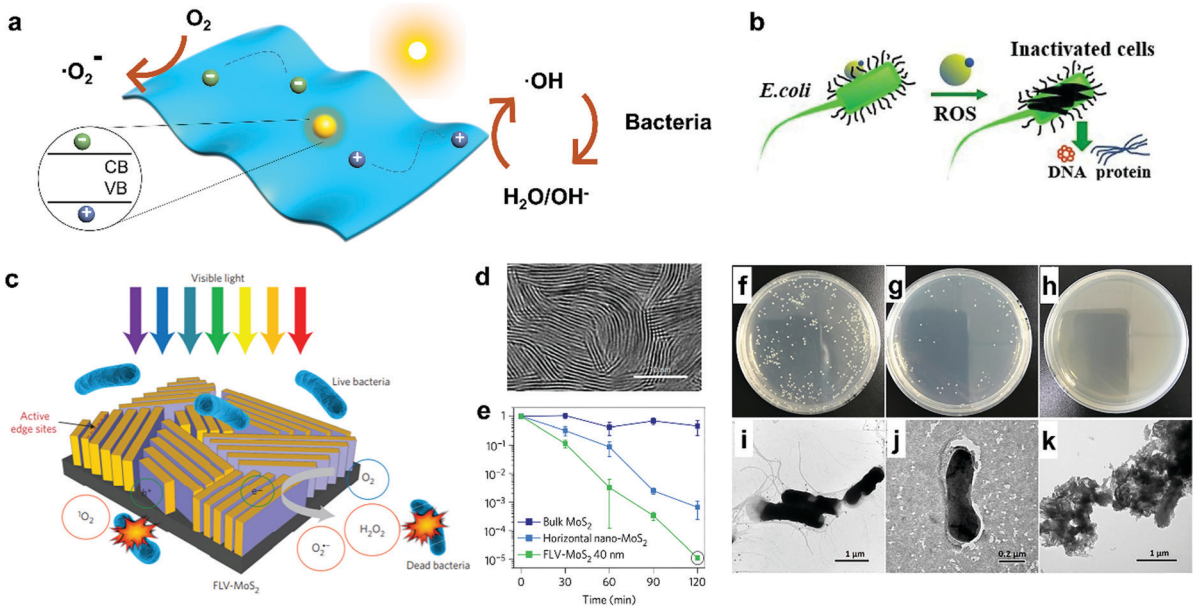

Fig. 15 Photocatalysts based on 2D nanomaterials for the removal of bacteria. (a) Simplified schematic showing the photocatalytic process of 2DM photocatalysts. (b) Examples of the antibacterial mechanism of Ag/ZnO photocatalyst. Reproduced with permission.[291] Copyright 2017, Elsevier B.V. (c) Schematic illustration of bacteria deactivation by FLV-MoS_2 in water. (d) TEM image of FLV-MoS_2 showing the vertically standing layers. (e) Disinfection performances of FLV-MoS_2 compared with that of bulk MoS_2 and horizontal nano-MoS_2. (c–e) Reproduced with permission.[42] Copyright 2016, Springer Nature. Photos and TEM images of *E. coli* before (f and i) and after photocatalysis for 2 h (g and j) and for 4 h (h and k) using porous g-C_3N_4 nanosheets. (f–k) Reproduced with permission.[293] Copyright 2017, the American Chemical Society.

abundant surface reactive sites and better capability of charge transfer than the bulk g-C_3N_4. Therefore, the performance of organic pollutant degradation and visible-light-driven photocatalytic disinfection of the nanosheets were significantly improved. The unexfoliated g-C_3N_4 could only inactivate some *E. coli* within 4 h, whereas the g-C_3N_4 nanosheet could inactivate all the *E. coli* cells completely, confirming the advantage of bandgap engineering based on the dimension-control method.[293]

Compared with bacteria, viruses have been regarded as more dangerous pathogens due to their higher illness risk and lower infectious dose under a similar level of exposure.[294] For example, exposure to one rotavirus particle can increase the chance of infection by up to 31%.[295] In addition, viruses possess extremely small sizes and unique surface properties, and thus physical removal methods are often unavailable. For example, in water treatment, granular activated carbon adsorption was reported to be effective in removing protozoan parasites and bacteria, but not viruses.[296] To deactivate viruses *via* photocatalysis, extensive efforts have also been made using a variety of 2D nanomaterials. Li *et al.* evaluated the virucidal performance and mechanism of g-C_3N_4.[297] During the photocatalysis, the authors found that a shape distortion, protein oxidation, and RNA damage occurred, leading to virus death (Fig. 16a–d). The virus inactivation performance of g-C_3N_4 was also comparatively analysed with other visible-light-driven photocatalysts, namely TiO_2, Bi_2WO_6 and Ag@AgCl, indicating that surface plasmon resonance and dissolved Ag^+ of Ag nanoparticles may further improve the performance (Fig. 16e and f). Inspired by the discovery of the photocatalytic reduction of GO to rGO by WO_3,[298–300] Akhavan *et al.* added GO nanosheets to WO_3 films to construct rGO–WO_3

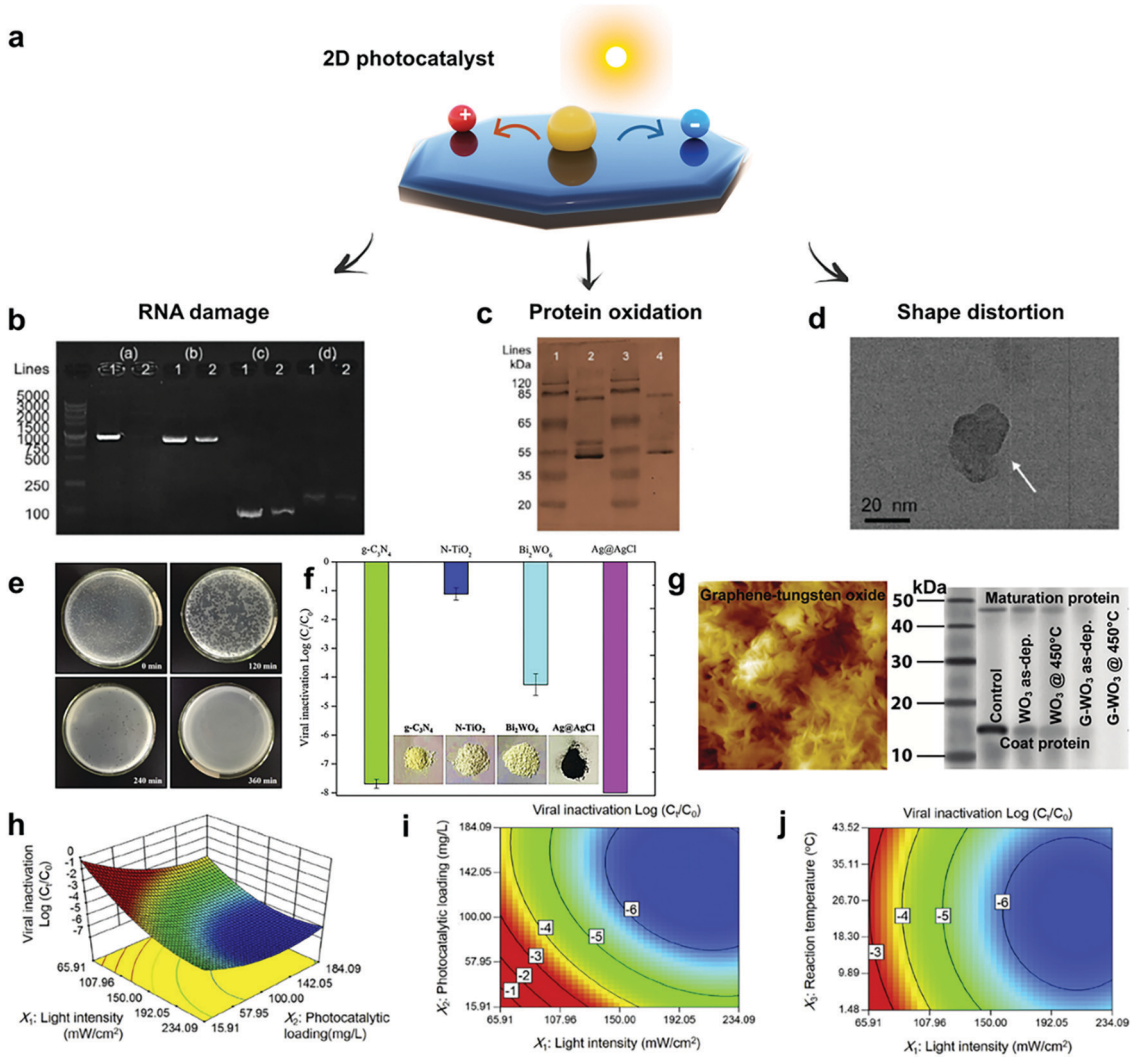

Fig. 16 Photocatalysts based on 2D nanomaterials for virus removal. (a) Main mechanisms of virus disinfection by 2D photocatalysts, including RNA damage (b), protein oxidation (c), and shape distortion (d). (e) g-C_3N_4 photocatalyst for viral disinfection under visible light. (f) Virucidal performance of g-C_3N_4 compared with other nanomaterials. (b–f) Reproduced with permission.[297] Copyright 2016, Elsevier B.V. (g) Virucidal performance of graphene–WO_3 composites. Reproduced with permission.[301] Copyright 2012, the American Chemical Society. (h) 3D response surface and (i) 2D contour plots of viral disinfection with light intensity (X_1) and g-C_3N_4 loading (X_2). (j) 2D contour plots of inactivation efficiency with light intensity (X_1) and temperature (X_3). (h–j) Reproduced with permission.[302] Copyright 2018, Elsevier B.V.

films, in which the composite film was shown to decrease the virus concentration from 2×10^6 PFU mL^{-1} to <5 PFU mL^{-1} within 3 h under visible-light irradiation (Fig. 16g).[301] To accelerate the disinfection process, Zhang *et al.* used the response surface methodology to optimize the operational conditions for photocatalysis.[302] The optimal conditions of 135.40 mg L^{-1} (photocatalyst), 24.05 °C and 199.80 mW cm^{-2} (light power), were obtained with the disinfection time of 240 min (Fig. 16h–j). Bio-disinfection of 2DM by other mechanisms such as the photothermal effect and Fenton reaction can be found in another recent review.[303]

4.2. Photocatalysts for removing organic pollutants

Compared with bio-disinfection, which only requires the deactivation of cell or proteins, removing organic pollutants requires the formation of sufficient reactive oxygen species that can destroy or mineralize organic contaminants completely.[304] To develop an effective photocatalyst, the band structures of 2DM need to be carefully designed since they play a crucial role in the redox potentials of photogenerated electron–hole pairs.[305] Compared with bulk 2D materials (Fig. 17a), monolayer or few-layer 2D nanoparticles (such as MoS_2) possess a larger bandgap to shift the band edge position to generate a redox potential, which favours ROS, even though the photocatalysis of these nanosheets sometimes only uses a narrow range of the solar spectrum.[49] Thus, to develop photocatalysts that utilize light in the desired wavelength range, several strategies, such as heterostructuring, element doping, and size control, have been utilized to modulate the band structure of 2D nanosheets.[306] To date, 0D nanoparticles and 1D nanorods/nanowires/nanotubes have been composited with 2D nanomaterials.[281,307–313] For example, some 2DM-based composites have been achieved by incorporating metal-containing nanoparticles, such as Pt,[310] RuO_2,[314] Au,[315] $Rh(OH)_3$,[316] into the space between the layers of metal oxide nanosheets. Recently, a new method that can intercalate metal nanoclusters, such as Pt, Pd, Rh, and Ru, into $KCa_2Nb_3O_{10}$ nanosheets, was reported by Oshima *et al.*[317] The prepared colloidal $KCa_2Nb_3O_{10}$ nanosheets with intercalating Pt exhibited a high photocatalytic performance due to the co-catalysts of the well-dispersed Pt nanocluster between the 2D layers.

Compared with 0D/2D and 1D/2D nanocomposites, 2D/2D heterostructures have unique coupling hetero-interfaces, facilitating the separation and transfer of photogenerated charge carriers, thereby leading to higher photocatalytic activity. Numerous studies have indicated that the properties of catalysts can be modulated by controlling the morphology and size of the semiconducting component in hybrid systems. For example, a systematic comparison study between 1D CNT–TiO_2 composite photocatalysts and 2D graphene–TiO_2 was conducted by Zhang *et al.*[318] The interfacial contact of graphene–TiO_2 sheets was shown to be superior in comparison with that of the CNT–TiO_2 heterostructure.[318] Yang *et al.* reported a comparative study of a TiO_2 photocatalyst, where

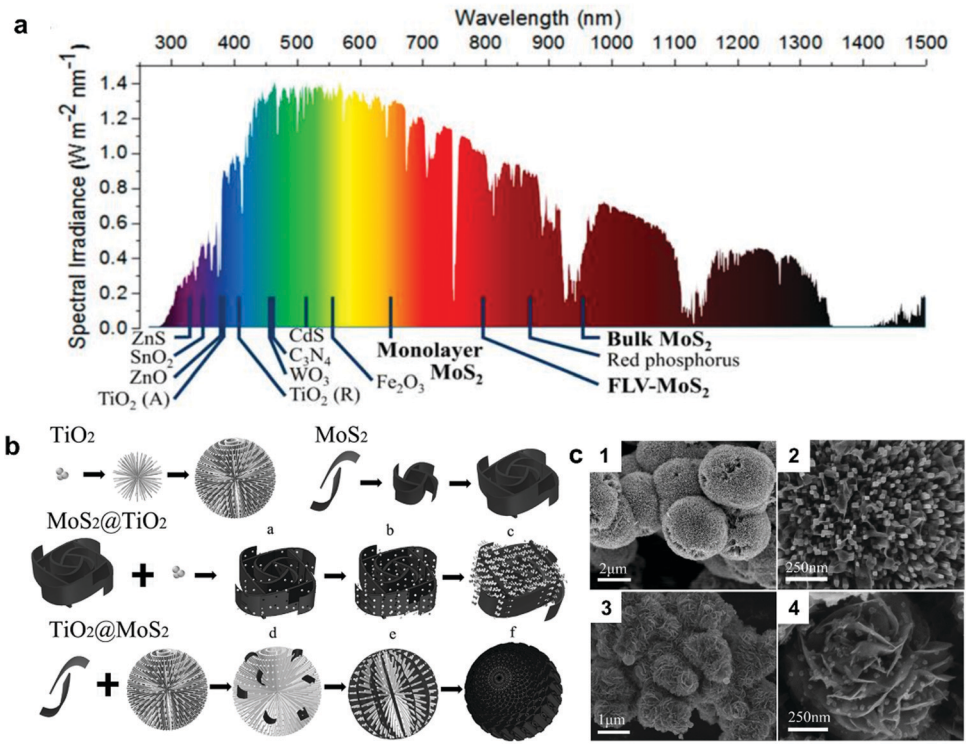

Fig. 17 Photocatalysts based on 2D nanomaterials for the removal of organic pollutants. (a) Adsorption spectra of various materials compared with sunlight spectrum. Reproduced with permission.[49] Copyright 2017, the American Chemical Society. (b) Schematic diagram of the growth mechanisms of hybrid nanocomposites. The black and silver colors represent MoS_2 and TiO_2, respectively. (c) SEM images of hybrid 2D composites of TiO_2@MoS_2 (1 and 2) and MoS_2@TiO_2 (3 and 4). (b and c) Reproduced with permission.[322] Copyright 2015, The Royal Society of Chemistry.

TiO_2–graphene, TiO_2–carbon nanotube, and TiO_2–fullerene (C_{60}) nanocomposite photocatalysts were prepared.[319] The authors found that the three types of TiO_2–carbon photocatalysts followed an analogous oxidation mechanism for the photocatalytic oxidation of benzyl alcohol. In addition, a graphene-based nanocomposite with different shapes of TiO_2 nanomaterials, including TiO_2 nanosheets, nanotubes, and nanoparticles, was developed.[320] It was discovered that compared with the other two composites, the TiO_2 nanosheet–rGO heterostructure possessed better photocatalytic performance for the degradation of 2,4-dichlorophenol and RhB. Through the analysis of the interfacial charge transfer kinetics, the 2D/2D hybrid structure was demonstrated to possess strong electronic coupling effects. The coupling effects can promote charge transfer across the interface of heterojunction, and thereby enhance the photocatalytic performance. Similar results were also obtained for graphene–CdS composite systems, including the graphene oxide–CdS (the shapes include nanoparticle, nanorod, and nanosheet) composites prepared by Bera *et al.*[321] It was shown that the pollutant degradation by the composites varied upon engineering the shape of the CdS nanocrystals. The CdS nanosheet/rGO heterostructure showed the highest photocatalytic result compared with CdS nanoparticle/rGO and CdS nanorod/rGO.

In pursuit of an optimized heterostructure, Fu *et al.* constructed two types of MoS_2/titania heterostructures (Fig. 17b), *i.e.*, MoS_2@TiO_2 and TiO_2@MoS_2.[322] The successful synthesis of these two nanocomposites was confirmed using SEM (Fig. 17c). The authors observed that TiO_2@MoS_2 exhibited a higher photocatalytic performance and better adsorption ability, which is primarily because of the large percentage of highly reactive (001) planes of TiO_2 nanorods and the formation of heterojunctions. Meanwhile, MoS_2@TiO_2 exhibited a better performance in field emission due to the wide distribution of TiO_2 nanoparticles, which led to sharp edges for emitting. Recently, the 1T and 2H phases of MoS_2 were chemically exfoliated successfully by Bai and co-workers, which were used to form a co-catalyst with TiO_2 nanocrystals.[323] Their results indicated that the photocatalytic activity of the 1T phase of MoS_2 is better than that of the 2H phase. The excellent performance of the 1T phase of MoS_2 originates from the higher conductivity of this metallic phase, which promotes the charge transfer kinetics. The authors suggested that the 1T-phase MoS_2 not only provides a high-mobility electron transfer path, but also possesses more reaction active sites on its basal plane.

In the context of the effective degradation of organic pollutants, oxidative species (*e.g.* H_2O_2) have been incorporated in the photocatalytic process to further improve the oxidation processes. For example, photo-Fenton systems, which contain hydrogen peroxide and Fe species, have been extensively studied. There are reports presenting that H_2O_2 can react with dissolved Fe species rapidly and the generated reactive hydroxyl radicals can oxidize organic compounds.[324–327] Yoon *et al.* combined the photo-Fenton system with traditional photocatalytic reaction, developing an innovative Fe-doped C_3N_4/WO_3 hybrid structure (Fig. 18a).[328] The authors found that compared with the pristine g-C_3N_4 sample, the hybrid structure enabled an improved efficiency from 10% to 90% using visible-light irradiation. The mechanism was studied using electron paramagnetic resonance analysis (Fig. 18b). Compared to the Fe(III) counterpart, the Fe(II)-doped sample exhibited a higher initial catalytic activity, as suggested by the cyclic mechanism of [$Fe^{2+} + H_2O_2 \rightarrow Fe^{3+} + OH^- + OH^{\bullet}$].[329,330] The Fe(II) concentration can be supplemented by the reduction of Fe(III) under visible-light irradiation.[324,331] As another example, Lin *et al.* developed iron-doped graphitic C_3N_4 (Fc-CN) *via* the Schiff base reaction of ferrocene (Fc) and C_3N_4 (Fig. 18c).[332] The results showed that the charge transfer/separation and the reaction of reversible photo-redox were significantly improved, which is due to the strong π conjugation between the aromatic C_3N_4 and Fc. Compared with C_3N_4, the obtained composited Fc-C_3N_4 showed considerably higher catalytic activity in activating hydrogen peroxide for the degradation of RhB (Fig. 18d and e). The photogenerated electrons from C_3N_4 can keep the bivalence state of Fe species in Fc effectively, which also leads to the activation of hydrogen peroxide.

4.3. Photocatalysts for the removal of inorganic pollutants

Some inorganic pollutants can be converted into less toxic or nontoxic forms by oxidative or reductive photocatalysis. These processes may involve the oxidation of NH_3 to N_2, H_2S to S, and the reduction of Cr(VI) to Cr(III). Prakash *et al.* (Fig. 19a) fabricated In_2S_3/CuS nanosheets, which photocatalytically converted toxic H_2S into nontoxic $S_2O_3^{2-}$ with the production of H_2.[333] Monolayer g-C_3N_4 was reported to have a good photocatalytic performance for the removal of total ammonia nitrogen (TAN) from contaminated water.[334] The oxidation of ammonia can thermodynamically proceed on g-C_3N_4 since the corresponding redox levels of ammonia are fully covered by the bandgap range of g-C_3N_4 (Fig. 19b). More importantly, the photocatalytic performance of the exfoliated g-C_3N_4 was noticeably better than that of the bulk g-C_3N_4 (Fig. 19c). As another example, flower-like MoS_2 was obtained *via* a hydrothermal method followed by further compositing with polyaniline (PANI).[335] The authors demonstrated a maximum capacity for the removal of Cr(VI) of up to ~600 mg g^{-1} under UV irradiation. This can be explained by the photocatalytic reduction of Cr(VI) to Cr(III), and following complexation with PANI. Deng *et al.* studied the photocatalytic oxidation of 2,4-dichlorophenol (2,4-DCP) and reduction of Cr(VI) simultaneously by doping phosphorus into porous g-C_3N_4 nanosheets (Fig. 19d–g).[336] The results showed the 2,4-DCP oxidation and Cr(VI) reduction can be enhanced by dissolved oxygen and low pH value. The photocatalytic efficiency for the 2,4-DCP oxidation and Cr(VI) reduction reached 90% and 75%, respectively, and no notable reduction in photocatalytic activity was observed in 5 cycling experiments.

To apply photocatalysts in the decontamination of pollutants in rivers, lakes, and oceans, the photocatalytic performance of nanomaterials in unstirred or weakly stirred conditions is of great importance for practical implementation.[337] Particle aggregation can occur due to the lack of photostability.[338]

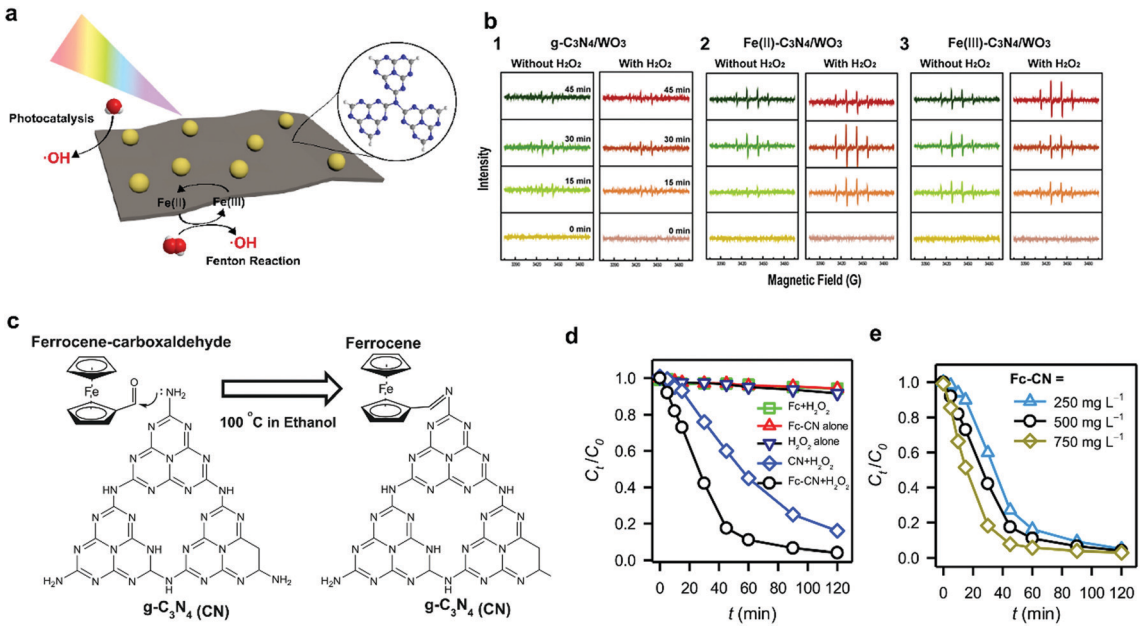

Fig. 18 Photocatalysts based on 2D nanomaterials by bandgap engineering. (a) Illustration of the photo-Fenton reaction on the 0D/2D hybrid photocatalyst with WO_3 nanoparticles on C_3N_4 nanosheets. (b) Electron paramagnetic resonance (EPR) spectra of hydroxyl radicals trapped by dimethylpyrroline-*N*-oxide (DMPO). Results obtained with (1) C_3N_4/WO_3, (2) $Fe_{(II)}–C_3N_4/WO_3$ and (3) $Fe_{(III)}–C_3N_4/WO_3$ under visible light illumination. (a and b) Reproduced with permission.[328] Copyright 2017, Elsevier B.V. (c) Scheme for the synthesis of ferrocene-functionalized C_3N_4 (Fc-CN). (d) Degradation of RhB under various conditions. (e) Fc-CN dosage effect on decontamination performance. (c–e) Reproduced with permission.[332] Copyright 2017, Elsevier B.V.

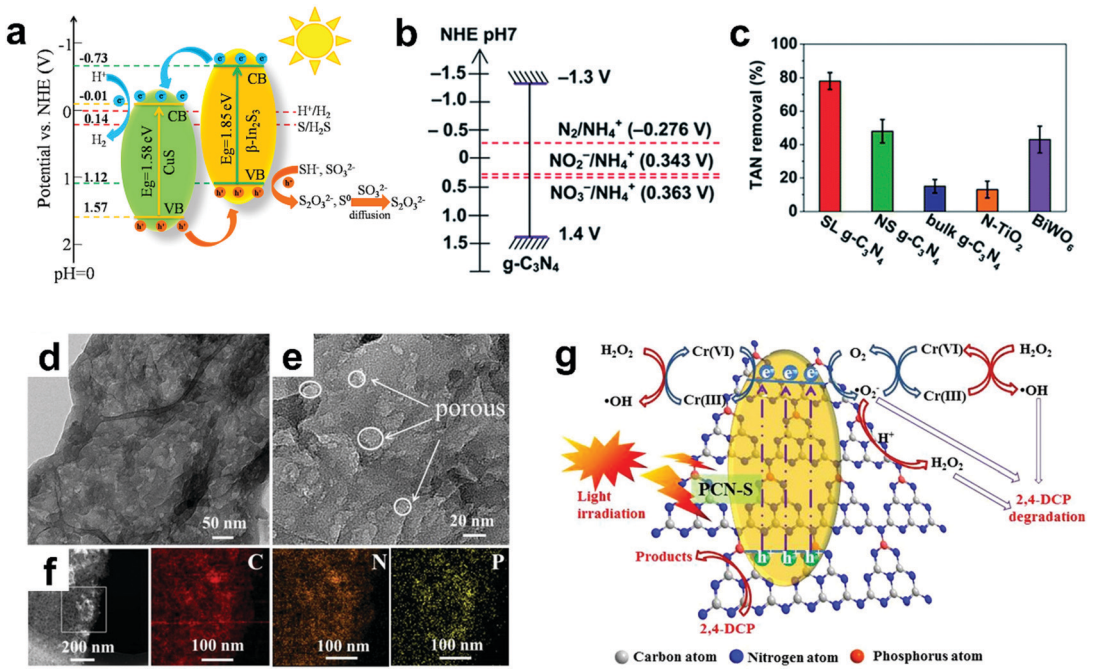

Fig. 19 Photocatalysts based on 2D nanomaterials for the removal of inorganic pollutants. (a) Photocatalytic degradation of H_2S by In_2S_3/CuS composites under visible light irradiation. Reproduced with permission.[333] Copyright 2018, Elsevier B.V. (b) Illustration of the band structure of g-C_3N_4 with redox levels for ammonia oxidation. (c) Comparison of the photocatalytic performance of samples of single-layer g-C_3N_4 (SL g-C_3N_4), g-C_3N_4 nanosheets (NS g-C_3N_4), bulk g-C_3N_4, N-doped TiO_2 (N-TiO_2), and Bi_2WO_6 for pollutant removal under Xe lamp irradiation. (b and c) Reproduced with permission.[334] Copyright 2014, the American Chemical Society. (d) Low- and (e) high-resolution of TEM images of P-doped C_3N_4 nanosheets (PCN-S), and (f) STEM of PCN-S and corresponding elemental mapping. (g) Schematic illustration of the simultaneous removal of $Cr_{(VI)}$ and 2,4-DCP using PCN-S photocatalyst. (d–g) Reproduced with permission.[336] Copyright 2017, Elsevier B.V.

During photocatalysis, oxidation and the subsequent desorption of ligands (*e.g.*, thiols) lead to a reduction in steric stabilization. In addition, electrostatic repulsion can decrease when the surface charge of a photocatalyst diminishes or the charged solute is depleted. The uncontrolled aggregation seriously reduces the effective surface area of photocatalysts. As discussed in Section 3.4 (Stokes' law), the terminal sedimentation rate is proportional to the square of the particle diameter, and thus uncontrolled aggregation leads to the fast removal of the photocatalyst from wastewater. This undesired aggregation may be mitigated by stirring the reaction mixture; however, the stirring of a lake may not be accessible in practice. Thus, to alleviate the detrimental effect of uncontrolled aggregation, judicious design of particle interaction, surface engineering of photocatalysts, and prudent selection of ligands have emerged as promising approaches.[41,48] For example, self-assembly or controlled aggregation, as opposed to uncontrolled aggregation, may be beneficial for photocatalysis.[339] In fact, the charge hopping among self-assembled nanoparticles alleviates the fast charge recombination. Park *et al.* demonstrated the improved photocatalytic reduction of Cr(VI) to Cr(III) by the controlled assembly of dye/TiO_2 with bare TiO_2.[340] As another example, CdSe/CdS quantum dots were self-assembled with a Pt co-catalyst, leading to significantly improved electron transfer between particles with a good internal quantum efficiency of 65%.[341]

5. Water pollutant sensors with 2D nanomaterials

The accurate, sensitive, and rapid detection of pollutants is crucial in water treatment processes since it quantitatively determines the effectiveness of water decontamination. A large number of nanomaterials have been investigated for detecting and monitoring pollutants in water.[342–344] Noteworthily, the ability of 2D nanomaterials to respond to external stimuli with ultrahigh surface sensitivity reveals key characteristics for water monitoring and pollutant sensing. Recently, 2D nanomaterials with remarkable optical/electrical properties have attracted tremendous interest for the development of high-performance pollutant sensors. Depending on the type of analyte, non-covalent interactions (*e.g.*, electrostatic force) and covalent linkages (*e.g.*, amide bonding) can be used to probe pollutants. In this section, we focus on the state-of-art of 2DM-based sensors for monitoring water pollutants by electrical[345–361] or optical outputs.[362–373] Specifically, fluorescent sensors, colorimetric sensors, electrochemical sensors, and field-effect-transistor-based sensors are highlighted, while several recent examples of these sensors are shown in Table 4.

5.1. Fluorescent sensors

Fluorescent sensors or photoluminescent sensors are based on pollutant-induced changes in fluorescence (intensity, wavelength, and lifetime).[385] These changes in light intensity or wavelength originate from the structure/composition alteration of the sensor upon binding of the pollutant. Since photoluminescence is related to energy transfer processes, the electronic bandgap structure of 2D nanomaterials is a crucial factor for the development of fluorescent sensors. As shown in Fig. 20a, 2D nanomaterials, ranging from large bandgap g-C_3N_4 (Fig. 20b and c) to ~zero bandgap graphene, have offered enormous opportunities in the field of sensing with a wide range of bandgap options.[51,386]

For some 2D nanomaterials with bandgaps in the UV-vis range, they can be used as fluorescent sensors directly or combined with other materials to form functional composites. For example, Rong *et al.* reported a fluorescence sensor for the label-free and selective detection of Cr(VI) based on g-C_3N_4 nanosheets (Fig. 20g).[387] With a low limit of detection (0.15 μM) and large linear sensing range (0.6 to 300 μM), the g-C_3N_4 dispersion showed an "on–off–on" fluorescence response by using a redox reaction between ascorbic acid and Cr(VI). Based on a similar strategy, a g-C_3N_4–MnO_2 nanocomposite was prepared to monitor the glutathione level in cells.[388] During the sensing process, MnO_2 is reduced to Mn^{2+} and restores the fluorescence of the g-C_3N_4 nanosheets, resulting in a turn-on fluorescence sensor.

For graphene, BP, and other low bandgap 2D nanomaterials, bandgap engineering has been demonstrated as a viable approach. As shown in Fig. 20d and e, the bandgap of graphene

Table 4 Different 2DM-based sensors for pollutant detection

Sensor type	Materials	Analyte	LOD	Working range	Ref.
Fluorescent	Gr QDs	TNT[a]	2.2 μM	10^{-4}–10^{-1} g L^{-1}	374
Fluorescent	MoS_2 QDs	Hg^{2+}	1.8 nM	0.005–41 μM	375
Fluorescent	N-Doped MoS_2	Hg^{2+}	0.02 μM	0.1–5 μM	376
Colorimetric	GO/MnO_2	Glucose	3.1 mg dL^{-1}	25–300 mg dL^{-1}	377
Colorimetric	LDH/CeO_2	H_2O_2	0.015 mM	0.05–2 mM	378
Electrochemical	Pt/Gr	H_2O_2	80 nM	1–500 μM	379
Electrochemical	rGO	NH_2NH_2	0.43 μM	2.5 μM–1.16 mM	380
Electrochemical	N-Doped Gr	Ascorbic acid	2.2 μM	5.0–1300 μM	381
FET	Gr	*E. coli*	10 CFU mL^{-1}	10–10^4 CFU mL^{-1}	382
FET	MoS_2	Hg^{2+}	0.1 nM	0.1–10 nM	353
FET	MoS_2	Streptavidin	100 fM	—	383
FET	SnS_2	NO_2	30 ppb	0.6–10 ppm	384
FET	BP	Pb^{2+}	1 ppb	10–10^5 ppb	372

[a] 2,4,6-Trinitrotoluene (TNT).

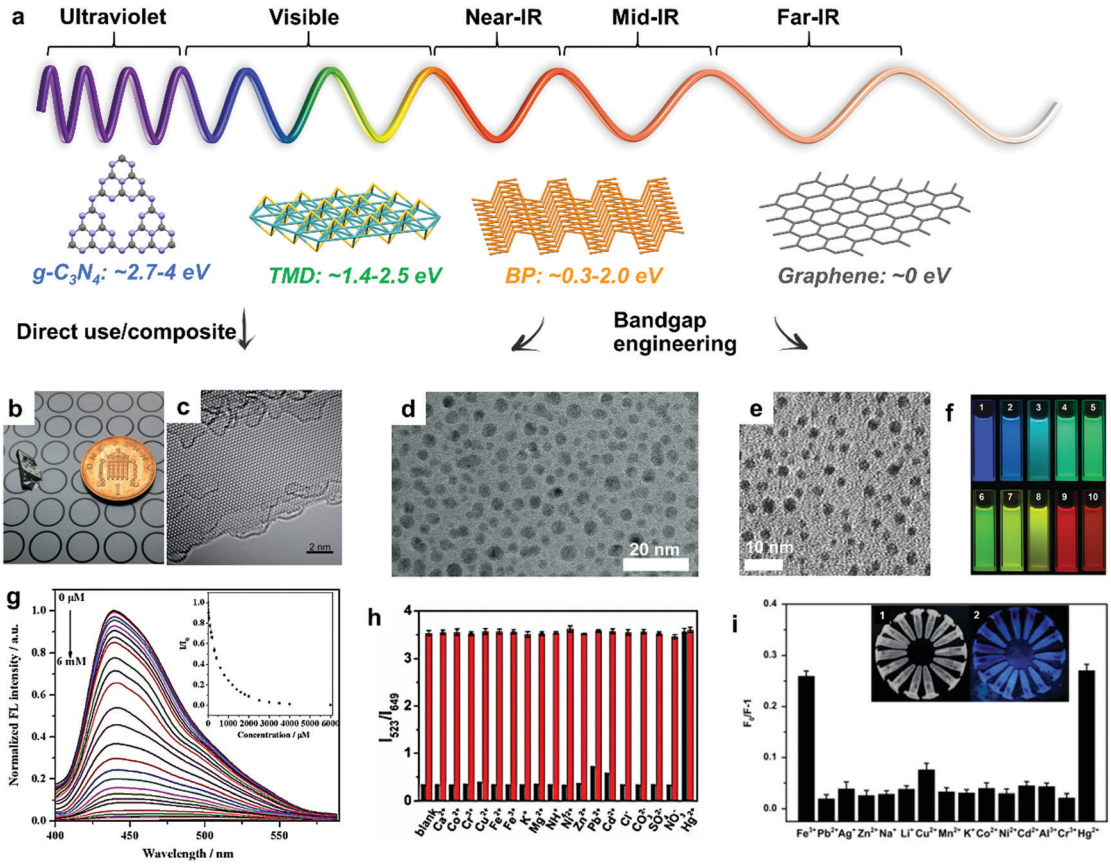

Fig. 20 Fluorescent sensors based on 2D nanomaterials and their photoluminescent derivatives. (a) Bandgap ranges of several 2D nanomaterials compared with the light spectrum. Reproduced with permission.[51] Copyright 2019, The Royal Society of Chemistry. (b) Macroscopic flake of g-C_3N_4. (c) TEM image of g-C_3N_4 nanosheets. (b and c) Reproduced with permission.[386] Copyright 2014, Wiley-VCH. (d) TEM image of BP QDs. Reproduced with permission.[398] Copyright 2018, Wiley-VCH. (e) TEM image of carbon-based graphene quantum dots. Reproduced with permission.[396] Copyright 2014, Wiley-VCH. (f) Optical image of luminescence carbon quantum dos prepared using different reaction conditions under different excitation light. The bandgap of the carbon quantum dots can be tuned by using citric acid and urea under different reaction conditions. Reproduced with permission.[399] Copyright 2017, Wiley-VCH. (g) Fluorescence responses of g-C_3N_4 nanosheets with Cr(VI). The inset shows the relationship between the fluorescence change (I/I_0) and the concentration of Cr(VI). Reproduced with permission.[387] Copyright 2015, Elsevier B.V. (h) Fluorescence sensor based on tetraphenylporphyrin tetrasulfonic acid (TPPS) and BP QDs, showing high selectivity for the detection of Hg^{2+}. Reproduced with permission.[373] Copyright 2017, the American Chemical Society. (i) Selective PL response of nitrogen-doped graphene quantum dots (N-GQDs) solution towards different metal ions. F_0 and F are the fluorescence intensities without and with the presence of metal ions, respectively. Inset shows photos of the fluorescence response of N-GQDs upon the addition of heavy metals under sunlight and UV light. Reproduced with permission.[397] Copyright 2014, Elsevier B.V.

and BP can be enlarged by reducing their particle dimensions, which leads to the formation of graphene quantum dots (GQDs) and BP quantum dots (QDs), respectively. Gu *et al.* fabricated BP QDs from bulk crystals using a sonication-assisted solvothermal approach (Fig. 20h).[373] The authors demonstrated the ability of the BP QDs to fluorescently probe Hg^{2+} in the aqueous phase. In addition to an ultralow detection limit (0.39 nM), the BP QDs showed strong tolerance to other heavy metal ions, such as Pb^{2+} and Cd^{2+}. Owing to the inner filter effect of tetraphenylporphyrin tetrasulfonic acid (TPPS) with BP QDs, the authors found no significant interference even when the concentration of Pb^{2+} was 1000% higher than that of Hg^{2+}. Similar to BP QDs, graphene QDs and carbon QDs (CQDs) are emerging semiconducting materials that have demonstrated potential in the fields of energy storage/conversion,[389,390] bioimaging/biosensing,[391,392] and Pickering nanosurfactants.[393,394] GQDs and CQDs are mono- or few-layer graphene platelets with lateral sizes smaller than 100 nm, while GQDs possess higher crystallinity.[395] Owing to the versatile surface chemistry of carbon, these carbon-based quantum dots can demonstrate a wide variety of colors by tuning their chemical structure and corresponding bandgaps (Fig. 20f).[399] In the field of pollutant sensing, Ananthanarayanan *et al.* synthesized fluorescent GQDs using CVD-synthesized graphene *via* a controlled electrochemical approach.[396] The authors also found that the change in fluorescence intensity in GQDs is moderately selective to Fe^{3+} (400 μM Fe^{3+} showed 68% fluorescence quenching), while another work by Ju *et al.* suggested the possible intervention by oxidative metal ions such as Hg^{2+} (Fig. 20i).[397] The doping strategy has also been widely investigated for tuning the bandgap of 2D nanomaterials. For example, doping MoS_2 nanosheets with B or N was found to greatly

improve their fluorescence properties.[37] These doped nanosheets could selective adsorb Hg^{2+}, and consequently fluorescence quenching occurred, leading to the development of label-free Hg^{2+} sensors.[367] Interestingly, some heavy metal dopants (*e.g.*, Pb^{2+}) were found to improve the fluorescence of MoS_2, which can be later quenched upon the addition of sulfide species. Based on this mechanism, Wang *et al.* proposed the use of fluorescent MoS_2 nanosheets for the detection of Pb^{2+} and sulfide ions.[368]

The capability of 2D nanomaterials to form long-range energy transfer has enabled many 2D nanomaterials to possess strong fluorescence quenching abilities. A variety of fluorescent dyes (*e.g.*, fluorescein) show strong fluorescence in dilute form, whereas fluorescence quenching occurs in the adsorbed state of fluorescent molecules on 2D nanomaterials, which is the so-called aggregation-caused quenching (ACQ) effect.[403,404] By designing appropriate target–probe interactions, numerous approaches have been utilized to design fluorescent ''turn-on'' sensors, such as fluorescence resonance energy transfer and photo-induced electron transfer. The quenching property of 2D nanomaterials has been studied in the fluorimetric sensing of heavy metals, DNA, RNA, proteins, and other small biomolecules.[405–408] As shown in Fig. 21a, a heavy metal sensor was developed based on the quenching of a silver-specific cytosine-rich DNA probe on the surface of GO.[364] The fluorescence intensity of the cytosine-rich oligonucleotide (SSO) probe increased considerably with an increase in Ag^+ concentration due to the desorption of SSO on GO. This mix-and-detect assay showed excellent selectivity toward the detection of Ag^+ over other interference metal ions. In addition, a dye-labelled single-stranded DNA (ssDNA) could interact with TMDs (*e.g.*, MoS_2) through van der Waals forces, which enabled TMDs nanosheets to adsorb the nucleotides and cause fluorescence quenching.[401,409,410] When ssDNA hybridizes with its complementary target DNA, the formed double-stranded DNA cannot be sufficiently bonded with the basal plane of the TMDs nanosheets, recovering the fluorescence. A DNA sensing platform was fabricated based on the high fluorescence quenching efficiency of monolayer MoS_2.[410] Similar to MoS_2, WS_2 monolayers have also been demonstrated to form fluorescence-based DNA sensors.[409] To further improve the sensitivity, sequence specific hairpins were integrated into an MoS_2-based sensing platform followed by rapid hybridization chain reactions (Fig. 21b).[400] With the target DNA, hybridization chain reactions enabled the enzyme-free recognition of DNA since the fluorescent-labelled probe desorbed from the MoS_2 nanosheets.[400] Furthermore, this ''off–on'' fluorescence analysis can be compatible with microfluidic techniques, leading to the high-speed, high-sensitivity, and possible high-throughput detection of multi-DNA.[411] Furthermore, the multiplexed recognition of DNA molecules has been demonstrated using the combination of different fluorescence probes in a TMD system (Fig. 21c).[401] A composite material consisting of multiple 2D nanomaterials may possess potential for the development of an efficient biosensing platform. A graphene/MoS_2 heterostructure was established to detect the sequence of DNA (Fig. 21d).[402] This PL-based graphene/MoS_2 heterostructure sensor could even differentiate a single base mismatch at a low DNA concentration.

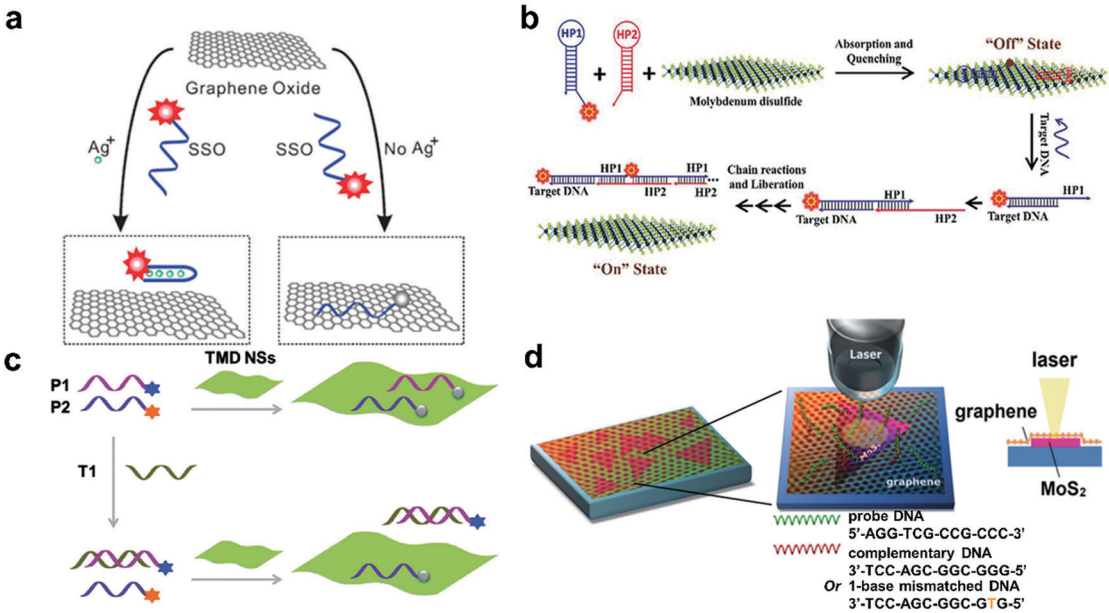

Fig. 21 Fluorescent sensors from high-quenching 2D nanomaterials and target–probe interaction. (a) Schematic showing the detection of Ag^+ using fluorescent silver specific oligonucleotide (SSO) and high-quenching GO nanosheets. Reproduced with permission.[364] Copyright 2010, The Royal Society of Chemistry. (b) Schematic drawing of 2DM-based DNA sensor based on the hybridization chain reactions of HP1 and HP2. HP1 and HP2 are two complementary hairpin probes. Reproduced with permission.[400] Copyright 2015, The Royal Society of Chemistry. (c) Fluorescent DNA sensing based on TMD nanosheets (MoS_2, TiS_2, and TaS_2 nanosheets). P1, P2, and T1 are 6-carboxyfluores-cein (FAM)-labeled ssDNA probe, Texas Red-labeled ssDNA probe, and the influenza A virus subtype H1N1 gene, respectively. Reproduced with permission.[401] Copyright 2015, Wiley-VCH. (d) MoS_2/graphene heterostructure sensor for fluorescent DNA sensing. Reproduced with permission.[402] Copyright 2014, Wiley-VCH.

In addition to the aggregation-caused quenching effect, innovative luminogenic strategies, *e.g.*, aggregation-induced emission (AIE), have been developed recently.[412] This recently discovered AIE mechanism, combined with 2DM, possesses huge potential since it allows a wide range of dye concentrations in biosensing.[413] Benefitting from luminogenic aggregation, developing ''turn-on'' sensors provides higher accuracy and better sensitivity in comparison with their conventional ACQ counterparts.[414] For example, Tang's group developed an AIE-based fluorene sensor for the detection of heparin.[415] By employing GO nanosheets, the authors significantly improved the sensitivity and selectivity of the AIE detector for sensing heparin. The AIE probe exhibited bright green emission only in the presence of heparin and tolerated the interference of heparin analogues, including hyaluronic acid and chondroitin-4-sulfate. This turn-on sensor could also quantify the heparin concentration with a low detection limit. Moreover, AIE-active ligands have been applied to develop MOFs/COFs to enable exceptional fluorescent properties.[416–418] Zhou's group cleverly developed a 2D MOF that can detect volatile organic compounds.[44] When volatile organic compounds fill the channels, the fluorescence quantum yield of the MOF–pollutant complexes increases dramatically. It is worth noting that a shift in the fluorescence peak was observed upon the contact with analytes. Therefore, the authors combined the change in emission enhancement with the emission shift to accurately to monitor various VOCs based on AIE-based MOF nanoplates.

5.2. Colorimetric sensors

Compared with fluorescence sensing, which often needs UV light or laser excitation, colorimetric sensors, which change their colours upon interaction with pollutants, can be just read out using the naked eye, allowing point-of-care testing of pollutants under sunlight. For example, nanomaterials that can mimic biological enzymes have been suggested as promising candidates for colorimetric detection.[419,420] Several nanoparticles with different geometries have been studied as artificial enzyme mimetics.[421,422] Lin *et al.* demonstrated that MoS_2 and WS_2 nanosheets could serve as peroxidase-like materials (Fig. 22a), which showed a color change upon the addition of the analytes.[423,424] The authors fabricated a colorimetric sensor for the visual detection of the glucose concentration in blood. By using the agarose hydrogel-based system, the authors demonstrated a portable test kit for measuring the glucose concentration in serum samples (Fig. 22b and c). Similarly, it was also found that g-C_3N_4 nanosheets can mimic the behavior of peroxidase. In the presence of H_2O_2, g-C_3N_4 nanosheets can initiate the catalytic oxidation of 3,3′,5,5′-tetramethylbenzidine, yielding a coloured solution. Similarly, a colorimetric approach was implemented for sensing blood glucose.[425] MnO_2 nanosheets were used to develop a colorimetric sensor array for detecting the antioxidant levels in bovine serum.[426] Since antioxidants (*e.g.* cysteine, ascorbic acid, and uric acids) have different reducing capabilities, the MnO_2 nanosheet-3,3′,5,5′-tetramethylbenzidine system generated different colorimetric feedback with peaks at 650, 450, and 370 nm. The authors realized the colorimetric detection of various antioxidants with a low detection limit ($\sim$20 μM).

To enhance the performance of pollutant sensing, composition-based strategies have been recently adopted for colorimetric detection. One example is to integrate noble metals with 2D nanosheets. Nirala *et al.* developed an Au-decorated TMD composite as a colorimetric sensor.[428] The authors observed that the Au-decorated MoS_2 nanosheets showed enhanced catalytic activity. Upon the addition of cholesterol oxidase, a colorimetric probe that could detect cholesterol in serum samples was realized. In addition, a hemin-functionalized MoS_2 sensor was developed by Li *et al.*[429] Based on the van der Waals force between hemin molecules and the nanosheets, the hemin-functionalized nanosheets exhibited excellent catalytic performance for H_2O_2. During this process, the authors observed both metallic and semiconducting phases of MoS_2, suggesting that phase transformation occurs for a portion of the MoS_2 nanosheets. Recently, an intriguing colorimetric probe was developed using the size-dependent optical property of MoS_2.[430] As salt can cause nanosheet aggregation, which changes the absorption spectrum of MoS_2, the authors developed a colorimetric biosensor for single nucleotide polymorphism detection. Specifically, MoS_2 nanosheets were first bonded with a ssDNA probe to form an ssDNA/MoS_2 complex, which inhibited the salt-induced aggregation process. In the presence of the target DNA, the bonded ssDNA will desorb from the MoS_2 nanosheets and form double-stranded DNA (dsDNA). During this process, the charged base groups of the nucleobases are shielded within the oppositely charged phosphate backbone of dsDNA, making dsDNA difficult to stabilize the MoS_2 nanosheets in saline conditions. Consequently, the characteristic adsorption peak shifts quantitatively due to the salt-induced aggregation of the MoS_2 nanosheets, leading to the label-free detection of DNA.

In addition to pigment-like color (coloration due to adsorption of certain light), structural color can also be used for sensing applications. Structural coloration commonly refers to ordered nanostructures that can produce colors owing to their interference/scattering of visible light. To achieve structural colors, the design of microscopically structured materials is particularly important. For instance, Liu *et al.*[431] developed a photonic hydrogel with interconnected porous cavities, which could detect methyl phosphonic acid. This photonic hydrogel showed a low limit of detection (10^{-6} mol L^{-1}). Upon the adsorption of methyl phosphonic acid, the color intensity of the photonic hydrogel decreased considerably. In addition to the detection of organic pollutants, strategies based on structural color have also been developed to probe heavy metal ions, including Ba^{2+} [432,433] and Hg^{2+}.[434] However, despite these significant advances, the development of photonic sensors has been largely limited to spherical nanoparticles, primarily due to the shortage of 2D photonic building blocks. Recently, 2D nanomaterials such as GO have been engineered to form photonic structures.[435–437] In particular, exfoliated TiO_2 nanosheets formed a co-facial geometry with a photonic colour that is controllable over the entire visible range by applying stimuli (Fig. 22d–f).[427] These photonic 2D nanomaterials, with appropriate

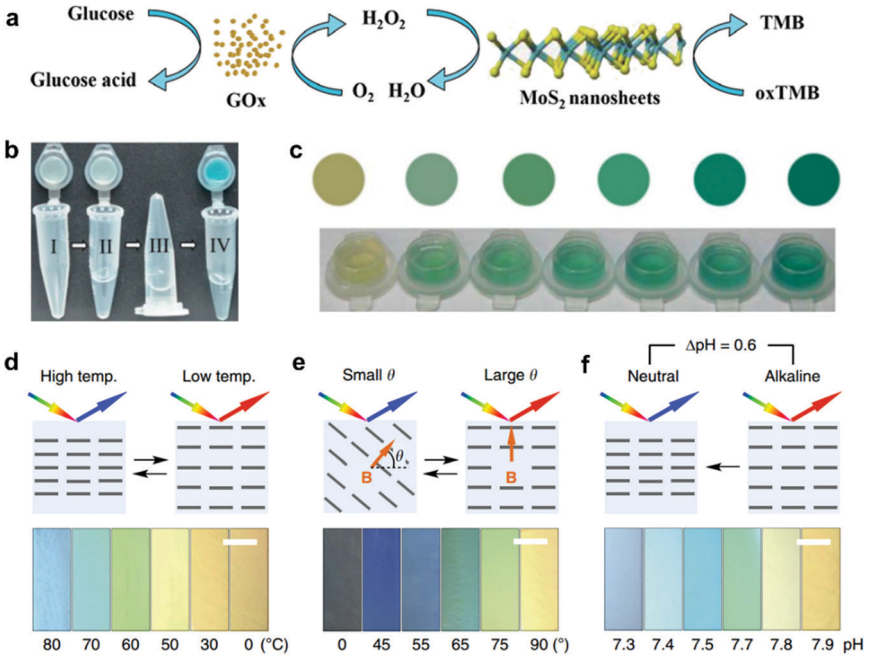

Fig. 22 Colorimetric sensors based on 2D nanomaterials with color-changing capability. (a) Colorimetric glucose sensor from MoS_2 nanosheets and glucose oxidase (GOx). (b) Procedure for glucose detection using the portable test kit, involving initiating the test kit (I), loading the serum sample (II), 60 min incubation at 37 °C (III), and observing the sample colour (IV). (c) Standard colorimetric card of glucose concentration (from left to right: 0, 3, 5, 7, 9, and 12 mM) and images of the hydrogel demonstrating the concentration of the serum glucose in the test kit. (a–c) Reproduced with permission.[423] Copyright 2014, The Royal Society of Chemistry. (d–f) Color changes of 2D TiO_2 dispersion in response to external stimuli. Optical images of the magnetically oriented photonic nanosheet dispersion on changing the temperature (d), angle of an externally applied magnetic flux (e) and the pH value (f). Scale bars are 5 mm in (d–f). (d–f) Reproduced with permission.[427] Copyright 2016, Springer Nature.

surface modification and large surface area, are expected to be valuable for sensing aqueous pollutants.[427]

5.3. Electrochemical sensors

The electrochemical detection of aqueous pollutants typically relies on detecting electrodes that can produce an observable electrical signal in response to electrochemical adsorption/reaction with analytes. A typical electrochemical sensing process involves the use of a working electrode, counter electrode, and reference electrode. The presence of pollutants can induce a change in current, resistance, capacitance, and potential, which will be recorded and analyzed. For example, a sensor prepared by screen-printing conductive inks on a polymer substrate followed by the introduction of Bi particles and ferricyanide was developed to detect Cd^{2+} and Pb^{2+} (Fig. 23a), where the electrochemical potential was evaluated.[438] Recently, SnS_2, WS_2, MoS_2, and other 2D nanostructures have been investigated to boost the efficiency of nanomaterial-based electrochemical sensors.[441–444] To improve the sensor signals, gold and other noble metals have also been implanted into these materials.[445–447] For instance, Zhao *et al.* developed a polypyrrole–rGO (PPy–rGO) nanocomposite-modified glassy carbon electrode for probing Hg^{2+}.[355] During the reducing reaction of adsorbed Hg^{2+} to Hg^0, the authors used square wave anodic stripping voltammetry to achieve high selectivity, where a low limit of detection (15 nM) and high sensitivity (0.124 μA nM^{-1}) were also attained. The authors found that rGO in the nanocomposite is crucial for high sensitivity. As another example, Zhou *et al.* reported Mn-mediated MoS_2 nanosheets for sensing Pb^{2+}.[439] The affinity of Pb^{2+} with S atoms from MoS_2 nanosheets was promoted by defect- and phase-engineering processes (Fig. 23b).

In addition to heavy metal sensing, 2DM-based electrochemical sensors can detect other pollutants. For example, a bisphenol sensor was fabricated by integrating MoS_2 nanoflowers into a chitosan/Au-based glassy carbon electrode.[448] It was shown that the MoS_2/chitosan/Au modified electrode has a strong anodic peak at around 0.9 V, and there was no reduction peak in the presence of bisphenol. This can be explained by the irreversible oxidation of bisphenol at this potential. In another study, Xia *et al.* reported a electrochemical sensor for the detection tryptophan, which was realized by compositing Ag-doped MoS_2 with chitosan.[449] In the sensing process, tryptophan undergoes an irreversible oxidation reaction *via* a two-electron transfer route. In addition, the electrochemical detection of acetaminophen was achieved by combining graphene with MoS_2-based electrodes.[450] In contrast to the pristine MoS_2, the graphene–MoS_2 electrodes showed a superior performance, possibly owing to the high carrier mobility of graphene. With a large linear range of 0.1 to 100 μM, the sensor showed a low sensing limit of 2.0×10^{-8} M. Huang *et al.* reported a WS_2–graphene composite for the simultaneous detection of catechol, resorcinol, and hydroquinone. In comparison with the pristine electrode and graphene-modified electrode, the

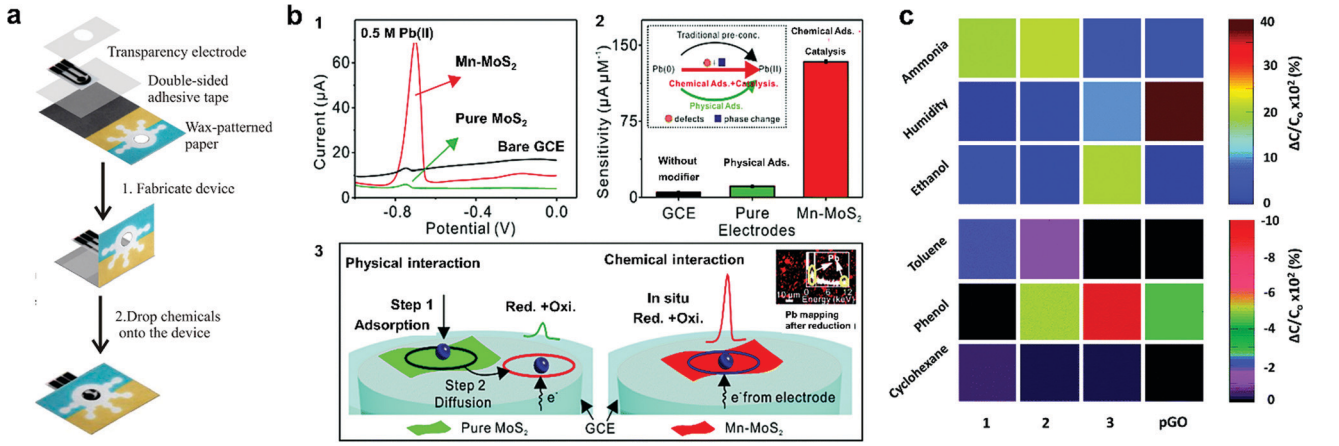

Fig. 23 Electrochemical sensors based on 2D nanomaterials. (a) Schematic illustration of the fabrication of electrochemical sensors for the detection of Pb^{2+} and Cd^{2+}. Reproduced with permission.[438] Copyright 2014, the American Chemical Society. (b) Electrochemical response (1) and sensitivity (2) of glassy carbon electrode (GCE), MoS_2, and Mn–MoS_2-modified GCE for Pb^{2+} sensing. The high response of Mn–MoS_2-modified GCE can be explained by the improved *in situ* redox reactions (3) with inset showing Pb mapping on the surface of Mn–MoS_2. Reproduced with permission.[439] Copyright 2018, The Royal Society of Chemistry. (c) Array-based color code identification of various pollutant vapors from sensors based on porous graphene oxide (pGO) and its chemically modified derivatives (phenyl–GO (1), dodecyl–GO (2), and ethanol–GO (3)). The colors are related to the percentage capacitance response with the color bars displayed on the right. Reproduced with permission.[440] Copyright 2017, The Royal Society of Chemistry.

WS_2–graphene electrode exhibited improved electrocatalytic behaviour for the oxidation of catechol, resorcinol and hydroquinone.[442]

For volatile pollutants (*e.g.*, NH_3 and toluene), gas sensors can also be useful for monitoring water quality. Here, we briefly introduce a few recent advances in gas sensing of common pollutants in water, and a comprehensive review on gas sensing with 2D nanomaterials can been found in a recent review paper.[37] The surface chemistry of 2D nanomaterials can be engineered to develop sensors for recognizing different gases. Yavari *et al.*[451] developed self-standing graphene foam *via* CVD growth on a porous nickel template, followed by template removal. This graphene foam showed an observable response to 1000 ppm of NH_3, although a slow recovery time was observed (~1000 s). GO nanosheets have emerged as a strong candidate for sensing hydrogen bonding donors owing to their oxygen-bearing groups, which make GO exceedingly hydrophilic.[452] Ruoff *et al.*[453] confirmed that the interaction between moisture and the oxygen-bearing groups of GO affects the device performance, and suggested that highly reduced GO may be unsuitable for sensing humidity or other hydrogen bonding donors. Jelinek *et al.*[440] reported a vapour sensor by integrating porous graphene oxide (pGO), anilinegrafted GO (phenyl-GO), dodecylamine-grafted GO (dodecyl-GO) and ethanolamine-grafted GO (ethanol-GO) onto interdigitated electrodes (IDEs). Due to the different surface chemistry of functionalized GO, this array could selectively probe several analytes, including NH_3, moisture, ethanol, toluene, phenol and cyclohexane (Fig. 23c).

5.4. Pollutant detection *via* field-effect transistors

2D nanomaterials have attracted increasing attention in FETs for pollutant sensing. For a typical FET-based sensor, the design strategy involves the adsorption of targeted pollutants on 2D nanosheets, which changes one or several key parameters of the FET, such as I_{on}/I_{off} ratio, threshold voltage, and field-effect mobility. In particular, semiconducting nanosheets have been heavily investigated owing to their excellent charge carrier mobility and suitable bandgaps. In addition, the large lateral size of 2DM enables them to have conformal contact with metal electrodes, which reduces the contact resistance in FET-based sensors. FET-based sensors possess several unique advantages. For instance, FETs are very responsive, whereas a relatively longer detection time is commonly expected in fluorescent sensors. In particular, 2DM-based FET sensors often feature small dimensions and low power consumption, facilitating the design of integrated and wearable sensors.

A classic FET-based sensor includes drain (D) electrodes, channel materials, source (S) electrodes, gate electrodes, and gate oxides (Fig. 24a). A typical working mechanism of FET-based sensors involves a conductance change in the channel material upon the introduction of analytes (*e.g.*, heavy metal ions) (Fig. 24b). Generally, charge transfer and electrostatic gating are the two main principles for sensing chemicals in water. For p-type semiconductors detecting positively charged heavy metal ions, these two mechanisms compete with each other since the charge transfer of electrons from p-type 2D nanomaterials to the heavy metal ions increases the current, while the current can be reduced by the effective gating effect (Fig. 24c).[345] Compared with conventional FETs, there are a few additional factors that determine the gating effect of FET-based sensors, such as analyte type and analyte concentration. For heavy metal ions, a larger electron negativity usually allows a stronger interaction with channel materials, and thus the gating effect may occur at a relatively low concentration. Taking Hg^{2+} ions as an example, the electron negativity of Hg^{2+} is 1.9, which is higher than that of Pb^{2+} (1.8),[454,455] and thus channel materials often show higher sensitivity to Hg^{2+} in comparison with Pb^{2+}.[456,457]

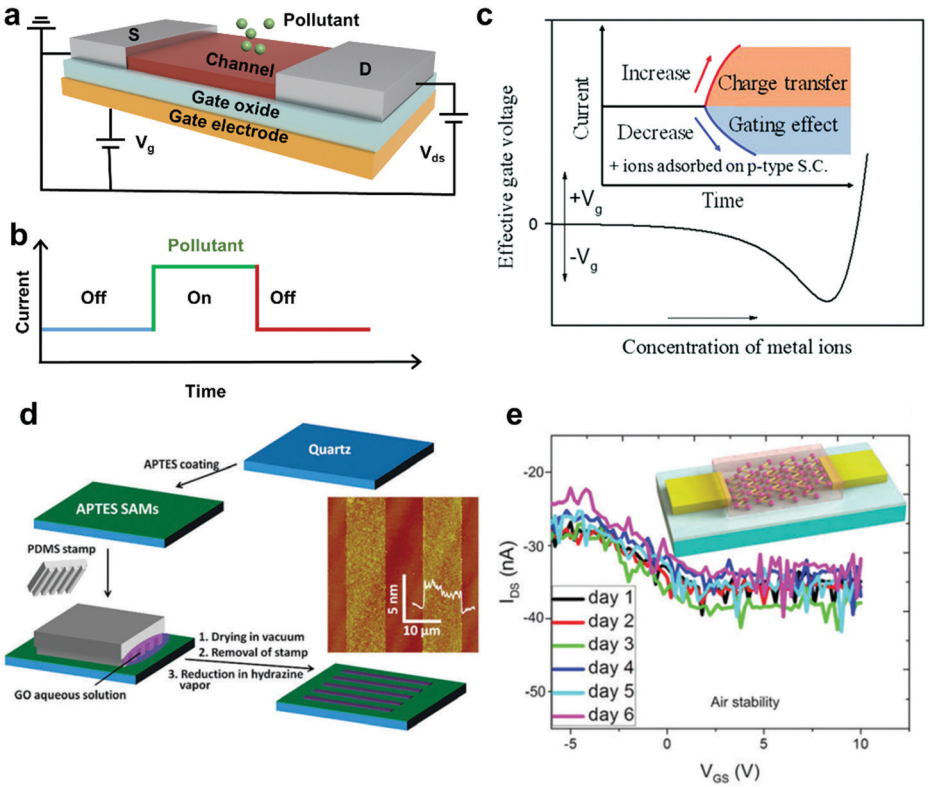

Fig. 24 2DM-based field-effect transistor (FET) for sensing applications. (a) Schematic drawing of a typical field-effect-transistor sensor. (b) Illustrational example of the current change after pollutant adsorption and desorption on a sensor. (c) Illustration of the effective gate voltage due to the metal ion adsorption on the channel materials. The inset shows a typical current change in a p-type channel because of the charge transfer or gating effect.[345] Reproduced with permission.[345] Copyright 2017, The Royal Society of Chemistry. (d) Schematic of the fabricating patterned rGO films on (3-aminopropyl)triethoxysilane (APTES)-coated quartz with their AFM analysis (inset). Reproduced with permission.[347] Copyright 2011, the American Chemical Society. (e) I_{ds}–V_{gs} plots of BP-based FET sensor with ionophore protection, showing insignificant I_{ds} variation over 6 days. The inset shows the FET design of the BP sensor with improved air stability. Reproduced with permission.[372] Copyright 2015, the American Chemical Society.

In pursuit of highly sensitive/selective FET sensors, the judicious selection of the channel material is a key element. Owing to their unique structures and exceptional electronic properties, 2D nanomaterials have been investigated for the development of FET-based sensors for water quality monitoring and pollutant detection. As a representative 2D nanomaterial, graphene has gained enormous interest for graphene field-effect transistor (GFET)-based sensors because of its large surface area, versatile chemical functionalization, and high carrier mobility.[458] For example, functionalized graphene field effect transistors have been demonstrated for Hg^{2+} sensing.[346] It was found that the self-assembly of 1-octadecanethiol forms a large monolayer on graphene. The adsorption of Hg^{2+} by the functionalized graphene was monitored using AFM, showing that the thickness of graphene increased to 1.6 nm upon exposure to mercury. The GFET-based sensor showed a low detection limit for Hg^{2+} of 10 ppm. With the goal of the practical application of GFET sensors, other strategies are being pursued, including solution-processable rGO,[347,348] and graphene derivatives.[345,349–351] As shown in Fig. 24d, a micropatterning approach was proposed to fabricate FET sensors for the detection of metal ions.[347] Serving as the gating materials, micropatterned rGO films were functionalized with metallothionein type II protein due to its high affinity with metal ions. This rGO–FET sensor showed an obvious current increase upon the addition of 1 nM mercury (Hg^{2+}), demonstrating high sensitivity with a low detection limit. The very same FET sensor also detected Cd^{2+} at 1 nM with a signal-to-noise ratio of 15–20.

In addition to graphene, the semiconducting properties of TMDs make them attractive candidates for applications in FET sensors.[459] For instance, mechanically exfoliated MoS_2 nanosheets have been used to fabricate FET sensors for the detection of Hg^{2+} ions.[352] The strong affinity between the S group and mercury ions allows the quick and robust binding of Hg^{2+} with MoS_2. The authors observed that the adsorption of mercury ions leads to p-type doping, and subsequently decreases the carrier concentration in n-type semiconducting MoS_2. These changes were reflected in the conductance of few-layer MoS_2, resulting in high sensitivity of FET sensors with an ultralow detection limit. In addition, a DNA-functionalized MoS_2/Au nanocomposite FET sensor was developed for mercury sensing.[353] A thin layer of Au NPs was sputter-coated on the exfoliated MoS_2, followed by the grafting of DNA molecules. This FET sensor was also examined under different Hg^{2+} concentrations, in which the sensor responded to Hg^{2+} within several seconds, confirming the dynamic response of Hg^{2+} in an aqueous environment.

For water-sensitive 2D nanomaterials, a thin film of protection layers, such as metal oxide, is often needed to prevent irreversible degradation of the channel materials. During the analysis of aqueous pollutants, an electrostatic double layer forms at the surface of the adsorbed target analytes, often causing negative effects on FET-based sensors. This is because the strong electrostatic double layer (*i.e.*, short Debye length) reduces the field produced by charged pollutants and/or gate potential.[460] Thus, to mitigate the screening effect on FET sensors, several direct and indirect strategies, such as involving a desalination process, use of thin top gate oxide, and the deposition of functional polymer on channel materials, have been reported.[460–464] Alternatively, Li *et al.* fabricated air-stable black phosphorus sensors by ionophore encapsulation (Fig. 24e).[372] The ionophore layer could reduce the oxidation from air, while it allowed the selective permeability of some molecules. After 7 days of ambient exposure, this ionophore-encapsulated BP FET sensor showed a source–drain current I_{ds} change smaller than 10%. More importantly, this sensor could effectively probe several hazardous ions with low detection limits, including Pb^{2+}, Cd^{2+}, Hg^{2+}, and AsO_2^-.

6. Conclusion and perspectives

The development of emerging water treatment methodologies that leverage sophisticated nanostructures of advanced functional materials to clean and monitor various water systems in a scalable, controllable, affordable, and sustainable manner presents great research opportunities and challenges for the next several decades. In this review, we summarized and evaluated the state-of-the-art works on emerging 2D nanomaterials and their applications in water treatment, highlighting the important role of their 2D nanostructure and exceptional properties in membrane separation, adsorption, photocatalysis, and pollutant detection. Although it is almost impossible to cover every research work or paper regarding 2DM, Table 5 aims to provide general information on various 2DM technologies that have already been successfully demonstrated in the fields of water decontamination and water quality monitoring.

To realize the large-scale application of 2DM in water purification, there are a number of challenges that need to be addressed. Firstly, the production cost of many 2DM remains relatively high compared with conventional materials, and thus significant cost reduction is desirable. Strategies that are based on high scalability and processability may help to lower the cost of 2DM. For example, solution-based top-down exfoliation can achieve the scalable production of 2DM in an affordable manner due to the use of cheap and abundant layered crystals (*e.g.* graphite).[541] Compared with 1D nanomaterials, which are mostly made from bottom-up approaches from molecular precursors (such as CVD growth), the top-down exfoliation techniques for 2D nanomaterials are relatively mature and readily scaled up in an industrial environment by exfoliating bulk-layered precursors using sonication or shear force.[542,543]

In addition, the sustainability of 2DM (including production sustainability and application sustainability) should be considered. Production sustainability is important to ensure that the continuous supply of 2DM is sustainable and will minimize any negative influence on the ecosystem and environment (*e.g.*, using less hazardous chemical reagents[544] or consuming minimal energy[545,546]). Since water treatment is essentially a decontamination process, the biocompatibility of 2DM has to be considered to avoid any possible recontamination of water from the materials, and thus environmental-friendly 2DM with low toxicity (*e.g.*, LDHs) should be prioritized.[35] Considering that most 2DM are made from earth abundant elements (*e.g.*, C, N, B, Mo, S, and Ti), the sustainability and the issue of material scarcity will be manageable when judicious measures (*e.g.*, materials recovery) are taken. From the application perspective, the continuous use of 2DM should not cause material loss, degradation, damage, and secondary pollution. Therefore, application sustainability is also an important factor. For example, the widely reported GO laminates are hydrophilic in nature and can be hydrated in water over time, leading to a change in their interlayer spacing during membrane separation. This hydration issue is unsustainable for long-term operations in water desalination. Thus, methods that can maintain precise nanochannels with long-standing operational stability need to be developed. For solar desalination membranes, the formation of high-throughput channels is essential for efficient water transport and high-performance solar desalination, and thus advanced self-assembly and directed assembly strategies that form ordered structures with high-throughput channels can be highly beneficial. For example, the self-assembly of 2D nanomaterials can lead to various ordered nanoarchitectures, ranging from orientationally ordered to positionally ordered structures.[547] Recently, Yang's

Table 5 Overview of several 2D nanomaterials with their applications in water decontamination and water quality monitoring

	Gr	TMDs	BP	MXene	h-BN	g-C_3N_4	LDH	MOF/COF
Filtration	+[465]	+[69]		+[70]	+[71]	+[72,98,466]	+[467]	+[468–470]
Solar desalination	+[471]	+[166]		+[167,472]		+[473]		+[474]
Adsorption	+[475]	+[476,477]	+[478]	+[100]	+[479]	+[480]	+[481–483]	+[484]
Photocatalysis	+[485,486]	+[487–489]	+[490,491]	+[492,493]	+[494]	+[495–499]	+[500–502]	+[503–507]
Fluorescent sensing	+[508]	+[509]	+[510]	+[511–513]	+[514]	+[515–517]	+[518]	+[519]
Electrochemical sensing	+[520]	+[521]	+[522,523]	+[524–526]	+[527]	+[528,529]	+[530]	+[531]
FET sensor[a]	+[532–534]	+[535,536]	+[537]	+[538]				+[539,540]

[a] Field-effect transistor (FET) sensors here only consider the use of 2D nanomaterials for channel materials, while non-conductive 2D nanomaterials (*e.g.* h-BN) may be also used as separators in FETs.

group developed a lamellar liquid-crystal phase of 2D MXene to achieve the vertical alignment of nanosheets for fast ion transport.[548] These self-assembly and directed assembly tools appear to be attractive approaches to fine-tune the transport channels of 2DM-based nanostructures, and thus the implementation of the above approaches in water treatment process needs more research attention.

For the processes of adsorption, photocatalysis, and sensing, efficient manipulation of the material–pollutant interaction is needed for the development of a new generation of intelligent nanostructures that are multifunctional, selective, adaptive, and programmable. Since weak and unspecific interactions with pollutants are seen in many pristine, defect-free 2D nanocrystals, the defect engineering of 2D nanomaterials can greatly improve the selectivity of pollutant absorption. This is often due to the presence of dangling groups on the surface of 2D nanomaterials, and appropriate defect engineering is often used to improve the performances of adsorption, catalysis, and detection. For example, according to the hard–soft-acid–base (HSAB) theory, TMD (such as MoS_2 and $MoSe_2$) nanosheets possess soft dangling groups including S and Se, and thus interact strongly with soft acids such as Hg^{2+} and Pb^{2+}, while the surface groups of MXene contain –F and –OH, leading to better adsorption on hard acids such as U(VI).[549] Furthermore, chemical programmability through the fabrication of multi-component assemblies and superlattice 2D nanomaterials[550] may achieve multiple functions (*e.g.*, removal of multiple pollutants) in a single material system. For example, combining photocatalysts with membranes can enable the photocatalytic degradation of organic foulants, alleviating organic fouling in membrane separation.[104] In the future, the field of 2D nanomaterials is expected to witness tremendous innovation in synthesis methodologies, device fabrication, post-processing, and performance characterization. Although some have yet to be directly used for water treatment, Table 6 and Fig. 25 aims to summarize the recent encouraging development of nanomaterial synthesis, device fabrication/processing and performance characterization related to 2D nanomaterials and potentially transformable to water-related applications.

In the past decade, the development of advanced robotics and manufacturing techniques in materials science has emerged as a rapidly expanding area of research. Remarkably, Masubuchi and co-workers demonstrated a robotic system that could autonomously assemble van der Waals heterostructures.[550,561] With the capability of autonomously detecting monolayers, the robotic system could stack four cycles of the designated 2D nanosheets per hour with minimal human intervention, realizing the production of a complex superlattice consisting of 29 alternating layers of graphene and h-BN. Recently, robotic arms have been integrated in layer-by-layer assembly processes, such as the fabrication of 2D clay-embedded polyelectrolyte multilayer membranes.[556] With the aid of robot arms, the numbers of polymer layers between clay depositions can be readily controlled, leading to the precise tuning of the interlayer spacing in separation membranes.[564–568] In addition, additive manufacturing (*e.g.*, 3D printing) has attracted tremendous interest from the industry and research community.[345,569–586] 3D printing allows the pervasiveness of desktop-size and relatively low-cost fabrication units, enabling tremendous opportunities for the rapid prototyping of 2DM-based devices.[51,562] Zhang *et al.* developed a 3D-printed graphene aerogel with unique mechanical and electrical properties.[587] Recently, Tour's group described the synthesis of structured graphene foam using a modified, automated 3D-printing process.[588] The authors further refined the graphene foam into more complex 3D shapes using laser techniques. Although these works are not directly related to water treatment, the advanced manufacturing may offer

Table 6 Examples of emerging technologies in the field of functional nanomaterials

	Emerging field	Examples	Capabilities & features
Nanomaterial synthesis	Robot-assisted synthesis	Autonomous robot assembly of van der Waals materials	Accelerated development of complex nanostructures with less human intervention[550]
	High-throughput synthesis	Continuous flow exfoliation method	Continuous production of high quality 2D nanomaterials with good consistency[551]
	Heteronanostructures	Block-by-block epitaxial growth of 2D heterostructures	Precise modulation of chemical compositions and electronic structures[552]
	Green chemistry	Electrochemical exfoliation of graphite	Providing a low hazard, and highly scalable method[553,554]
Device fabrication	3D printing	3D printing of 2D nanomaterials and their composites	Fast prototyping and flexible fabrication of 2DM-based devices[51,555]
	Robotic assembly	Robot-assisted LbL assembly	Fabricating multilayer membranes for wastewater & effluent treatment[556]
	Orientation engineering	Liquid-crystalline assembly	Liquid-crystalline 2D nanosheets can form structures with high orientational ordering[437,548]
	Large-scale manufacturing	Roll-to-roll production of 2DM-based photoelectronics	Reducing the production cost and enabling possible industrial applications[557]
Post-processing & characterization & analysis	Fast processing techniques	Photonic sintering	Improved conductivity of printed films on polymer substrates within seconds[558]
	Data-centric informatics	Machine learning	Rapid prediction of the bandgaps of 2D nanomaterials[559]
	Advanced imaging & probing	Cryogenic electron microscopy	Clarifying micro-/nanostructures[560]

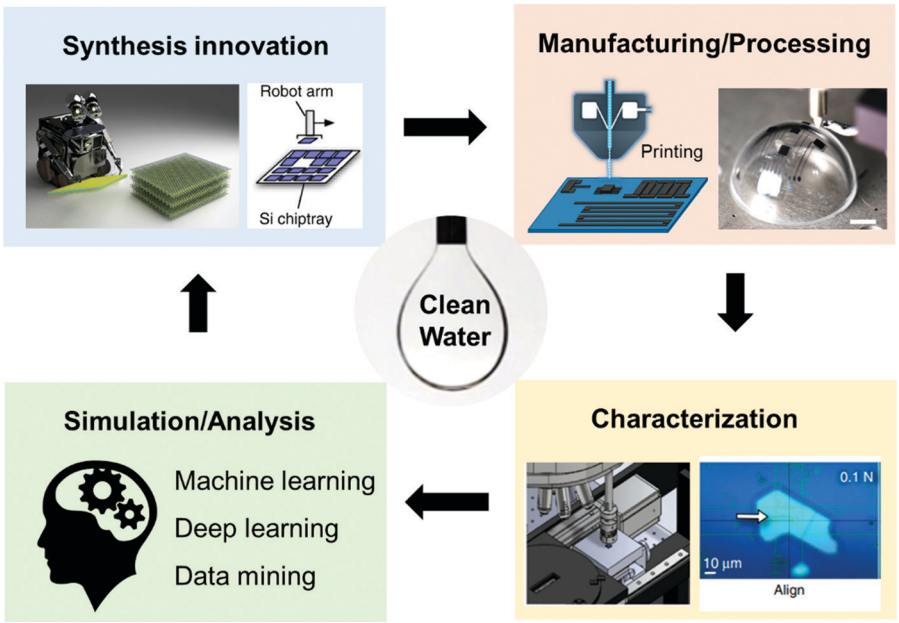

Fig. 25 Overview of the recent innovations in synthesis, manufacturing/processing, characterization, and simulation/analysis, which may potentially improve and optimize current water technologies. Reproduced with permission.[550,561] Copyright 2018, Springer Nature. Reproduced with permission.[51] Copyright 2019, The Royal Society of Chemistry. Reproduced with permission.[562] Copyright 2020, Wiley-VCH. Reproduced with permissions. Copyright 2019,[563] the American Chemical Society.

unique opportunities to develop innovative 2DM and 2DM-based composites for water-related applications.

In pursuit of a new generation of intelligent materials for water treatment, it remains extremely important to build a fundamental structure–processing–performance relationship using innovative theoretic approaches (*e.g.*, machine-learning method). Thanks to the recent algorithmic developments, data-driven approaches are starting to play a significant role in materials engineering.[589–605] These data-driven methods, *e.g.*, machine learning, data mining, and artificial neural network, have demonstrated the ability of fast predicting material structures/properties based on past data instead of by performing experiments and simulations.[563] Machine learning can be particularly helpful for predicting the properties of 2D nanomaterials when measuring/computing using traditional methods is expensive or time consuming. For instance, the machine-learning approach was used to predict the bandgap of MXene using several machine-learning algorithms.[559] Among these algorithms, the authors found the calculated bandgap with lowest root-mean-squared error (RMSE) of 0.14 eV. However, despite increasing data-driven efforts on 2DM in the energy field,[606] the investigation of 2DM-based water treatment remains an underexplored avenue, and thus certainly needs more attention.

High-throughput manufacturing of stable 2D materials with high quality and low cost is critical toward the realization of mass commercialization. Production cost, scalability, processability, stability, and the quality of 2DM are important and sometimes interdependent factors that should be considered simultaneously for large-scale implementation.[607] For example, improving scalability *via* roll-to-roll manufacturing will also lead to a lower production cost for 2DM.[608] In the case of stability, the challenge of maintaining long-term stability and high performance simultaneously may be even more urgent under the current scenario. In fact, many water treatments involve harsh conditions, such as strong chemicals, extreme pH values, high salinity and high humidity. Recent progress in device passivation and packaging has provided improved stability for various 2D nanosystems against oxygen and moisture;[609] however, techniques that can maintain the high quality of 2DM over an extended period of time (10+ years) under severe conditions have yet to be developed. Addressing this challenge not only requires material innovation (such as surface chemistry and compositional nano-structuring), but also calls for fundamental understanding of the underlying physics/mechanism of these processes. Therefore, future pioneering research from diverse and multidisciplinary areas is needed to advance the fundamental understanding of the structure-behavior-property relationship and facilitate the development of multifunctional, selective, adaptive, programmable 2DM-based devices for water treatment applications.

Conflicts of interest

There are no conflicts to declare.

Acknowledgements

The authors would like to acknowledge financial support from Texas A&M Water Seed Grant (TEES-163024). L. W. thanks the

support from the National Natural Science Foundation of China (No. 51973155).

References

1 H. Bi, X. Wang, H. Liu, Y. He, W. Wang, W. Deng, X. Ma, Y. Wang, W. Rao, Y. Chai, H. Ma, R. Li, J. Chen, Y. Wang and M. Xue, *Adv. Mater.*, 2020, **32**, 2000074.
2 L. Chen, L. Cao, X. Ji, S. Hou, Q. Li, J. Chen, C. Yang, N. Eidson and C. Wang, *Nat. Commun.*, 2020, **11**, 2638.
3 G. Denecker, E. Hoste, B. Gilbert, T. Hochepied, P. Ovaere, S. Lippens, C. Van den Broecke, P. Van Damme, K. D'Herde, J.-P. Hachem, G. Borgonie, R. B. Presland, L. Schoonjans, C. Libert, J. Vandekerckhove, K. Gevaert, P. Vandenabeele and W. Declercq, *Nat. Cell Biol.*, 2007, **9**, 666–674.
4 Y. Fu, L. Li, B. Xie, C. Dong, M. Wang, B. Jia, L. Shao, Y. Dong, S. Deng, H. Liu, G. Liu, B. Liu, D. Hu and H. Liu, *Astrobiology*, 2016, **16**, 925–936.
5 K. Aagaard and E. C. Carmack, *J. Geophys. Res.: Oceans*, 1989, **94**, 14485–14498.
6 P. H. Gleick, *The world's water 2000-2001: the biennial report on freshwater resources*, Island Press, 2000.
7 C. A. Dieter, M. A. Maupin, R. R. Caldwell, M. A. Harris, T. I. Ivahnenko, J. K. Lovelace, N. L. Barber and K. S. Linsey, Estimated use of water in the United States in 2015, Report 1441, Reston, VA, 2018.
8 B. Chen, M. Han, K. Peng, S. Zhou, L. Shao, X. Wu, W. Wei, S. Liu, Z. Li and J. Li, *Sci. Total Environ*, 2018, **613**, 931–943.
9 P. Zhao, P. J. J. Alvarez, X. Li and C. Pan, *Anal. Methods*, 2018, **10**, 757–766.
10 S. A. Snyder, P. Westerhoff, Y. Yoon and D. L. Sedlak, *Environ. Eng. Sci.*, 2003, **20**, 449–469.
11 K. J. Godri Pollitt, J.-H. Kim, J. Peccia, M. Elimelech, Y. Zhang, G. Charkoftaki, B. Hodges, I. Zucker, H. Huang, N. C. Deziel, K. Murphy, M. Ishii, C. H. Johnson, A. Boissevain, E. O'Keefe, P. T. Anastas, D. Orlicky, D. C. Thompson and V. Vasiliou, *Sci. Total Environ*, 2019, **690**, 853–866.
12 L. Wu, D. Ning, B. Zhang, Y. Li, P. Zhang, X. Shan, Q. Zhang, M. R. Brown, Z. Li, J. D. Van Nostrand, F. Ling, N. Xiao, Y. Zhang, J. Vierheilig, G. F. Wells, Y. Yang, Y. Deng, Q. Tu, A. Wang, D. Acevedo, M. Agullo-Barcelo, P. J. J. Alvarez, L. Alvarez-Cohen, G. L. Andersen, J. C. de Araujo, K. F. Boehnke, P. Bond, C. B. Bott, P. Bovio, R. K. Brewster, F. Bux, A. Cabezas, L. Cabrol, S. Chen, C. S. Criddle, Y. Deng, C. Etchebehere, A. Ford, D. Frigon, J. Sanabria, J. S. Griffin, A. Z. Gu, M. Habagil, L. Hale, S. D. Hardeman, M. Harmon, H. Horn, Z. Hu, S. Jauffur, D. R. Johnson, J. Keller, A. Keucken, S. Kumari, C. D. Leal, L. A. Lebrun, J. Lee, M. Lee, Z. M. P. Lee, Y. Li, Z. Li, M. Li, X. Li, F. Ling, Y. Liu, R. G. Luthy, L. C. Mendonça-Hagler, F. G. R. de Menezes, A. J. Meyers, A. Mohebbi, P. H. Nielsen, D. Ning, A. Oehmen, A. Palmer, P. Parameswaran, J. Park, D. Patsch, V. Reginatto, F. L. de los Reyes, B. E. Rittmann, A. Noyola, S. Rossetti, X. Shan, J. Sidhu, W. T. Sloan, K. Smith, O. V. de Sousa, D. A. Stahl, K. Stephens, R. Tian, J. M. Tiedje, N. B. Tooker, Q. Tu, J. D. Van Nostrand, D. De los Cobos Vasconcelos, J. Vierheilig, M. Wagner, S. Wakelin, A. Wang, B. Wang, J. E. Weaver, G. F. Wells, S. West, P. Wilmes, S.-G. Woo, L. Wu, J.-H. Wu, L. Wu, C. Xi, N. Xiao, M. Xu, T. Yan, Y. Yang, M. Yang, M. Young, H. Yue, B. Zhang, P. Zhang, Q. Zhang, Y. Zhang, T. Zhang, Q. Zhang, W. Zhang, Y. Zhang, H. Zhou, J. Zhou, X. Wen, T. P. Curtis, Q. He, Z. He, M. R. Brown, T. Zhang, Z. He, J. Keller, P. H. Nielsen, P. J. J. Alvarez, C. S. Criddle, M. Wagner, J. M. Tiedje, Q. He, T. P. Curtis, D. A. Stahl, L. Alvarez-Cohen, B. E. Rittmann, X. Wen and J. Zhou, *Nat. Microbiol.*, 2019, **4**, 1183–1195.
13 F. Fu and Q. Wang, *J. Environ. Manage.*, 2011, **92**, 407–418.
14 S. Bolisetty, M. Peydayesh and R. Mezzenga, *Chem. Soc. Rev.*, 2019, **48**, 463–487.
15 A. Prüss-Ustün, J. Bartram, T. Clasen, J. M. Colford Jr, O. Cumming, V. Curtis, S. Bonjour, A. D. Dangour, J. De France, L. Fewtrell, M. C. Freeman, B. Gordon, P. R. Hunter, R. B. Johnston, C. Mathers, D. Mäusezahl, K. Medlicott, M. Neira, M. Stocks, J. Wolf and S. Cairncross, *Trop. Med. Int. Health*, 2014, **19**, 894–905.
16 C. Marolla, *Information and Communication Technology for Sustainable Development*, CRC Press, 2018.
17 M. A. Shannon, P. W. Bohn, M. Elimelech, J. G. Georgiadis, B. J. Mariñas and A. M. Mayes, *Nature*, 2008, **452**, 301.
18 J. Bartram, J. Cotruvo, M. Exner, C. Fricker and A. Glasmacher, *Heterotrophic plate counts and drinking-water safety*, IWA Publishing, 2003.
19 Y.-F. Guan, M. Marcos-Hernández, X. Lu, W. Cheng, H.-Q. Yu, M. Elimelech and D. Villagrán, *Environ. Sci. Technol.*, 2019, **53**, 13302–13311.
20 M. V. Riquelme, W. Leng, M. Carzolio, A. Pruden and P. Vikesland, *J. Environ. Sci.*, 2017, **62**, 49–59.
21 H. Su, Y. Wei, X. Qu, C. Yu, Q. Li, P. J. J. Alvarez and M. Long, *Chem. Eng. J.*, 2020, **385**, 123923.
22 J. E. Padilla, J. Melendez, L. A. Barrera, Y. Wu, K. Ventura, J. M. Veleta, M. T. Islam, C. A. Chavez, S. K. Katla, D. Villagrán and J. C. Noveron, *J. Environ. Chem. Eng.*, 2018, **6**, 1027–1032.
23 S. K. Loeb, J. Kim, C. Jiang, L. S. Early, H. Wei, Q. Li and J.-H. Kim, *Environ. Sci. Technol.*, 2019, **53**, 7621–7631.
24 X. Zhu, A. V. Dudchenko, C. M. Khor, X. He, G. Z. Ramon and D. Jassby, *Environ. Sci. Technol.*, 2018, **52**, 11591–11600.
25 M.-J. Suh, Y. Shen, C. K. Chan and J.-H. Kim, *Langmuir*, 2019, **35**, 8699–8708.
26 M. Li, L. M. Farmen and C. K. Chan, *Ind. Eng. Chem. Res.*, 2017, **56**, 2458–2465.
27 C. Thamaraiselvan, J. Wang, D. K. James, P. Narkhede, S. P. Singh, D. Jassby, J. M. Tour and C. J. Arnusch, *Mater. Today*, 2019, **34**, 115–131.
28 C. Chu, J. Yang, D. Huang, J. Li, A. Wang, P. J. J. Alvarez and J.-H. Kim, *Environ. Sci. Technol.*, 2019, **53**, 10352–10360.
29 R. Zhou, L. Zhao, Y. Wang, S. Hameed, J. Ping, L. Xie and Y. Ying, *TrAC, Trends Anal. Chem.*, 2020, **127**, 115884.

30 F. Zhao, Y. Yao, C. Jiang, Y. Shao, D. Barceló, Y. Ying and J. Ping, *J. Hazard. Mater.*, 2020, **384**, 121358.
31 Y. Yao and J. Ping, *TrAC, Trends Anal. Chem.*, 2018, **105**, 75–88.
32 Y. Yao, C. Jiang and J. Ping, *Biosens. Bioelectron.*, 2019, **123**, 178–184.
33 Y. Yao, L. Lan, X. Li, X. Liu, Y. Ying and J. Ping, *Small*, 2020, **16**, 1907282.
34 J. S. Santos, M. S. Pontes, E. F. Santiago, A. R. Fiorucci and G. J. Arruda, *Sci. Total Environ*, 2020, **749**, 142385.
35 D. Chimene, D. L. Alge and A. K. Gaharwar, *Adv. Mater.*, 2015, **27**, 7261–7284.
36 C. Tan, X. Cao, X.-J. Wu, Q. He, J. Yang, X. Zhang, J. Chen, W. Zhao, S. Han, G.-H. Nam, M. Sindoro and H. Zhang, *Chem. Rev.*, 2017, **117**, 6225–6331.
37 C. Anichini, W. Czepa, D. Pakulski, A. Aliprandi, A. Ciesielski and P. Samorì, *Chem. Soc. Rev.*, 2018, **47**, 4860–4908.
38 G. Wei, X. Quan, S. Chen and H. Yu, *ACS Nano*, 2017, **11**, 1920–1926.
39 S. P. Surwade, S. N. Smirnov, I. V. Vlassiouk, R. R. Unocic, G. M. Veith, S. Dai and S. M. Mahurin, *Nat. Nanotechnol.*, 2015, **10**, 459.
40 J. Ge, L.-A. Shi, Y.-C. Wang, H.-Y. Zhao, H.-B. Yao, Y.-B. Zhu, Y. Zhang, H.-W. Zhu, H.-A. Wu and S.-H. Yu, *Nat. Nanotechnol.*, 2017, **12**, 434.
41 F. Haque, T. Daeneke, K. Kalantar-zadeh and J. Z. Ou, *Nano-Micro Lett.*, 2018, **10**, 23.
42 C. Liu, D. Kong, P.-C. Hsu, H. Yuan, H.-W. Lee, Y. Liu, H. Wang, S. Wang, K. Yan, D. Lin, P. A. Maraccini, K. M. Parker, A. B. Boehm and Y. Cui, *Nat. Nanotechnol.*, 2016, **11**, 1098.
43 Y. Oh, D. L. Armstrong, C. Finnerty, S. Zheng, M. Hu, A. Torrents and B. Mi, *J. Membr. Sci.*, 2017, **541**, 235–243.
44 M. Zhang, G. Feng, Z. Song, Y.-P. Zhou, H.-Y. Chao, D. Yuan, T. T. Y. Tan, Z. Guo, Z. Hu, B. Z. Tang, B. Liu and D. Zhao, *J. Am. Chem. Soc.*, 2014, **136**, 7241–7244.
45 V. Nicolosi, M. Chhowalla, M. G. Kanatzidis, M. S. Strano and J. N. Coleman, *Science*, 2013, **340**, 1226419.
46 L. Fu, H. Yang, A. Tang and Y. Hu, *Nano Res.*, 2017, **10**, 2782–2799.
47 U. S. G. Survey, One estimate of global water distribution, http://water.usgs.gov/edu/gallery/watercyclekids/earth-water-distribution.html, accessed May 25, 2020.
48 B. Luo, G. Liu and L. Wang, *Nanoscale*, 2016, **8**, 6904–6920.
49 Z. Wang and B. Mi, *Environ. Sci. Technol.*, 2017, **51**, 8229–8244.
50 Z. Zheng, R. Grünker and X. Feng, *Adv. Mater.*, 2016, **28**, 6529–6545.
51 M. Zeng and Y. Zhang, *J. Mater. Chem. A*, 2019, **7**, 23301–23336.
52 M. Fathizadeh, W. L. Xu, F. Zhou, Y. Yoon and M. Yu, *Adv. Mater. Interfaces*, 2017, **4**, 1600918.
53 G. Liu, W. Jin and N. Xu, *Angew. Chem., Int. Ed.*, 2016, **55**, 13384–13397.
54 M. Zeng, I. Echols, P. Wang, S. Lei, J. Luo, B. Peng, L. He, L. Zhang, D. Huang, C. Mejia, L. Wang, M. S. Mannan and Z. Cheng, *ACS Sustainable Chem. Eng.*, 2018, **6**, 3879–3887.
55 P. M. Biesheuvel, L. Zhang, P. Gasquet, B. Blankert, M. Elimelech and W. G. J. van der Meer, *Environ. Sci. Technol. Lett.*, 2020, **7**, 42–47.
56 J. Zhu, J. Hou, A. Uliana, Y. Zhang, M. Tian and B. Van der Bruggen, *J. Mater. Chem. A*, 2018, **6**, 3773–3792.
57 S. Homaeigohar and M. Elbahri, *NPG Asia Mater.*, 2017, **9**, e427.
58 J. R. Werber, C. O. Osuji and M. Elimelech, *Nat. Rev. Mater.*, 2016, **1**, 16018.
59 P. Wang, *Environ. Sci.: Nano*, 2018, **5**, 1078–1089.
60 G. Liu, J. Xu and K. Wang, *Nano Energy*, 2017, **41**, 269–284.
61 A. K. Ghosh, B.-H. Jeong, X. Huang and E. M. V. Hoek, *J. Membr. Sci.*, 2008, **311**, 34–45.
62 N. Wang, S. Ji, G. Zhang, J. Li and L. Wang, *Chem. Eng. J.*, 2012, **213**, 318–329.
63 J. Zhu, M. Tian, J. Hou, J. Wang, J. Lin, Y. Zhang, J. Liu and B. Van der Bruggen, *J. Mater. Chem. A*, 2016, **4**, 1980–1990.
64 Q. Nan, P. Li and B. Cao, *Appl. Surf. Sci.*, 2016, **387**, 521–528.
65 G. S. Lai, W. J. Lau, P. S. Goh, A. F. Ismail, N. Yusof and Y. H. Tan, *Desalination*, 2016, **387**, 14–24.
66 M. Safarpour, V. Vatanpour, A. Khataee and M. Esmaeili, *Sep. Purif. Technol.*, 2015, **154**, 96–107.
67 Z. Wang, A. Sim, J. J. Urban and B. Mi, *Environ. Sci. Technol.*, 2018, **52**, 9741–9748.
68 L. Sun, H. Huang and X. Peng, *Chem. Commun.*, 2013, **49**, 10718–10720.
69 L. Sun, Y. Ying, H. Huang, Z. Song, Y. Mao, Z. Xu and X. Peng, *ACS Nano*, 2014, **8**, 6304–6311.
70 L. Ding, Y. Wei, Y. Wang, H. Chen, J. Caro and H. Wang, *Angew. Chem., Int. Ed.*, 2017, **56**, 1825–1829.
71 Y. Yu, H. Chen, Y. Liu, V. S. J. Craig, C. Wang, L. H. Li and Y. Chen, *Adv. Mater. Interfaces*, 2015, **2**, 1400267.
72 H. Zhao, S. Chen, X. Quan, H. Yu and H. Zhao, *Appl. Catal., B*, 2016, **194**, 134–140.
73 M. D. Fischbein and M. Drndić, *Appl. Phys. Lett.*, 2008, **93**, 113107.
74 S. C. O'Hern, M. S. H. Boutilier, J.-C. Idrobo, Y. Song, J. Kong, T. Laoui, M. Atieh and R. Karnik, *Nano Lett.*, 2014, **14**, 1234–1241.
75 J. Feng, M. Graf, K. Liu, D. Ovchinnikov, D. Dumcenco, M. Heiranian, V. Nandigana, N. R. Aluru, A. Kis and A. Radenovic, *Nature*, 2016, **536**, 197.
76 D. Cohen-Tanugi and J. C. Grossman, *Nano Lett.*, 2012, **12**, 3602–3608.
77 W. Li, Y. Yang, J. K. Weber, G. Zhang and R. Zhou, *ACS Nano*, 2016, **10**, 1829–1835.
78 A. Nicolaï, B. G. Sumpter and V. Meunier, *Phys. Chem. Chem. Phys.*, 2014, **16**, 8646–8654.
79 M. Hu and B. Mi, *Environ. Sci. Technol.*, 2013, **47**, 3715–3723.
80 S. Garaj, S. Liu, J. A. Golovchenko and D. Branton, *Proc. Natl. Acad. Sci. U. S. A.*, 2013, **110**, 12192–12196.
81 S. C. O'Hern, C. A. Stewart, M. S. H. Boutilier, J.-C. Idrobo, S. Bhaviripudi, S. K. Das, J. Kong, T. Laoui, M. Atieh and R. Karnik, *ACS Nano*, 2012, **6**, 10130–10138.

82 C. J. Russo and J. A. Golovchenko, *Proc. Natl. Acad. Sci. U. S. A.*, 2012, **109**, 5953–5957.
83 S. P. Koenig, L. Wang, J. Pellegrino and J. S. Bunch, *Nat. Nanotechnol.*, 2012, **7**, 728.
84 Y. C. Cheng, T. P. Kaloni, Z. Y. Zhu and U. Schwingenschlögl, *Appl. Phys. Lett.*, 2012, **101**, 073110.
85 S. Wu, R. Yang, D. Shi and G. Zhang, *Nanoscale*, 2012, **4**, 2005–2009.
86 J. Feng, K. Liu, M. Graf, M. Lihter, R. D. Bulushev, D. Dumcenco, D. T. L. Alexander, D. Krasnozhon, T. Vuletic, A. Kis and A. Radenovic, *Nano Lett.*, 2015, **15**, 3431–3438.
87 S. C. O'Hern, D. Jang, S. Bose, J.-C. Idrobo, Y. Song, T. Laoui, J. Kong and R. Karnik, *Nano Lett.*, 2015, **15**, 3254–3260.
88 D. Cohen-Tanugi, L.-C. Lin and J. C. Grossman, *Nano Lett.*, 2016, **16**, 1027–1033.
89 B. Mi, *Science*, 2014, **343**, 740–742.
90 L. Chen, G. Shi, J. Shen, B. Peng, B. Zhang, Y. Wang, F. Bian, J. Wang, D. Li, Z. Qian, G. Xu, G. Liu, J. Zeng, L. Zhang, Y. Yang, G. Zhou, M. Wu, W. Jin, J. Li and H. Fang, *Nature*, 2017, **550**, 380–383.
91 L. Nie, K. Goh, Y. Wang, J. Lee, Y. Huang, H. E. Karahan, K. Zhou, M. D. Guiver and T.-H. Bae, *Sci. Adv.*, 2020, **6**, eaaz9184.
92 B. X. Chen, W. F. Zhang, X. H. Zhou, X. Huang, X. M. Zhao, H. T. Wang, M. Liu, Y. L. Lu and S. F. Yang, *Nano Energy*, 2013, **2**, 906–915.
93 C.-H. Tsou, Q.-F. An, S.-C. Lo, M. De Guzman, W.-S. Hung, C.-C. Hu, K.-R. Lee and J.-Y. Lai, *J. Membr. Sci.*, 2015, **477**, 93–100.
94 W. L. Xu, C. Fang, F. Zhou, Z. Song, Q. Liu, R. Qiao and M. Yu, *Nano Lett.*, 2017, **17**, 2928–2933.
95 J. Borges and J. F. Mano, *Chem. Rev.*, 2014, **114**, 8883–8942.
96 Y. Gao, M. Hu and B. Mi, *J. Membr. Sci.*, 2014, **455**, 349–356.
97 J. Zhao, Y. Zhu, F. Pan, G. He, C. Fang, K. Cao, R. Xing and Z. Jiang, *J. Membr. Sci.*, 2015, **487**, 162–172.
98 Y. Wang, L. Li, Y. Wei, J. Xue, H. Chen, L. Ding, J. Caro and H. Wang, *Angew. Chem., Int. Ed.*, 2017, **56**, 8974–8980.
99 L. Ding, L. Li, Y. Liu, Y. Wu, Z. Lu, J. Deng, Y. Wei, J. Caro and H. Wang, *Nat. Sustain.*, 2020, **3**, 296–302.
100 X. Xie, C. Chen, N. Zhang, Z.-R. Tang, J. Jiang and Y.-J. Xu, *Nat. Sustain.*, 2019, **2**, 856–862.
101 R. K. Joshi, P. Carbone, F. C. Wang, V. G. Kravets, Y. Su, I. V. Grigorieva, H. A. Wu, A. K. Geim and R. R. Nair, *Science*, 2014, **343**, 752–754.
102 Y. Long, K. Wang, G. Xiang, K. Song, G. Zhou and X. Wang, *Adv. Mater.*, 2017, **29**, 1606093.
103 H. B. Park, J. Kamcev, L. M. Robeson, M. Elimelech and B. D. Freeman, *Science*, 2017, **356**, eaab0530.
104 R. Zhang, Y. Liu, M. He, Y. Su, X. Zhao, M. Elimelech and Z. Jiang, *Chem. Soc. Rev.*, 2016, **45**, 5888–5924.
105 X. Lu, X. Feng, J. R. Werber, C. Chu, I. Zucker, J.-H. Kim, C. O. Osuji and M. Elimelech, *Proc. Natl. Acad. Sci. U. S. A.*, 2017, **114**, E9793–E9801.
106 F. Perreault, A. F. de Faria, S. Nejati and M. Elimelech, *ACS Nano*, 2015, **9**, 7226–7236.
107 A. F. Faria, C. Liu, M. Xie, F. Perreault, L. D. Nghiem, J. Ma and M. Elimelech, *J. Membr. Sci.*, 2017, **525**, 146–156.
108 K. Zodrow, L. Brunet, S. Mahendra, D. Li, A. Zhang, Q. Li and P. J. J. Alvarez, *Water Res.*, 2009, **43**, 715–723.
109 L. Zhou, Y. Tan, J. Wang, W. Xu, Y. Yuan, W. Cai, S. Zhu and J. Zhu, *Nat. Photonics*, 2016, **10**, 393.
110 P. Zhang, J. Li, L. Lv, Y. Zhao and L. Qu, *ACS Nano*, 2017, **11**, 5087–5093.
111 C.-H. Liu, Y.-C. Chang, T. B. Norris and Z. Zhong, *Nat. Nanotechnol.*, 2014, **9**, 273.
112 H. Ghasemi, G. Ni, A. M. Marconnet, J. Loomis, S. Yerci, N. Miljkovic and G. Chen, *Nat. Commun.*, 2014, **5**, 4449.
113 O. Neumann, C. Feronti, A. D. Neumann, A. Dong, K. Schell, B. Lu, E. Kim, M. Quinn, S. Thompson, N. Grady, P. Nordlander, M. Oden and N. J. Halas, *Proc. Natl. Acad. Sci. U. S. A.*, 2013, **110**, 11677–11681.
114 A. Lenert, D. M. Bierman, Y. Nam, W. R. Chan, I. Celanović, M. Soljačić and E. N. Wang, *Nat. Nanotechnol.*, 2014, **9**, 126.
115 J. B. Chou, Y. X. Yeng, Y. E. Lee, A. Lenert, V. Rinnerbauer, I. Celanovic, M. Soljačić, N. X. Fang, E. N. Wang and S.-G. Kim, *Adv. Mater.*, 2014, **26**, 8041–8045.
116 J.-H. Lee, Y.-S. Kim, K. Constant and K.-M. Ho, *Adv. Mater.*, 2007, **19**, 791–794.
117 K. A. Arpin, M. D. Losego, A. N. Cloud, H. Ning, J. Mallek, N. P. Sergeant, L. Zhu, Z. Yu, B. Kalanyan, G. N. Parsons, G. S. Girolami, J. R. Abelson, S. Fan and P. V. Braun, *Nat. Commun.*, 2013, **4**, 2630.
118 J. Zhu, Z. Yu, G. F. Burkhard, C.-M. Hsu, S. T. Connor, Y. Xu, Q. Wang, M. McGehee, S. Fan and Y. Cui, *Nano Lett.*, 2009, **9**, 279–282.
119 J. P. Mailoa, A. J. Akey, C. B. Simmons, D. Hutchinson, J. Mathews, J. T. Sullivan, D. Recht, M. T. Winkler, J. S. Williams, J. M. Warrender, P. D. Persans, M. J. Aziz and T. Buonassisi, *Nat. Commun.*, 2014, **5**, 3011.
120 F. J. García-Vidal, J. M. Pitarke and J. B. Pendry, *Phys. Rev. Lett.*, 1997, **78**, 4289–4292.
121 J. Q. Xi, M. F. Schubert, J. K. Kim, E. F. Schubert, M. Chen, S.-Y. Lin, W. Liu and J. A. Smart, *Nat. Photonics*, 2007, **1**, 176.
122 L. Zhou, Y. Tan, D. Ji, B. Zhu, P. Zhang, J. Xu, Q. Gan, Z. Yu and J. Zhu, *Sci. Adv.*, 2016, **2**, e1501227.
123 Z. Yu, A. Raman and S. Fan, *Proc. Natl. Acad. Sci. U. S. A.*, 2010, **107**, 17491–17496.
124 S. Wu, G. Xiong, H. Yang, Y. Tian, B. Gong, H. Wan, Y. Wang, T. S. Fisher, J. Yan, K. Cen, Z. Bo and K. Ostrikov, *Matter*, 2019, **1**, 1017–1032.
125 B. Huo, D. Jiang, X. Cao, H. Liang, Z. Liu, C. Li and J. Liu, *Carbon*, 2019, **142**, 13–19.
126 Z. Hong, J. Pei, Y. Wang, B. Cao, M. Mao, H. Liu, H. Jiang, Q. An, X. Liu and X. Hu, *Energy Convers. Manage.*, 2019, **199**, 112019.
127 N. Yousefi, X. Lu, M. Elimelech and N. Tufenkji, *Nat. Nanotechnol.*, 2019, **14**, 107–119.
128 F. Wang, D. Wei, Y. Li, T. Chen, P. Mu, H. Sun, Z. Zhu, W. Liang and A. Li, *J. Mater. Chem. A*, 2019, **7**, 18311–18317.

129 P. Qiao, J. Wu, H. Li, Y. Xu, L. Ren, K. Lin and W. Zhou, *ACS Appl. Mater. Interfaces*, 2019, **11**, 7066–7073.
130 S. Lei, M. Zeng, D. Huang, L. Wang, L. Zhang, B. Xi, W. Ma, G. Chen and Z. Cheng, *ACS Sustainable Chem. Eng.*, 2019, **7**, 13708–13716.
131 A. Klinkova, R. M. Choueiri and E. Kumacheva, *Chem. Soc. Rev.*, 2014, **43**, 3976–3991.
132 S. Dutta, A. Bhaumik and K. C. W. Wu, *Energy Environ. Sci.*, 2014, **7**, 3574–3592.
133 Z. Nie, A. Petukhova and E. Kumacheva, *Nat. Nanotechnol.*, 2009, **5**, 15.
134 M. Grzelczak, J. Vermant, E. M. Furst and L. M. Liz-Marzán, *ACS Nano*, 2010, **4**, 3591–3605.
135 M. R. Gartia, A. Hsiao, A. Pokhriyal, S. Seo, G. Kulsharova, B. T. Cunningham, T. C. Bond and G. L. Liu, *Adv. Opt. Mater.*, 2013, **1**, 68–76.
136 X. Sheng, J. Liu, I. Kozinsky, A. M. Agarwal, J. Michel and L. C. Kimerling, *Adv. Mater.*, 2011, **23**, 843–847.
137 W. Lee, R. Ji, U. Gösele and K. Nielsch, *Nat. Mater.*, 2006, **5**, 741.
138 N. I. Landy, S. Sajuyigbe, J. J. Mock, D. R. Smith and W. J. Padilla, *Phys. Rev. Lett.*, 2008, **100**, 207402.
139 K. Aydin, V. E. Ferry, R. M. Briggs and H. A. Atwater, *Nat. Commun.*, 2011, **2**, 517.
140 T. Søndergaard, S. M. Novikov, T. Holmgaard, R. L. Eriksen, J. Beermann, Z. Han, K. Pedersen and S. I. Bozhevolnyi, *Nat. Commun.*, 2012, **3**, 969.
141 Y. Cui, K. H. Fung, J. Xu, H. Ma, Y. Jin, S. He and N. X. Fang, *Nano Lett.*, 2012, **12**, 1443–1447.
142 X. Xiong, S.-C. Jiang, Y.-H. Hu, R.-W. Peng and M. Wang, *Adv. Mater.*, 2013, **25**, 3994–4000.
143 J. Zhou, A. F. Kaplan, L. Chen and L. J. Guo, *ACS Photonics*, 2014, **1**, 618–624.
144 J. A. Bossard, L. Lin, S. Yun, L. Liu, D. H. Werner and T. S. Mayer, *ACS Nano*, 2014, **8**, 1517–1524.
145 M. L. Brongersma, N. J. Halas and P. Nordlander, *Nat. Nanotechnol.*, 2015, **10**, 25.
146 S. Shukla, K.-T. Kim, A. Baev, Y. K. Yoon, N. M. Litchinitser and P. N. Prasad, *ACS Nano*, 2010, **4**, 2249–2255.
147 R. A. Pala, J. S. Q. Liu, E. S. Barnard, D. Askarov, E. C. Garnett, S. Fan and M. L. Brongersma, *Nat. Commun.*, 2013, **4**, 2095.
148 A. P. Raman, M. A. Anoma, L. Zhu, E. Rephaeli and S. Fan, *Nature*, 2014, **515**, 540.
149 F. Cao, K. McEnaney, G. Chen and Z. Ren, *Energy Environ. Sci.*, 2014, **7**, 1615–1627.
150 M. Wang, J. Zhang, P. Wang, C. Li, X. Xu and Y. Jin, *Nano Res.*, 2018, **11**, 3854–3863.
151 F. Zhao, X. Zhou, Y. Shi, X. Qian, M. Alexander, X. Zhao, S. Mendez, R. Yang, L. Qu and G. Yu, *Nat. Nanotechnol.*, 2018, **13**, 489–495.
152 K. Bae, G. Kang, S. K. Cho, W. Park, K. Kim and W. J. Padilla, *Nat. Commun.*, 2015, **6**, 10103.
153 M. S. Zielinski, J.-W. Choi, T. La Grange, M. Modestino, S. M. H. Hashemi, Y. Pu, S. Birkhold, J. A. Hubbell and D. Psaltis, *Nano Lett.*, 2016, **16**, 2159–2167.
154 C. Li, Y. Goswami and E. Stefanakos, *Renewable Sustainable Energy Rev.*, 2013, **19**, 136–163.
155 Z. Liu, H. Song, D. Ji, C. Li, A. Cheney, Y. Liu, N. Zhang, X. Zeng, B. Chen, J. Gao, Y. Li, X. Liu, D. Aga, S. Jiang, Z. Yu and Q. Gan, *Global Challenges*, 2017, **1**, 1600003.
156 X. Li, W. Xu, M. Tang, L. Zhou, B. Zhu, S. Zhu and J. Zhu, *Proc. Natl. Acad. Sci. U. S. A.*, 2016, **113**, 13953–13958.
157 M. Elimelech and W. A. Phillip, *Science*, 2011, **333**, 712–717.
158 L. Zhang, B. Tang, J. Wu, R. Li and P. Wang, *Adv. Mater.*, 2015, **27**, 4889–4894.
159 J. Jean, P. R. Brown, R. L. Jaffe, T. Buonassisi and V. Bulović, *Energy Environ. Sci.*, 2015, **8**, 1200–1219.
160 M. S. Romano, N. Li, D. Antiohos, J. M. Razal, A. Nattestad, S. Beirne, S. Fang, Y. Chen, R. Jalili, G. G. Wallace, R. Baughman and J. Chen, *Adv. Mater.*, 2013, **25**, 6602–6606.
161 X. Hu, W. Xu, L. Zhou, Y. Tan, Y. Wang, S. Zhu and J. Zhu, *Adv. Mater.*, 2017, **29**, 1604031.
162 Y. Ito, Y. Tanabe, J. Han, T. Fujita, K. Tanigaki and M. Chen, *Adv. Mater.*, 2015, **27**, 4302–4307.
163 W. Li, M. C. Tekell, Y. Huang, K. Bertelsmann, M. Lau and D. Fan, *Adv. Energy Mater.*, 2018, **8**, 1802108.
164 S. N. Shirodkar and U. V. Waghmare, *Phys. Rev. Lett.*, 2014, **112**, 157601.
165 Y.-C. Lin, D. O. Dumcenco, Y.-S. Huang and K. Suenaga, *Nat. Nanotechnol.*, 2014, **9**, 391.
166 D. Ghim, Q. Jiang, S. Cao, S. Singamaneni and Y.-S. Jun, *Nano Energy*, 2018, **53**, 949–957.
167 X. Zhao, X.-J. Zha, J.-H. Pu, L. Bai, R.-Y. Bao, Z.-Y. Liu, M.-B. Yang and W. Yang, *J. Mater. Chem. A*, 2019, **7**, 10446–10455.
168 R. Li, L. Zhang, L. Shi and P. Wang, *ACS Nano*, 2017, **11**, 3752–3759.
169 X. Li, R. Lin, G. Ni, N. Xu, X. Hu, B. Zhu, G. Lv, J. Li, S. Zhu and J. Zhu, *Natl. Sci. Rev.*, 2018, **5**, 70–77.
170 J. Zhao, Y. Yang, C. Yang, Y. Tian, Y. Han, J. Liu, X. Yin and W. Que, *J. Mater. Chem. A*, 2018, **6**, 16196–16204.
171 P. D. Dongare, A. Alabastri, S. Pedersen, K. R. Zodrow, N. J. Hogan, O. Neumann, J. Wu, T. Wang, A. Deshmukh and M. Elimelech, *Proc. Natl. Acad. Sci. U. S. A.*, 2017, **114**, 6936–6941.
172 W. Xu, X. Hu, S. Zhuang, Y. Wang, X. Li, L. Zhou, S. Zhu and J. Zhu, *Adv. Energy Mater.*, 2018, **8**, 1702884.
173 Y. Yang, X. Yang, L. Fu, M. Zou, A. Cao, Y. Du, Q. Yuan and C.-H. Yan, *ACS Energy Lett.*, 2018, **3**, 1165–1171.
174 G. Li, W.-C. Law and K. C. Chan, *Green Chem.*, 2018, **20**, 3689–3695.
175 Q. Zhao, C. Du, Y. Jia, J. Yuan, G. Song, X. Zhou, S. Sun, C. Zhou, L. Zhao and S. Yang, *Chem. Eng. J.*, 2020, **387**, 124131.
176 H.-N. Li, J. Yang and Z.-K. Xu, *Adv. Mater. Interfaces*, 2020, 1902064.
177 D.-D. Qin, Y.-J. Zhu, R.-L. Yang and Z.-C. Xiong, *Nanoscale*, 2020, **12**, 6717–6728.
178 A. Jernelöv, *Nature*, 2010, **466**, 182.
179 C. H. Peterson, S. D. Rice, J. W. Short, D. Esler, J. L. Bodkin, B. E. Ballachey and D. B. Irons, *Science*, 2003, **302**, 2082–2086.

180 E. B. Kujawinski, M. C. Kido Soule, D. L. Valentine, A. K. Boysen, K. Longnecker and M. C. Redmond, *Environ. Sci. Technol.*, 2011, **45**, 1298–1306.
181 X. Wang, M. Zeng, Y.-H. Yu, H. Wang, M. S. Mannan and Z. Cheng, *ACS Appl. Mater. Interfaces*, 2017, **9**, 7852–7858.
182 J. Luo, M. Zeng, B. Peng, Y. Tang, L. Zhang, P. Wang, L. He, D. Huang, L. Wang, X. Wang, M. Chen, S. Lei, P. Lin, Y. Chen and Z. Cheng, *Angew. Chem., Int. Ed.*, 2018, **57**, 11752–11757.
183 L. Zhang, Q. Lei, J. Luo, M. Zeng, L. Wang, D. Huang, X. Wang, S. Mannan, B. Peng and Z. Cheng, *Sci. Rep.*, 2019, **9**, 163.
184 A. Vidyasagar, K. Handore and K. M. Sureshan, *Angew. Chem., Int. Ed.*, 2011, **50**, 8021–8024.
185 I. Buist, J. McCourt, S. Potter, S. Ross and K. Trudel, *Pure Appl. Chem.*, 1999, **71**, 43–65.
186 V. Broje and A. A. Keller, *Environ. Sci. Technol.*, 2006, **40**, 7914–7918.
187 D. Mullangi, S. Shalini, S. Nandi, B. Choksi and R. Vaidhyanathan, *J. Mater. Chem. A*, 2017, **5**, 8376–8384.
188 A. Cassie, *Trans. Faraday Soc.*, 1944, **40**, 546.
189 R. N. Wenzel, *Ind. Eng. Chem.*, 1936, **28**, 988–994.
190 K. Jayaramulu, K. K. R. Datta, C. Rösler, M. Petr, M. Otyepka, R. Zboril and R. A. Fischer, *Angew. Chem., Int. Ed.*, 2016, **55**, 1178–1182.
191 A. Lafuma and D. Quéré, *Nat. Mater.*, 2003, **2**, 457.
192 R. Blossey, *Nat. Mater.*, 2003, **2**, 301.
193 T. Sun, G. Wang, H. Liu, L. Feng, L. Jiang and D. Zhu, *J. Am. Chem. Soc.*, 2003, **125**, 14996–14997.
194 L. Jiang, Y. Zhao and J. Zhai, *Angew. Chem.*, 2004, **116**, 4438–4441.
195 H.-W. Liang, Q.-F. Guan, L.-F. Chen, Z. Zhu, W.-J. Zhang and S.-H. Yu, *Angew. Chem., Int. Ed.*, 2012, **51**, 5101–5105.
196 L. L. Li, G. H. Wu, G. H. Yang, J. Peng, J. W. Zhao and J. J. Zhu, *Nanoscale*, 2013, **5**, 4015–4039.
197 H.-P. Cong, X.-C. Ren, P. Wang and S.-H. Yu, *ACS Nano*, 2012, **6**, 2693–2703.
198 R. Du, X. Gao, Q. Feng, Q. Zhao, P. Li, S. Deng, L. Shi and J. Zhang, *Adv. Mater.*, 2016, **28**, 936–942.
199 J. Hou, C. Cao, F. Idrees and X. Ma, *ACS Nano*, 2015, **9**, 2556–2564.
200 S. Cai, D. Zhang, L. Shi, J. Xu, L. Zhang, L. Huang, H. Li and J. Zhang, *Nanoscale*, 2014, **6**, 7346–7353.
201 W. Jiang, M. S. Pacella, D. Athanasiadou, V. Nelea, H. Vali, R. M. Hazen, J. J. Gray and M. D. McKee, *Nat. Commun.*, 2017, **8**, 15066.
202 W. J. Roth, B. Gil, W. Makowski, B. Marszalek and P. Eliášová, *Chem. Soc. Rev.*, 2016, **45**, 3400–3438.
203 R. Schreiber, J. Do, E.-M. Roller, T. Zhang, V. J. Schüller, P. C. Nickels, J. Feldmann and T. Liedl, *Nat. Nanotechnol.*, 2014, **9**, 74–78.
204 M. Zeng, P. Wang, J. Luo, B. Peng, B. Ding, L. Zhang, L. Wang, D. Huang, I. Echols, E. Abo Deeb, E. Bordovsky, C.-H. Choi, C. Ybanez, P. Meras, E. Situ, M. S. Mannan and Z. Cheng, *ACS Appl. Mater. Interfaces*, 2018, **10**, 22793–22800.
205 I. Ali, *Chem. Rev.*, 2012, **112**, 5073–5091.
206 N. Ahmad, H. A. Younus, A. H. Chughtai, K. Van Hecke, Z. A. K. Khattak, Z. Gaoke, M. Danish and F. Verpoort, *Catal. Sci. Technol.*, 2018, **8**, 4010–4017.
207 J.-J. Li, C.-C. Wang, H.-f. Fu, J.-R. Cui, P. Xu, J. Guo and J.-R. Li, *Dalton Trans.*, 2017, **46**, 10197–10201.
208 A. T. Massey, R. Gusain, S. Kumari and O. P. Khatri, *Ind. Eng. Chem. Res.*, 2016, **55**, 7124–7131.
209 X. Wang, J. Ding, S. Yao, X. Wu, Q. Feng, Z. Wang and B. Geng, *J. Mater. Chem. A*, 2014, **2**, 15958–15963.
210 S. Wang, H. Sun, H. M. Ang and M. O. Tadé, *Chem. Eng. J.*, 2013, **226**, 336–347.
211 X. Gao, X. Wang, X. Ouyang and C. Wen, *Sci. Rep.*, 2016, **6**, 27207.
212 H. Tang, H. Huang, X. Wang, K. Wu, G. Tang and C. Li, *Appl. Surf. Sci.*, 2016, **379**, 296–303.
213 H. J. Song, S. You, X. H. Jia and J. Yang, *Ceram. Int.*, 2015, **41**, 13896–13902.
214 J. H. Duffus, *Pure Appl. Chem.*, 2002, **74**, 793–807.
215 C. Zhu, Z. Luan, Y. Wang and X. Shan, *Sep. Purif. Technol.*, 2007, **57**, 161–169.
216 A. B. Pérez-Marín, V. M. Zapata, J. F. Ortuño, M. Aguilar, J. Sáez and M. Lloréns, *J. Hazard. Mater.*, 2007, **139**, 122–131.
217 F.-S. Zhang, J. O. Nriagu and H. Itoh, *Water Res.*, 2005, **39**, 389–395.
218 C. Green-Ruiz, *Bioresour. Technol.*, 2006, **97**, 1907–1911.
219 G. Bayramoğlu and M. Y. Arica, *J. Hazard. Mater.*, 2007, **144**, 449–457.
220 H. Sigel, *Metal Ions in Biological Systems: Volume 20: Concepts on Metal Ion Toxicity*, CRC Press, 1986.
221 D. Z. John, *Handbook of Drinking Water Quality: Standards and Controls*, Van Nostrand Reinhold, New York, 1990.
222 L. Jie, L. Jing, X. Xuewen, Z. Xinghua, X. Yanming, M. Jiao, M. Zhaojun, F. Ying, H. Long, Y. Xiaojing, Z. Jun, M. Fanbin, Y. Songdong and T. Chengchun, *Nanotechnology*, 2013, **24**, 155603.
223 H. Yang, J.-H. Bahk, T. Day, A. M. S. Mohammed, B. Min, G. J. Snyder, A. Shakouri and Y. Wu, *Nano Lett.*, 2014, **14**, 5398–5404.
224 Z. Liu, Y. Fang, H. Jia, C. Wang, Q. Song, L. Li, J. Lin, Y. Huang, C. Yu and C. Tang, *Sci. Rep.*, 2018, **8**, 1104.
225 J. Wan, S. D. Lacey, J. Dai, W. Bao, M. S. Fuhrer and L. Hu, *Chem. Soc. Rev.*, 2016, **45**, 6742–6765.
226 L. Wang, W. Tao, L. Yuan, Z. Liu, Q. Huang, Z. Chai, J. K. Gibson and W. Shi, *Chem. Commun.*, 2017, **53**, 12084–12087.
227 Z. Chen, Y. Liang, D. Jia, W. Chen, Z. Cui and X. Wang, *Environ. Sci.: Nano*, 2017, **4**, 1851–1858.
228 F. Zhao, M. Peydayesh, Y. Ying, R. Mezzenga and J. Ping, *ACS Appl. Mater. Interfaces*, 2020, **12**, 24521–24530.
229 N. Huang, L. Zhai, H. Xu and D. Jiang, *J. Am. Chem. Soc.*, 2017, **139**, 2428–2434.
230 G. Abate and J. C. Masini, *Colloids Surf., A*, 2005, **262**, 33–39.
231 O. Abollino, A. Giacomino, M. Malandrino and E. Mentasti, *Appl. Clay Sci.*, 2008, **38**, 227–236.

232 A. A. El-Bayaa, N. A. Badawy and E. A. AlKhalik, *J. Hazard. Mater.*, 2009, **170**, 1204–1209.
233 M. Malandrino, O. Abollino, A. Giacomino, M. Aceto and E. Mentasti, *J. Colloid Interface Sci.*, 2006, **299**, 537–546.
234 D. Yang, Z. Zheng, H. Liu, H. Zhu, X. Ke, Y. Xu, D. Wu and Y. Sun, *J. Phys. Chem. C*, 2008, **112**, 16275–16280.
235 S. Sarina, A. Bo, D. Liu, H. Liu, D. Yang, C. Zhou, N. Maes, S. Komarneni and H. Zhu, *Chem. Mater.*, 2014, **26**, 4788–4795.
236 J. Cai, M. Lei, Q. Zhang, J.-R. He, T. Chen, S. Liu, S.-H. Fu, T.-T. Li, G. Liu and P. Fei, *Composites, Part A*, 2017, **92**, 10–16.
237 S.-H. Lin and R.-S. Juang, *J. Hazard. Mater.*, 2002, **92**, 315–326.
238 B. C. Kross, A. D. Ayebo and L. J. Fuortes, *Am. Fam. Physician*, 1992, **46**, 183–188.
239 D. A. Almasri, T. Rhadfi, M. A. Atieh, G. McKay and S. Ahzi, *Chem. Eng. J.*, 2018, **335**, 1–12.
240 Y. Ying, Y. Liu, X. Wang, Y. Mao, W. Cao, P. Hu and X. Peng, *ACS Appl. Mater. Interfaces*, 2015, **7**, 1795–1803.
241 J. Das, B. S. Patra, N. Baliarsingh and K. M. Parida, *Appl. Clay Sci.*, 2006, **32**, 252–260.
242 S. Mandal and S. Mayadevi, *Appl. Clay Sci.*, 2008, **40**, 54–62.
243 A. Legrouri, M. Lakraimi, A. Barroug, A. De Roy and J. P. Besse, *Water Res.*, 2005, **39**, 3441–3448.
244 Y. You, H. Zhao and G. F. Vance, *Colloids Surf., A*, 2002, **205**, 161–172.
245 X. Wu, X. Tan, S. Yang, T. Wen, H. Guo, X. Wang and A. Xu, *Water Res.*, 2013, **47**, 4159–4168.
246 L. Ma, S. M. Islam, H. Liu, J. Zhao, G. Sun, H. Li, S. Ma and M. G. Kanatzidis, *Chem. Mater.*, 2017, **29**, 3274–3284.
247 H.-R. Fu, Z.-X. Xu and J. Zhang, *Chem. Mater.*, 2015, **27**, 205–210.
248 Y. L. F. Musico, C. M. Santos, M. L. P. Dalida and D. F. Rodrigues, *J. Mater. Chem. A*, 2013, **1**, 3789–3796.
249 B.-M. Jun, N. Her, C. M. Park and Y. Yoon, *Environ. Sci.: Water Res. Technol.*, 2020, **6**, 173–180.
250 Y. Wang, S. Liang, B. Chen, F. Guo, S. Yu and Y. Tang, *PLoS One*, 2013, **8**, e65634.
251 R. Li, H. Deng, X. Zhang, J. J. Wang, M. K. Awasthi, Q. Wang, R. Xiao, B. Zhou, J. Du and Z. Zhang, *Bioresour. Technol.*, 2019, **273**, 335–340.
252 F. Zhang, B. Wang, S. He and R. Man, *J. Chem. Eng. Data*, 2014, **59**, 1719–1726.
253 X. Li, H. Zhou, W. Wu, S. Wei, Y. Xu and Y. Kuang, *J. Colloid Interface Sci.*, 2015, **448**, 389–397.
254 S. Kumar, R. R. Nair, P. B. Pillai, S. N. Gupta, M. A. R. Iyengar and A. K. Sood, *ACS Appl. Mater. Interfaces*, 2014, **6**, 17426–17436.
255 D. Zhao, L. Chen, M. Xu, S. Feng, Y. Ding, M. Wakeel, N. S. Alharbi and C. Chen, *ACS Sustainable Chem. Eng.*, 2017, **5**, 10290–10297.
256 K. Zhang, H. Li, X. Xu and H. Yu, *Microporous Mesoporous Mater.*, 2018, **255**, 7–14.
257 Y. Fang, Q. Huang, P. Liu, J. Shi and G. Xu, *Colloids Surf., A*, 2018, **540**, 112–122.
258 C. Tian, X. Xiang, J. Wu, B. Li, C. Cai, B. Khan, H. Chen, Y. Yuan and X. Zu, *J. Chem. Eng. Data*, 2018, **63**, 3966–3974.
259 H. Dang, L. Chen, L. Chen, M. Yuan, Z. Yan and M. Li, *Mater. Lett.*, 2019, **254**, 42–45.
260 N.-N. Wang, H. Wang, Y.-Y. Wang, Y.-H. Wei, J.-Y. Si, A. C. Y. Yuen, J.-S. Xie, B. Yu, S.-E. Zhu, H.-D. Lu, W. Yang, Q. N. Chan and G.-H. Yeoh, *ACS Appl. Mater. Interfaces*, 2019, **11**, 40512–40523.
261 M. Bystrzejewski, A. Huczko and H. Lange, *Mater. Chem. Phys.*, 2008, **107**, 322–327.
262 X. Chen, S. Shen, L. Guo and S. S. Mao, *Chem. Rev.*, 2010, **110**, 6503–6570.
263 M. D. Kärkäs, O. Verho, E. V. Johnston and B. Åkermark, *Chem. Rev.*, 2014, **114**, 11863–12001.
264 H. Wang, L. Zhang, Z. Chen, J. Hu, S. Li, Z. Wang, J. Liu and X. Wang, *Chem. Soc. Rev.*, 2014, **43**, 5234–5244.
265 C. S. Turchi and D. F. Ollis, *J. Catal.*, 1990, **122**, 178–192.
266 X. Zhao, D. Pan, X. Chen, R. Li, T. Jiang, W. Wang, G. Li and D. Y. C. Leung, *Appl. Surf. Sci.*, 2019, **467–468**, 658–665.
267 M. Zhou, X. W. Lou and Y. Xie, *Nano Today*, 2013, **8**, 598–618.
268 Y. Xu, M. Kraft and R. Xu, *Chem. Soc. Rev.*, 2016, **45**, 3039–3052.
269 J. Nawrocki and B. Kasprzyk-Hordern, *Appl. Catal., B*, 2010, **99**, 27–42.
270 G. Boczkaj and A. Fernandes, *Chem. Eng. J.*, 2017, **320**, 608–633.
271 S. O. Ganiyu, M. Zhou and C. A. Martínez-Huitle, *Appl. Catal., B*, 2018, **235**, 103–129.
272 E. Brillas and C. A. Martínez-Huitle, *Appl. Catal., B*, 2015, **166–167**, 603–643.
273 F. C. Moreira, R. A. R. Boaventura, E. Brillas and V. J. P. Vilar, *Appl. Catal., B*, 2017, **202**, 217–261.
274 J. L. Wang and L. J. Xu, *Crit. Rev. Environ. Sci. Technol.*, 2012, **42**, 251–325.
275 Q. Huang, S. Tian, D. Zeng, X. Wang, W. Song, Y. Li, W. Xiao and C. Xie, *ACS Catal.*, 2013, **3**, 1477–1485.
276 Q.-P. Luo, X.-Y. Yu, B.-X. Lei, H.-Y. Chen, D.-B. Kuang and C.-Y. Su, *J. Phys. Chem. C*, 2012, **116**, 8111–8117.
277 D. Xu, B. Liu, W. Zou, H. Wang and C. Zhang, *Appl. Surf. Sci.*, 2019, **487**, 91–100.
278 X. Yu, J. Liu, Y. Yu, S. Zuo and B. Li, *Carbon*, 2014, **68**, 718–724.
279 Z. Zhang, C. Shao, X. Li, Y. Sun, M. Zhang, J. Mu, P. Zhang, Z. Guo and Y. Liu, *Nanoscale*, 2013, **5**, 606–618.
280 Y. Li, L. Fang, R. Jin, Y. Yang, X. Fang, Y. Xing and S. Song, *Nanoscale*, 2015, **7**, 758–764.
281 M. Zhang, Y. Liu, L. Li, H. Gao and X. Zhang, *Catal. Commun.*, 2015, **58**, 122–126.
282 X. An, J. C. Yu and J. Tang, *J. Mater. Chem. A*, 2014, **2**, 1000–1005.
283 X. Liu, L. Pan, T. Lv, G. Zhu, Z. Sun and C. Sun, *Chem. Commun.*, 2011, **47**, 11984–11986.
284 Y. Hou, Z. Wen, S. Cui, X. Guo and J. Chen, *Adv. Mater.*, 2013, **25**, 6291–6297.
285 Y. Qu, X. Song, X. Chen, X. Fan and G. Zhang, *Chem. Eng. J.*, 2020, **382**, 123048.

286 W. Tu, Y. Zhou, Q. Liu, Z. Tian, J. Gao, X. Chen, H. Zhang, J. Liu and Z. Zou, *Adv. Funct. Mater.*, 2012, **22**, 1215–1221.
287 P. Yu, X. Zhou, Y. Yan, Z. Li and T. Zheng, *Colloids Surf., B*, 2019, **179**, 170–179.
288 S. Ma, S. Zhan, Y. Xia, P. Wang, Q. Hou and Q. Zhou, *Catal. Today*, 2019, **330**, 179–188.
289 B. Wu, Y. Li, K. Su, L. Tan, X. Liu, Z. Cui, X. Yang, Y. Liang, Z. Li, S. Zhu, K. W. K. Yeung and S. Wu, *J. Hazard. Mater.*, 2019, **377**, 227–236.
290 D. Sarkar, B. Mondal, A. Som, S. J. Ravindran, S. K. Jana, C. K. Manju and T. Pradeep, *Global Challenges*, 2018, **2**, 1800052.
291 S.-M. Lam, J.-A. Quek and J.-C. Sin, *J. Photochem. Photobiol., A*, 2018, **353**, 171–184.
292 Y. Jia, S. Zhan, S. Ma and Q. Zhou, *ACS Appl. Mater. Interfaces*, 2016, **8**, 6841–6851.
293 J. Xu, Z. Wang and Y. Zhu, *ACS Appl. Mater. Interfaces*, 2017, **9**, 27727–27735.
294 K. E. Gibson, *Curr. Opin. Virol.*, 2014, **4**, 50–57.
295 A. M. Gall, B. J. Mariñas, Y. Lu and J. L. Shisler, *PLoS Pathog.*, 2015, **11**, e1004867.
296 W. A. M. Hijnen, G. M. H. Suylen, J. A. Bahlman, A. Brouwer-Hanzens and G. J. Medema, *Water Res.*, 2010, **44**, 1224–1234.
297 Y. Li, C. Zhang, D. Shuai, S. Naraginti, D. Wang and W. Zhang, *Water Res.*, 2016, **106**, 249–258.
298 J. Qin, M. Cao, N. Li and C. Hu, *J. Mater. Chem.*, 2011, **21**, 17167–17174.
299 R. Babarao, S. Dai and D. E. Jiang, *J. Phys. Chem. B*, 2011, **115**, 9789–9794.
300 J. Guo, Y. Li, S. Zhu, Z. Chen, Q. Liu, D. Zhang, W.-J. Moon and D.-M. Song, *RSC Adv.*, 2012, **2**, 1356–1363.
301 O. Akhavan, M. Choobtashani and E. Ghaderi, *J. Phys. Chem. C*, 2012, **116**, 9653–9659.
302 C. Zhang, Y. Li, W. Zhang, P. Wang and C. Wang, *Chemosphere*, 2018, **195**, 551–558.
303 H. Miao, Z. Teng, C. Wang, H. Chong and G. Wang, *Chem. – Eur. J.*, 2019, **25**, 929–944.
304 S. P. Sahu, M. Qanbarzadeh, M. Ateia, H. Torkzadeh, A. S. Maroli and E. L. Cates, *Environ. Sci. Technol. Lett.*, 2018, **5**, 533–538.
305 S. K. Loeb, P. J. J. Alvarez, J. A. Brame, E. L. Cates, W. Choi, J. Crittenden, D. D. Dionysiou, Q. Li, G. Li-Puma, X. Quan, D. L. Sedlak, T. David Waite, P. Westerhoff and J.-H. Kim, *Environ. Sci. Technol.*, 2019, **53**, 2937–2947.
306 Y. Gong, Z. Liu, A. R. Lupini, G. Shi, J. Lin, S. Najmaei, Z. Lin, A. L. Elías, A. Berkdemir, G. You, H. Terrones, M. Terrones, R. Vajtai, S. T. Pantelides, S. J. Pennycook, J. Lou, W. Zhou and P. M. Ajayan, *Nano Lett.*, 2014, **14**, 442–449.
307 J. Ran, J. Zhang, J. Yu, M. Jaroniec and S. Z. Qiao, *Chem. Soc. Rev.*, 2014, **43**, 7787–7812.
308 X. Li, W. Bi, L. Zhang, S. Tao, W. Chu, Q. Zhang, Y. Luo, C. Wu and Y. Xie, *Adv. Mater.*, 2016, **28**, 2427–2431.
309 W. Bi, X. Li, L. Zhang, T. Jin, L. Zhang, Q. Zhang, Y. Luo, C. Wu and Y. Xie, *Nat. Commun.*, 2015, **6**, 8647.
310 Y. Ebina, T. Sasaki, M. Harada and M. Watanabe, *Chem. Mater.*, 2002, **14**, 4390–4395.
311 Z. Xing, X. Zong, Y. Zhu, Z. Chen, Y. Bai and L. Wang, *Catal. Today*, 2016, **264**, 229–235.
312 J. Tian, P. Hao, N. Wei, H. Cui and H. Liu, *ACS Catal.*, 2015, **5**, 4530–4536.
313 X. Yang, H. Xue, J. Xu, X. Huang, J. Zhang, Y.-B. Tang, T.-W. Ng, H.-L. Kwong, X.-M. Meng and C.-S. Lee, *ACS Appl. Mater. Interfaces*, 2014, **6**, 9078–9084.
314 Y. Ebina, K. Akatsuka, K. Fukuda and T. Sasaki, *Chem. Mater.*, 2012, **24**, 4201–4208.
315 H. Hata, S. Kubo, Y. Kobayashi and T. E. Mallouk, *J. Am. Chem. Soc.*, 2007, **129**, 3064–3065.
316 H. Hata, Y. Kobayashi, V. Bojan, W. J. Youngblood and T. E. Mallouk, *Nano Lett.*, 2008, **8**, 794–799.
317 T. Oshima, D. Lu, O. Ishitani and K. Maeda, *Angew. Chem., Int. Ed.*, 2015, **54**, 2698–2702.
318 Y. Zhang, Z.-R. Tang, X. Fu and Y.-J. Xu, *ACS Nano*, 2011, **5**, 7426–7435.
319 M.-Q. Yang, N. Zhang and Y.-J. Xu, *ACS Appl. Mater. Interfaces*, 2013, **5**, 1156–1164.
320 J. Sun, H. Zhang, L.-H. Guo and L. Zhao, *ACS Appl. Mater. Interfaces*, 2013, **5**, 13035–13041.
321 R. Bera, S. Kundu and A. Patra, *ACS Appl. Mater. Interfaces*, 2015, **7**, 13251–13259.
322 H. Fu, K. Yu, H. Li, J. Li, B. Guo, Y. Tan, C. Song and Z. Zhu, *Dalton Trans.*, 2015, **44**, 1664–1672.
323 S. Bai, L. Wang, X. Chen, J. Du and Y. Xiong, *Nano Res.*, 2015, **8**, 175–183.
324 C. Vilchèze, T. Hartman, B. Weinrick and W. R. Jacobs Jr, *Nat. Commun.*, 2013, **4**, 1881.
325 R. Gonzalez-Olmos, M. J. Martin, A. Georgi, F.-D. Kopinke, I. Oller and S. Malato, *Appl. Catal., B*, 2012, **125**, 51–58.
326 R. Gonzalez-Olmos, F. Holzer, F. D. Kopinke and A. Georgi, *Appl. Catal., A*, 2011, **398**, 44–53.
327 H. Bataineh, O. Pestovsky and A. Bakac, *Chem. Sci.*, 2012, **3**, 1594–1599.
328 M. Yoon, Y. Oh, S. Hong, J. S. Lee, R. Boppella, S. H. Kim, F. Marques Mota, S. O. Kim and D. H. Kim, *Appl. Catal., B*, 2017, **206**, 263–270.
329 V. Kavitha and K. Palanivelu, *Chemosphere*, 2004, **55**, 1235–1243.
330 G. Ruppert, R. Bauer and G. Heisler, *Chemosphere*, 1994, **28**, 1447–1454.
331 S.-M. Kim and A. Vogelpohl, *Chem. Eng. Technol.*, 1998, **21**, 187–191.
332 K.-Y. A. Lin and J.-T. Lin, *Chemosphere*, 2017, **182**, 54–64.
333 A. Prakash, M. Dan, S. Yu, S. Wei, Y. Li, F. Wang and Y. Zhou, *Sol. Energy Mater. Sol. Cells*, 2018, **180**, 205–212.
334 H. Wang, Y. Su, H. Zhao, H. Yu, S. Chen, Y. Zhang and X. Quan, *Environ. Sci. Technol.*, 2014, **48**, 11984–11990.
335 Y. Gao, C. Chen, X. Tan, H. Xu and K. Zhu, *J. Colloid Interface Sci.*, 2016, **476**, 62–70.
336 Y. Deng, L. Tang, G. Zeng, Z. Zhu, M. Yan, Y. Zhou, J. Wang, Y. Liu and J. Wang, *Appl. Catal., B*, 2017, **203**, 343–354.

337 A. P. Gondikas, F. v. d. Kammer, R. B. Reed, S. Wagner, J. F. Ranville and T. Hofmann, *Environ. Sci. Technol.*, 2014, **48**, 5415–5422.
338 D. Jassby, J. Farner Budarz and M. Wiesner, *Environ. Sci. Technol.*, 2012, **46**, 6934–6941.
339 J. K. Stolarczyk, S. Bhattacharyya, L. Polavarapu and J. Feldmann, *ACS Catal.*, 2018, **8**, 3602–3635.
340 Y. Park, W. Kim, D. Monllor-Satoca, T. Tachikawa, T. Majima and W. Choi, *J. Phys. Chem. Lett.*, 2013, **4**, 189–194.
341 X.-B. Li, Y.-J. Gao, Y. Wang, F. Zhan, X.-Y. Zhang, Q.-Y. Kong, N.-J. Zhao, Q. Guo, H.-L. Wu, Z.-J. Li, Y. Tao, J.-P. Zhang, B. Chen, C.-H. Tung and L.-Z. Wu, *J. Am. Chem. Soc.*, 2017, **139**, 4789–4796.
342 Y.-n. Zhang, Q. Niu, X. Gu, N. Yang and G. Zhao, *Nanoscale*, 2019, **11**, 11992–12014.
343 X. Yan, H. Li and X. Su, *TrAC, Trends Anal. Chem.*, 2018, **103**, 1–20.
344 Z. Farka, T. Juřík, D. Kovář, L. Trnková and P. Skládal, *Chem. Rev.*, 2017, **117**, 9973–10042.
345 S. Mao, J. Chang, H. Pu, G. Lu, Q. He, H. Zhang and J. Chen, *Chem. Soc. Rev.*, 2017, **46**, 6872–6904.
346 T. Zhang, Z. Cheng, Y. Wang, Z. Li, C. Wang, Y. Li and Y. Fang, *Nano Lett.*, 2010, **10**, 4738–4741.
347 H. G. Sudibya, Q. He, H. Zhang and P. Chen, *ACS Nano*, 2011, **5**, 1990–1994.
348 G. Zhou, J. Chang, S. Cui, H. Pu, Z. Wen and J. Chen, *ACS Appl. Mater. Interfaces*, 2014, **6**, 19235–19241.
349 J. H. An, S. J. Park, O. S. Kwon, J. Bae and J. Jang, *ACS Nano*, 2013, **7**, 10563–10571.
350 W. Fu, C. Nef, A. Tarasov, M. Wipf, R. Stoop, O. Knopfmacher, M. Weiss, M. Calame and C. Schönenberger, *Nanoscale*, 2013, **5**, 12104–12110.
351 K. Maehashi, Y. Sofue, S. Okamoto, Y. Ohno, K. Inoue and K. Matsumoto, *Sens. Actuators, B*, 2013, **187**, 45–49.
352 S. Jiang, R. Cheng, R. Ng, Y. Huang and X. Duan, *Nano Res.*, 2015, **8**, 257–262.
353 G. Zhou, J. Chang, H. Pu, K. Shi, S. Mao, X. Sui, R. Ren, S. Cui and J. Chen, *ACS Sens.*, 2016, **1**, 295–302.
354 P. Li, D. Zhang, C. Jiang, X. Zong and Y. Cao, *Biosens. Bioelectron.*, 2017, **98**, 68–75.
355 Z.-Q. Zhao, X. Chen, Q. Yang, J.-H. Liu and X.-J. Huang, *Chem. Commun.*, 2012, **48**, 2180–2182.
356 P. K. Sahoo, B. Panigrahy, S. Sahoo, A. K. Satpati, D. Li and D. Bahadur, *Biosens. Bioelectron.*, 2013, **43**, 293–296.
357 Y. Wei, C. Gao, F.-L. Meng, H.-H. Li, L. Wang, J.-H. Liu and X.-J. Huang, *J. Phys. Chem. C*, 2012, **116**, 1034–1041.
358 J. Li, S. Guo, Y. Zhai and E. Wang, *Electrochem. Commun.*, 2009, **11**, 1085–1088.
359 S. Chaiyo, E. Mehmeti, K. Žagar, W. Siangproh, O. Chailapakul and K. Kalcher, *Anal. Chim. Acta*, 2016, **918**, 26–34.
360 R. Seenivasan, W.-J. Chang and S. Gunasekaran, *ACS Appl. Mater. Interfaces*, 2015, **7**, 15935–15943.
361 J. Cui, S. Xu and L. Wang, *Sci. China Mater.*, 2017, **60**, 352–360.
362 Z. S. Qian, X. Y. Shan, L. J. Chai, J. R. Chen and H. Feng, *Biosens. Bioelectron.*, 2015, **68**, 225–231.
363 M. Li, X. Zhou, W. Ding, S. Guo and N. Wu, *Biosens. Bioelectron.*, 2013, **41**, 889–893.
364 Y. Wen, F. Xing, S. He, S. Song, L. Wang, Y. Long, D. Li and C. Fan, *Chem. Commun.*, 2010, **46**, 2596–2598.
365 K. Mao, Z. Wu, Y. Chen, X. Zhou, A. Shen and J. Hu, *Talanta*, 2015, **132**, 658–663.
366 Y. Yang, T. Liu, L. Cheng, G. Song, Z. Liu and M. Chen, *ACS Appl. Mater. Interfaces*, 2015, **7**, 7526–7533.
367 X. Liu, L. Li, Y. Wei, Y. Zheng, Q. Xiao and B. Feng, *Analyst*, 2015, **140**, 4654–4661.
368 Y. Wang, J. Hu, Q. Zhuang and Y. Ni, *ACS Sustainable Chem. Eng.*, 2016, **4**, 2535–2541.
369 X. Zuo, H. Zhang, Q. Zhu, W. Wang, J. Feng and X. Chen, *Biosens. Bioelectron.*, 2016, **85**, 464–470.
370 B. L. Li, J. Wang, H. L. Zou, S. Garaj, C. T. Lim, J. Xie, N. B. Li and D. T. Leong, *Adv. Funct. Mater.*, 2016, **26**, 7034–7056.
371 C. Liu, Z. Sun, L. Zhang, J. Lv, X. F. Yu, L. Zhang and X. Chen, *Sens. Actuators, B*, 2018, **257**, 1093–1098.
372 P. Li, D. Zhang, J. Liu, H. Chang, Y. e. Sun and N. Yin, *ACS Appl. Mater. Interfaces*, 2015, **7**, 24396–24402.
373 W. Gu, X. Pei, Y. Cheng, C. Zhang, J. Zhang, Y. Yan, C. Ding and Y. Xian, *ACS Sens.*, 2017, **2**, 576–582.
374 L. Fan, Y. Hu, X. Wang, L. Zhang, F. Li, D. Han, Z. Li, Q. Zhang, Z. Wang and L. Niu, *Talanta*, 2012, **101**, 192–197.
375 X. Guo, J. Huang, Y. Wei, Q. Zeng and L. Wang, *J. Hazard. Mater.*, 2020, **381**, 120969.
376 X. Li, J. Liu, X. Gong, T. Qing, P. Zhang and B. Feng, *J. Mater. Chem. C*, 2019, **7**, 4096–4101.
377 P.-C. Lee, N.-S. Li, Y.-P. Hsu, C. Peng and H.-W. Yang, *Analyst*, 2019, **144**, 3038–3044.
378 W. Yang, J. Li, J. Yang, Y. Liu, Z. Xu, X. Sun, F. Wang and D. H. L. Ng, *J. Alloys Compd.*, 2020, **815**, 152276.
379 S. Guo, D. Wen, Y. Zhai, S. Dong and E. Wang, *ACS Nano*, 2010, **4**, 3959–3968.
380 F. Gao, Q. Wang, N. Gao, Y. Yang, F. Cai, M. Yamane, F. Gao and H. Tanaka, *Biosens. Bioelectron.*, 2017, **97**, 238–245.
381 Z.-H. Sheng, X.-Q. Zheng, J.-Y. Xu, W.-J. Bao, F.-B. Wang and X.-H. Xia, *Biosens. Bioelectron.*, 2012, **34**, 125–131.
382 Y. Huang, X. Dong, Y. Liu, L.-J. Li and P. Chen, *J. Mater. Chem.*, 2011, **21**, 12358–12362.
383 D. Sarkar, W. Liu, X. Xie, A. C. Anselmo, S. Mitragotri and K. Banerjee, *ACS Nano*, 2014, **8**, 3992–4003.
384 J. Z. Ou, W. Ge, B. Carey, T. Daeneke, A. Rotbart, W. Shan, Y. Wang, Z. Fu, A. F. Chrimes, W. Wlodarski, S. P. Russo, Y. X. Li and K. Kalantar-zadeh, *ACS Nano*, 2015, **9**, 10313–10323.
385 K. P. Carter, A. M. Young and A. E. Palmer, *Chem. Rev.*, 2014, **114**, 4564–4601.
386 G. Algara-Siller, N. Severin, S. Y. Chong, T. Björkman, R. G. Palgrave, A. Laybourn, M. Antonietti, Y. Z. Khimyak, A. V. Krasheninnikov, J. P. Rabe, U. Kaiser, A. I. Cooper, A. Thomas and M. J. Bojdys, *Angew. Chem.*, 2014, **126**, 7580–7585.
387 M. Rong, L. Lin, X. Song, Y. Wang, Y. Zhong, J. Yan, Y. Feng, X. Zeng and X. Chen, *Biosens. Bioelectron.*, 2015, **68**, 210–217.

388 X.-L. Zhang, C. Zheng, S.-S. Guo, J. Li, H.-H. Yang and G. Chen, *Anal. Chem.*, 2014, **86**, 3426–3434.
389 Z. L. Zhu, J. A. Ma, Z. L. Wang, C. Mu, Z. T. Fan, L. L. Du, Y. Bai, L. Z. Fan, H. Yan, D. L. Phillips and S. H. Yang, *J. Am. Chem. Soc.*, 2014, **136**, 3760–3763.
390 J. K. Kim, M. J. Park, S. J. Kim, D. H. Wang, S. P. Cho, S. Bae, J. H. Park and B. H. Hong, *ACS Nano*, 2013, **7**, 7207–7212.
391 R. Gokhale and P. Singh, *Part. Part. Syst. Charact.*, 2014, **31**, 433–438.
392 Q. Liu, B. D. Guo, Z. Y. Rao, B. H. Zhang and J. R. Gong, *Nano Lett.*, 2013, **13**, 2436–2441.
393 H. Yang, D. J. Kang, K. H. Ku, H. H. Cho, C. H. Park, J. Lee, D. C. Lee, P. M. Ajayan and B. J. Kim, *ACS Macro Lett.*, 2014, **3**, 985–990.
394 H. H. Cho, H. Yang, D. J. Kang and B. J. Kim, *ACS Appl. Mater. Interfaces*, 2015, **7**, 8615–8621.
395 X. T. Zheng, A. Ananthanarayanan, K. Q. Luo and P. Chen, *Small*, 2015, **11**, 1620–1636.
396 A. Ananthanarayanan, X. Wang, P. Routh, B. Sana, S. Lim, D.-H. Kim, K.-H. Lim, J. Li and P. Chen, *Adv. Funct. Mater.*, 2014, **24**, 3021–3026.
397 J. Ju and W. Chen, *Biosens. Bioelectron.*, 2014, **58**, 219–225.
398 T. Guo, Y. Wu, Y. Lin, X. Xu, H. Lian, G. Huang, J. Z. Liu, X. Wu and H. H. Yang, *Small*, 2018, **14**, 1702815.
399 X. Miao, D. Qu, D. Yang, B. Nie, Y. Zhao, H. Fan and Z. Sun, *Adv. Mater.*, 2017, **30**, 1704740.
400 J. Huang, L. Ye, X. Gao, H. Li, J. Xu and Z. Li, *J. Mater. Chem. B*, 2015, **3**, 2395–2401.
401 Y. Zhang, B. Zheng, C. Zhu, X. Zhang, C. Tan, H. Li, B. Chen, J. Yang, J. Chen, Y. Huang, L. Wang and H. Zhang, *Adv. Mater.*, 2015, **27**, 935–939.
402 P. T. K. Loan, W. Zhang, C.-T. Lin, K.-H. Wei, L.-J. Li and C.-H. Chen, *Adv. Mater.*, 2014, **26**, 4838–4844.
403 Y.-z. Li, Z.-h. Fu and G. Xu, *Coord. Chem. Rev.*, 2019, **388**, 79–106.
404 M. I. Halawa, F. Wu, M. N. Zafar, I. M. Mostafa, A. Abdussalam, S. Han and G. Xu, *J. Mater. Chem. B*, 2020, **8**, 3542–3549.
405 S. He, B. Song, D. Li, C. Zhu, W. Qi, Y. Wen, L. Wang, S. Song, H. Fang and C. Fan, *Adv. Funct. Mater.*, 2010, **20**, 453–459.
406 C.-H. Lu, H.-H. Yang, C.-L. Zhu, X. Chen and G.-N. Chen, *Angew. Chem., Int. Ed.*, 2009, **48**, 4785–4787.
407 K. P. Loh, Q. Bao, G. Eda and M. Chhowalla, *Nat. Chem.*, 2010, **2**, 1015.
408 W. T. Huang, Y. Shi, W. Y. Xie, H. Q. Luo and N. B. Li, *Chem. Commun.*, 2011, **47**, 7800–7802.
409 Y. Yuan, R. Li and Z. Liu, *Anal. Chem.*, 2014, **86**, 3610–3615.
410 C. Zhu, Z. Zeng, H. Li, F. Li, C. Fan and H. Zhang, *J. Am. Chem. Soc.*, 2013, **135**, 5998–6001.
411 Y. Huang, Y. Shi, H. Y. Yang and Y. Ai, *Nanoscale*, 2015, **7**, 2245–2249.
412 D. Wang and B. Z. Tang, *Acc. Chem. Res.*, 2019, **52**, 2559–2570.
413 Y. Chen, J. W. Y. Lam, R. T. K. Kwok, B. Liu and B. Z. Tang, *Mater. Horiz.*, 2019, **6**, 428–433.
414 Y. Hong, J. W. Y. Lam and B. Z. Tang, *Chem. Commun.*, 2009, 4332–4353, DOI: 10.1039/B904665H.
415 R. T. K. Kwok, J. Geng, J. W. Y. Lam, E. Zhao, G. Wang, R. Zhan, B. Liu and B. Z. Tang, *J. Mater. Chem. B*, 2014, **2**, 4134–4141.
416 N. Li, L. Zhang, Y. Chen, M. Fang, J. Zhang and H. Wang, *Adv. Funct. Mater.*, 2012, **22**, 835–841.
417 H. Liu, H. Wang and X. Zhang, *Adv. Mater.*, 2015, **27**, 249–254.
418 G.-R. Xu, S.-H. Wang, H.-L. Zhao, S.-B. Wu, J.-M. Xu, L. Li and X.-Y. Liu, *J. Membr. Sci.*, 2015, **493**, 428–443.
419 Y. Song, W. Wei and X. Qu, *Adv. Mater.*, 2011, **23**, 4215–4236.
420 Y. Wang, X. Zhang, Z. Luo, X. Huang, C. Tan, H. Li, B. Zheng, B. Li, Y. Huang, J. Yang, Y. Zong, Y. Ying and H. Zhang, *Nanoscale*, 2014, **6**, 12340–12344.
421 H. Wei and E. Wang, *Chem. Soc. Rev.*, 2013, **42**, 6060–6093.
422 Y. Lin, J. Ren and X. Qu, *Acc. Chem. Res.*, 2014, **47**, 1097–1105.
423 T. Lin, L. Zhong, L. Guo, F. Fu and G. Chen, *Nanoscale*, 2014, **6**, 11856–11862.
424 T. Lin, L. Zhong, Z. Song, L. Guo, H. Wu, Q. Guo, Y. Chen, F. Fu and G. Chen, *Biosens. Bioelectron.*, 2014, **62**, 302–307.
425 T. Lin, L. Zhong, J. Wang, L. Guo, H. Wu, Q. Guo, F. Fu and G. Chen, *Biosens. Bioelectron.*, 2014, **59**, 89–93.
426 W. Huang, Y. Deng and Y. He, *Biosens. Bioelectron.*, 2017, **91**, 89–94.
427 K. Sano, Y. S. Kim, Y. Ishida, Y. Ebina, T. Sasaki, T. Hikima and T. Aida, *Nat. Commun.*, 2016, **7**, 12559.
428 N. R. Nirala, S. Pandey, A. Bansal, V. K. Singh, B. Mukherjee, P. S. Saxena and A. Srivastava, *Biosens. Bioelectron.*, 2015, **74**, 207–213.
429 B. L. Li, H. Q. Luo, J. L. Lei and N. B. Li, *RSC Adv.*, 2014, **4**, 24256–24262.
430 B. L. Li, H. L. Zou, L. Lu, Y. Yang, J. L. Lei, H. Q. Luo and N. B. Li, *Adv. Funct. Mater.*, 2015, **25**, 3541–3550.
431 F. Liu, S. Huang, F. Xue, Y. Wang, Z. Meng and M. Xue, *Biosens. Bioelectron.*, 2012, **32**, 273–277.
432 J. H. Holtz and S. A. Asher, *Nature*, 1997, **389**, 829–832.
433 J.-T. Zhang, L. Wang, J. Luo, A. Tikhonov, N. Kornienko and S. A. Asher, *J. Am. Chem. Soc.*, 2011, **133**, 9152–9155.
434 D. Arunbabu, A. Sannigrahi and T. Jana, *Soft Matter*, 2011, **7**, 2592–2599.
435 P. Li, M. Wong, X. Zhang, H. Yao, R. Ishige, A. Takahara, M. Miyamoto, R. Nishimura and H.-J. Sue, *ACS Photonics*, 2014, **1**, 79–86.
436 T.-Z. Shen, S.-H. Hong, B. Lee and J.-K. Song, *NPG Asia Mater.*, 2016, **8**, e296.
437 M. Zeng, D. King, D. Huang, C. Do, L. Wang, M. Chen, S. Lei, P. Lin, Y. Chen and Z. Cheng, *Proc. Natl. Acad. Sci. U. S. A.*, 2019, **116**, 18322–18327.
438 P. Rattanarat, W. Dungchai, D. Cate, J. Volckens, O. Chailapakul and C. S. Henry, *Anal. Chem.*, 2014, **86**, 3555–3562.
439 W.-Y. Zhou, S.-S. Li, X.-Y. Xiao, S.-H. Chen, J.-H. Liu and X.-J. Huang, *Chem. Commun.*, 2018, **54**, 9329–9332.

440 N. L. Teradal, S. Marx, A. Morag and R. Jelinek, *J. Mater. Chem. C*, 2017, **5**, 1128–1135.
441 S. Wu, Z. Zeng, Q. He, Z. Wang, S. J. Wang, Y. Du, Z. Yin, X. Sun, W. Chen and H. Zhang, *Small*, 2012, **8**, 2264–2270.
442 K.-J. Huang, L. Wang, Y.-J. Liu, T. Gan, Y.-M. Liu, L.-L. Wang and Y. Fan, *Electrochim. Acta*, 2013, **107**, 379–387.
443 J. Li, Z. Yang, Y. Tang, Y. Zhang and X. Hu, *Biosens. Bioelectron.*, 2013, **41**, 698–703.
444 T.-W. Lin, C.-J. Liu and C.-S. Dai, *Appl. Catal., B*, 2014, **154-155**, 213–220.
445 H. Sun, J. Chao, X. Zuo, S. Su, X. Liu, L. Yuwen, C. Fan and L. Wang, *RSC Adv.*, 2014, **4**, 27625–27629.
446 Y. Sun, S. Wang, C. Li, P. Luo, L. Tao, Y. Wei and G. Shi, *Phys. Chem. Chem. Phys.*, 2013, **15**, 9907–9913.
447 J. Li, Z. Yang, Y. Zhang, S. Yu, Q. Xu, Q. Qu and X. Hu, *Microchim. Acta*, 2012, **179**, 265–272.
448 K.-J. Huang, Y.-J. Liu, Y.-M. Liu and L.-L. Wang, *J. Hazard. Mater.*, 2014, **276**, 207–215.
449 X. Xia, Z. Zheng, Y. Zhang, X. Zhao and C. Wang, *Sens. Actuators, B*, 2014, **192**, 42–50.
450 K.-J. Huang, L. Wang, J. Li and Y.-M. Liu, *Sens. Actuators, B*, 2013, **178**, 671–677.
451 F. Yavari, Z. Chen, A. V. Thomas, W. Ren, H.-M. Cheng and N. Koratkar, *Sci. Rep.*, 2011, **1**, 166.
452 D. R. Dreyer, S. Park, C. W. Bielawski and R. S. Ruoff, *Chem. Soc. Rev.*, 2010, **39**, 228–240.
453 I. Jung, D. Dikin, S. Park, W. Cai, S. L. Mielke and R. S. Ruoff, *J. Phys. Chem. C*, 2008, **112**, 20264–20268.
454 J. A. Dean, *Lange's handbook of chemistry*, McGraw-Hill, Inc., New York, London, 1999.
455 L. Pauling, *The chemical bond; a brief introduction to modern structural chemistry*, Cornell University Press, Ithaca, N.Y., 1967.
456 O. Knopfmacher, M. L. Hammock, A. L. Appleton, G. Schwartz, J. Mei, T. Lei, J. Pei and Z. Bao, *Nat. Commun.*, 2014, **5**, 2954.
457 J. Tu, Y. Gan, T. Liang, Q. Hu, Q. Wang, T. Ren, Q. Sun, H. Wan and P. Wang, *Front. Chem.*, 2018, **6**, 333.
458 A. K. Geim and K. S. Novoselov, *Nat. Mater.*, 2007, **6**, 183.
459 Y. Huang, J. Guo, Y. Kang, Y. Ai and C. M. Li, *Nanoscale*, 2015, **7**, 19358–19376.
460 N. Gao, W. Zhou, X. Jiang, G. Hong, T.-M. Fu and C. M. Lieber, *Nano Lett.*, 2015, **15**, 2143–2148.
461 G. Palazzo, D. De Tullio, M. Magliulo, A. Mallardi, F. Intranuovo, M. Y. Mulla, P. Favia, I. Vikholm-Lundin and L. Torsi, *Adv. Mater.*, 2015, **27**, 911–916.
462 E. Stern, R. Wagner, F. J. Sigworth, R. Breaker, T. M. Fahmy and M. A. Reed, *Nano Lett.*, 2007, **7**, 3405–3409.
463 G. Zheng, F. Patolsky, Y. Cui, W. U. Wang and C. M. Lieber, *Nat. Biotechnol.*, 2005, **23**, 1294–1301.
464 E. Stern, A. Vacic, N. K. Rajan, J. M. Criscione, J. Park, B. R. Ilic, D. J. Mooney, M. A. Reed and T. M. Fahmy, *Nat. Nanotechnol.*, 2010, **5**, 138–142.
465 J. Sun, X. Qian, Z. Wang, F. Zeng, H. Bai and N. Li, *J. Membr. Sci.*, 2020, **599**, 117838.
466 F. Li, Z. Yu, H. Shi, Q. Yang, Q. Chen, Y. Pan, G. Zeng and L. Yan, *Chem. Eng. J.*, 2017, **322**, 33–45.
467 H. Zeng, Z. Yu, Y. Peng and L. Zhu, *Appl. Clay Sci.*, 2019, **183**, 105322.
468 R. Dai, X. Zhang, M. Liu, Z. Wu and Z. Wang, *J. Membr. Sci.*, 2019, **573**, 46–54.
469 H. Zhang, J. Hou, Y. Hu, P. Wang, R. Ou, L. Jiang, J. Z. Liu, B. D. Freeman, A. J. Hill and H. Wang, *Sci. Adv.*, 2018, **4**, eaaq0066.
470 X. Shi, A. Xiao, C. Zhang and Y. Wang, *J. Membr. Sci.*, 2019, **576**, 116–122.
471 J. Tian, X. Huang and W. Wu, *Ind. Eng. Chem. Res.*, 2020, **59**, 1135–1141.
472 Q. Zhang, G. Yi, Z. Fu, H. Yu, S. Chen and X. Quan, *ACS Nano*, 2019, **13**, 13196–13207.
473 H. Su, J. Zhou, L. Miao, J. Shi, Y. Gu, P. Wang, Y. Tian, X. Mu, A. Wei, L. Huang, S. Chen and Z. Deng, *Sustainable Mater. Technol.*, 2019, **20**, e00095.
474 S. Ma, W. Qarony, M. I. Hossain, C. T. Yip and Y. H. Tsang, *Sol. Energy Mater. Sol. Cells*, 2019, **196**, 36–42.
475 S. Bao, W. Yang, Y. Wang, Y. Yu and Y. Sun, *J. Hazard. Mater.*, 2020, **381**, 120914.
476 Y. Tian and I. Chowdhury, *Environ. Eng. Sci.*, 2018, **36**, 305–315.
477 T. Krasian, W. Punyodom and P. Worajittiphon, *Chem. Eng. J.*, 2019, **369**, 563–575.
478 Y. Yuan, B. Niu, Q. Yu, X. Guo, Z. Guo, J. Wen, T. Liu, H. Zhang and N. Wang, *Angew. Chem.*, 2019, **132**, 1236–1243.
479 W. Lei, D. Liu and Y. Chen, *Adv. Mater. Interfaces*, 2015, **2**, 1400529.
480 X. Cai, J. He, L. Chen, K. Chen, Y. Li, K. Zhang, Z. Jin, J. Liu, C. Wang, X. Wang, L. Kong and J. Liu, *Chemosphere*, 2017, **171**, 192–201.
481 I. Clark, J. Smith, R. L. Gomes and E. Lester, *J. Environ. Chem. Eng.*, 2019, **7**, 103175.
482 H. Zhou, Z. Jiang and S. Wei, *Appl. Clay Sci.*, 2018, **153**, 29–37.
483 O. Rahmanian, M. Dinari and M. K. Abdolmaleki, *Appl. Surf. Sci.*, 2018, **428**, 272–279.
484 M. Sarker, J. Y. Song and S. H. Jhung, *Chem. Eng. J.*, 2018, **335**, 74–81.
485 R. Zou, T. Xu, X. Lei, Q. Wu and S. Xue, *Solid State Sci.*, 2020, **99**, 106067.
486 P. Kuang, M. Sayed, J. Fan, B. Cheng and J. Yu, *Adv. Energy Mater.*, 2020, **10**, 1903802.
487 S. Luo, S. Dong, C. Lu, C. Yu, Y. Ou, L. Luo, J. Sun and J. Sun, *J. Colloid Interface Sci.*, 2018, **513**, 389–399.
488 S. Li, Z. Zhao, D. Yu, J.-Z. Zhao, Y. Su, Y. Liu, Y. Lin, W. Liu, H. Xu and Z. Zhang, *Nano Energy*, 2019, **66**, 104083.
489 M. Guo, Z. Xing, T. Zhao, Z. Li, S. Yang and W. Zhou, *Appl. Catal., B*, 2019, **257**, 117913.
490 X. Wang, Y. Xiang, B. Zhou, Y. Zhang, J. Wu, R. Hu, L. Liu, J. Song and J. Qu, *J. Colloid Interface Sci.*, 2019, **534**, 1–11.
491 J. Hu, D. Chen, Z. Mo, N. Li, Q. Xu, H. Li, J. He, H. Xu and J. Lu, *Angew. Chem.*, 2019, **131**, 2095–2099.
492 C. Cui, R. Guo, H. Xiao, E. Ren, Q. Song, C. Xiang, X. Lai, J. Lan and S. Jiang, *Appl. Surf. Sci.*, 2020, **505**, 144595.
493 A. Shahzad, K. Rasool, M. Nawaz, W. Miran, J. Jang, M. Moztahida, K. A. Mahmoud and D. S. Lee, *Chem. Eng. J.*, 2018, **349**, 748–755.

494 Y. Sheng, J. Yang, F. Wang, L. Liu, H. Liu, C. Yan and Z. Guo, *Appl. Surf. Sci.*, 2019, **465**, 154–163.
495 H. S. El-Sheshtawy, H. M. El-Hosainy, K. R. Shoueir, I. M. El-Mehasseb and M. El-Kemary, *Appl. Surf. Sci.*, 2019, **467-468**, 268–276.
496 Y. Sheng, Z. Wei, H. Miao, W. Yao, H. Li and Y. Zhu, *Chem. Eng. J.*, 2019, **370**, 287–294.
497 F. Li, M. Tang, T. Li, L. Zhang and C. Hu, *Appl. Catal., B*, 2020, **268**, 118397.
498 N. F. F. Moreira, M. J. Sampaio, A. R. Ribeiro, C. G. Silva, J. L. Faria and A. M. T. Silva, *Appl. Catal., B*, 2019, **248**, 184–192.
499 H.-Y. Liu, C. Liang, C.-G. Niu, D.-W. Huang, Y.-B. Du, H. Guo, L. Zhang, Y.-Y. Yang and G.-M. Zeng, *Appl. Surf. Sci.*, 2019, **475**, 421–434.
500 M. Darie, E. M. Seftel, M. Mertens, R. G. Ciocarlan, P. Cool and G. Carja, *Appl. Clay Sci.*, 2019, **182**, 105250.
501 F. Mohamed, M. R. Abukhadra and M. Shaban, *Sci. Total Environ*, 2018, **640–641**, 352–363.
502 G. Zhao, C. Li, X. Wu, J. Yu, X. Jiang, W. Hu and F. Jiao, *Appl. Surf. Sci.*, 2018, **434**, 251–259.
503 Y. Pi, X. Li, Q. Xia, J. Wu, Y. Li, J. Xiao and Z. Li, *Chem. Eng. J.*, 2018, **337**, 351–371.
504 D. Yu, L. Li, M. Wu and J. C. Crittenden, *Appl. Catal., B*, 2019, **251**, 66–75.
505 H. Ramezanalizadeh and F. Manteghi, *J. Cleaner Prod.*, 2018, **172**, 2655–2666.
506 A. Gómez-Avilés, M. Peñas-Garzón, J. Bedia, D. D. Dionysiou, J. J. Rodríguez and C. Belver, *Appl. Catal., B*, 2019, **253**, 253–262.
507 J. Huang, X. Zhang, H. Song, C. Chen, F. Han and C. Wen, *Appl. Surf. Sci.*, 2018, **441**, 85–98.
508 L. Sheng, B. Huangfu, Q. Xu, W. Tian, Z. Li, A. Meng and S. Tan, *J. Alloys Compd.*, 2020, **820**, 153191.
509 Q. Wu, X. Wang, Y. Jiang, W. Sun, C. Wang, M. Yang and C. Zhang, *ChemistrySelect*, 2018, **3**, 2326–2331.
510 Q. Yue, Y. Hu, L. Tao, B. Zhang, C. Liu, Y. Wang, C. Chen, J. Zhao and C.-Z. Li, *Microchim. Acta*, 2019, **186**, 640.
511 X. Chen, X. Sun, W. Xu, G. Pan, D. Zhou, J. Zhu, H. Wang, X. Bai, B. Dong and H. Song, *Nanoscale*, 2018, **10**, 1111–1118.
512 Q. Guan, J. Ma, W. Yang, R. Zhang, X. Zhang, X. Dong, Y. Fan, L. Cai, Y. Cao, Y. Zhang, N. Li and Q. Xu, *Nanoscale*, 2019, **11**, 14123–14133.
513 X. Zhu, X. Pang, Y. Zhang and S. Yao, *J. Mater. Chem. B*, 2019, **7**, 7729–7735.
514 Y. Zhan, J. Yang, L. Guo, F. Luo, B. Qiu, G. Hong and Z. Lin, *Sens. Actuators, B*, 2019, **279**, 61–68.
515 A. N. Kadam, M. Moniruzzaman and S.-W. Lee, *Molecules*, 2019, **24**, 450.
516 M. Li, B. Wang, X. An, Z. Li, H. Zhu, B. Mao, D. G. Calatayud and T. D. James, *Dyes Pigm.*, 2019, **170**, 107476.
517 H. Xie, J. Dong, J. Duan, J. Hou, S. Ai and X. Li, *Sens. Actuators, B*, 2019, **278**, 147–152.
518 M. S. Haroone, Y. Hu, P. Zhang, R. Ma, X. Zhang, Q. M. Kaleem, M. B. Khan and J. Lu, *Dyes Pigm.*, 2019, **166**, 422–432.
519 X.-Y. Xu and B. Yan, *Adv. Funct. Mater.*, 2017, **27**, 1700247.
520 T. C. Pereira and N. R. Stradiotto, *Microchim. Acta*, 2019, **186**, 764.
521 T.-W. Chen, U. Rajaji, S.-M. Chen and R. Jothi Ramalingam, *Ultrason. Sonochem.*, 2019, **54**, 79–89.
522 J. Xu, X. Qiao, Y. Wang, Q. Sheng, T. Yue, J. Zheng and M. Zhou, *Microchim. Acta*, 2019, **186**, 238.
523 Z. Song, Y. Ma and J. Ye, *J. Electroanal. Chem.*, 2020, **856**, 113595.
524 R. Zhang, J. Liu and Y. Li, *ACS Sens.*, 2019, **4**, 2058–2064.
525 X. Zhu, B. Liu, L. Li, L. Wu, S. Chen, L. Huang, J. Yang, S. Liang, K. Xiao, J. Hu and H. Hou, *Microchim. Acta*, 2019, **186**, 776.
526 D. Wu, M. Wu, J. Yang, H. Zhang, K. Xie, C.-T. Lin, A. Yu, J. Yu and L. Fu, *Mater. Lett.*, 2019, **236**, 412–415.
527 Y. Yue, L. Zeng, X. Wang, L. Su, M. Sun, B. Wu and S. Yan, *Sci. Rep.*, 2019, **9**, 3864.
528 Z.-W. Wang, H.-J. Liu, C.-Y. Li, X. Chen, R. Weerasooriya, J. Wei, J. Lv, P. Lv and Y.-C. Wu, *Talanta*, 2020, **208**, 120410.
529 J. Zou, S. Wu, Y. Liu, Y. Sun, Y. Cao, J.-P. Hsu, A. T. Shen Wee and J. Jiang, *Carbon*, 2018, **130**, 652–663.
530 Y. Ma, Y. Wang, D. Xie, Y. Gu, X. Zhu, H. Zhang, G. Wang, Y. Zhang and H. Zhao, *Chem. Eng. J.*, 2018, **347**, 953–962.
531 J.-C. Jin, J. Wu, G.-P. Yang, Y.-L. Wu and Y.-Y. Wang, *Chem. Commun.*, 2016, **52**, 8475–8478.
532 D. Kwong Hong Tsang, T. J. Lieberthal, C. Watts, I. E. Dunlop, S. Ramadan, A. E. del Rio Hernandez and N. Klein, *Sci. Rep.*, 2019, **9**, 13946.
533 T. Pham, P. Ramnani, C. C. Villarreal, J. Lopez, P. Das, I. Lee, M. R. Neupane, Y. Rheem and A. Mulchandani, *Carbon*, 2019, **142**, 504–512.
534 K. S. Bhat, U. T. Nakate, J.-Y. Yoo, Y. Wang, T. Mahmoudi and Y.-B. Hahn, *ACS Omega*, 2019, **4**, 8373–8380.
535 X. Chen, S. Hao, B. Zong, C. Liu and S. Mao, *Biosens. Bioelectron.*, 2019, **145**, 111711.
536 P. Zhang, S. Yang, R. Pineda-Gómez, B. Ibarlucea, J. Ma, M. R. Lohe, T. F. Akbar, L. Baraban, G. Cuniberti and X. Feng, *Small*, 2019, **15**, 1901265.
537 J. Chang, H. Pu, S. A. Wells, K. Shi, X. Guo, G. Zhou, X. Sui, R. Ren, S. Mao, Y. Chen, M. C. Hersam and J. Chen, *Mol. Syst. Des. Eng.*, 2019, **4**, 491–502.
538 B. Xu, M. Zhu, W. Zhang, X. Zhen, Z. Pei, Q. Xue, C. Zhi and P. Shi, *Adv. Mater.*, 2016, **28**, 3333–3339.
539 H. Tian, H. Fan, M. Li and L. Ma, *ACS Sens.*, 2016, **1**, 243–250.
540 B. Liu, *J. Mater. Chem.*, 2012, **22**, 10094–10101.
541 X. Cai, Y. Luo, B. Liu and H.-M. Cheng, *Chem. Soc. Rev.*, 2018, **47**, 6224–6266.
542 E. Varrla, C. Backes, K. R. Paton, A. Harvey, Z. Gholamvand, J. McCauley and J. N. Coleman, *Chem. Mater.*, 2015, **27**, 1129–1139.
543 J. Stafford, A. Patapas, N. Uzo, O. K. Matar and C. Petit, *AIChE J.*, 2018, **64**, 3246–3276.
544 J. Zhang, H. Yang, G. Shen, P. Cheng, J. Zhang and S. Guo, *Chem. Commun.*, 2010, **46**, 1112–1114.
545 L. Huang, Y. Liu, L.-C. Ji, Y.-Q. Xie, T. Wang and W.-Z. Shi, *Carbon*, 2011, **49**, 2431–2436.

546 X. Liu, T. Chen, H. Chu, L. Niu, Z. Sun, L. Pan and C. Q. Sun, *Electrochim. Acta*, 2015, **166**, 12–16.
547 P. Davidson, C. Penisson, D. Constantin and J.-C. P. Gabriel, *Proc. Natl. Acad. Sci. U. S. A.*, 2018, 201802692.
548 Y. Xia, T. S. Mathis, M.-Q. Zhao, B. Anasori, A. Dang, Z. Zhou, H. Cho, Y. Gogotsi and S. Yang, *Nature*, 2018, **557**, 409.
549 X. Li, W. Ma, H. Li, Q. Zhang and H. Liu, *Coord. Chem. Rev.*, 2020, **408**, 213191.
550 S. Masubuchi, M. Morimoto, S. Morikawa, M. Onodera, Y. Asakawa, K. Watanabe, T. Taniguchi and T. Machida, *Nat. Commun.*, 2018, **9**, 1413.
551 R. Rizvi, E. P. Nguyen, M. D. Kowal, W. H. Mak, S. Rasel, M. A. Islam, A. Abdelaal, A. S. Joshi, S. Zekriardehani, M. R. Coleman and R. B. Kaner, *Adv. Mater.*, 2018, **30**, 1800200.
552 Z. Zhang, P. Chen, X. Duan, K. Zang, J. Luo and X. Duan, *Science*, 2017, **357**, 788–792.
553 T. C. Achee, W. Sun, J. T. Hope, S. G. Quitzau, C. B. Sweeney, S. A. Shah, T. Habib and M. J. Green, *Sci. Rep.*, 2018, **8**, 14525.
554 S. Pei, Q. Wei, K. Huang, H.-M. Cheng and W. Ren, *Nat. Commun.*, 2018, **9**, 145.
555 S. D. Lacey, D. J. Kirsch, Y. Li, J. T. Morgenstern, B. C. Zarket, Y. Yao, J. Dai, L. Q. Garcia, B. Liu, T. Gao, S. Xu, S. R. Raghavan, J. W. Connell, Y. Lin and L. Hu, *Adv. Mater.*, 2018, **30**, 1705651.
556 O. Sanyal, Z. Liu, J. Yu, B. M. Meharg, J. S. Hong, W. Liao and I. Lee, *J. Membr. Sci.*, 2016, **512**, 21–28.
557 X. Hu, L. Chen, T. Ji, Y. Zhang, A. Hu, F. Wu, G. Li and Y. Chen, *Adv. Mater. Interfaces*, 2015, **2**, 1500445.
558 M. Saeidi-Javash, W. Kuang, C. Dun and Y. Zhang, *Adv. Funct. Mater.*, 2019, **29**, 1901930.
559 A. C. Rajan, A. Mishra, S. Satsangi, R. Vaish, H. Mizuseki, K.-R. Lee and A. K. Singh, *Chem. Mater.*, 2018, **30**, 4031–4038.
560 H. Wang, Y. Li, Y. Li, Y. Liu, D. Lin, C. Zhu, G. Chen, A. Yang, K. Yan, H. Chen, Y. Zhu, J. Li, J. Xie, J. Xu, Z. Zhang, R. Vilá, A. Pei, K. Wang and Y. Cui, *Nano Lett.*, 2019, **19**, 1326–1335.
561 R. Frisenda and A. Castellanos-Gomez, *Nat. Nanotechnol.*, 2018, **13**, 441–442.
562 M. Zeng, W. Kuang, I. Khan, D. Huang, Y. Du, M. Saeidi-Javash, L. Zhang, Z. Cheng, A. J. Hoffman and Y. Zhang, *Adv. Mater.*, 2020, **32**, e2003081.
563 M. Zeng, S. Yuan, D. Huang and Z. Cheng, *ACS Appl. Mater. Interfaces*, 2019, **11**, 40099–40106.
564 M. A. Priolo, K. M. Holder, S. M. Greenlee, B. E. Stevens and J. C. Grunlan, *Chem. Mater.*, 2013, **25**, 1649–1655.
565 F. Xiang, D. Parviz, T. M. Givens, P. Tzeng, E. M. Davis, C. M. Stafford, M. J. Green and J. C. Grunlan, *Adv. Funct. Mater.*, 2016, **26**, 2143–2149.
566 B. Stevens, T. Guin, O. Sarwar, A. John, K. R. Paton, J. N. Coleman and J. C. Grunlan, *Macromol. Rapid Commun.*, 2016, **37**, 1790–1794.
567 S. Lazar, F. Carosio, A.-L. Davesne, M. Jimenez, S. Bourbigot and J. Grunlan, *ACS Appl. Mater. Interfaces*, 2018, **10**, 31686–31696.
568 P. Tzeng, B. Stevens, I. Devlaming and J. C. Grunlan, *Langmuir*, 2015, **31**, 5919–5927.
569 A. Ambrosi and M. Pumera, *Chem. Soc. Rev.*, 2016, **45**, 2740–2755.
570 X. Cao, C. Tan, X. Zhang, W. Zhao and H. Zhang, *Adv. Mater.*, 2016, **28**, 6167–6196.
571 K. Chen, W. Gao, S. Emaminejad, D. Kiriya, H. Ota, H. Y. Y. Nyein, K. Takei and A. Javey, *Adv. Mater.*, 2016, **28**, 4397–4414.
572 K. Fu, Y. Yao, J. Dai and L. Hu, *Adv. Mater.*, 2017, **29**, 1603486.
573 S. K. Garlapati, M. Divya, B. Breitung, R. Kruk, H. Hahn and S. Dasgupta, *Adv. Mater.*, 2018, **30**, 1707600.
574 T. Jungst, W. Smolan, K. Schacht, T. Scheibel and J. Groll, *Chem. Rev.*, 2016, **116**, 1496–1539.
575 Y. S. Lui, W. T. Sow, L. P. Tan, Y. Wu, Y. Lai and H. Li, *Acta Biomater.*, 2019, **92**, 19–36.
576 M. Orrill and S. LeBlanc, *J. Appl. Polym. Sci.*, 2017, **134**, 44256.
577 S. Seyedin, P. Zhang, M. Naebe, S. Qin, J. Chen, X. Wang and J. M. Razal, *Mater. Horiz.*, 2019, **6**, 219–249.
578 D. Tian, Y. Song and L. Jiang, *Chem. Soc. Rev.*, 2013, **42**, 5184–5209.
579 F. Torrisi and T. Carey, *Nano Today*, 2018, **23**, 73–96.
580 W. Xu and D. H. Gracias, *ACS Nano*, 2019, **13**, 4883–4892.
581 P. Zhang, F. Wang, M. Yu, X. Zhuang and X. Feng, *Chem. Soc. Rev.*, 2018, **47**, 7426–7451.
582 B. Zhu, S. Gong and W. Cheng, *Chem. Soc. Rev.*, 2019, **48**, 1668–1711.
583 P. Chang, H. Mei, S. Zhou, K. G. Dassios and L. Cheng, *J. Mater. Chem. A*, 2019, **7**, 4230–4258.
584 G. Hu, J. Kang, L. W. T. Ng, X. Zhu, R. C. T. Howe, C. G. Jones, M. C. Hersam and T. Hasan, *Chem. Soc. Rev.*, 2018, **47**, 3265–3300.
585 J.-Y. Kim and N. A. Kotov, *Chem. Mater.*, 2014, **26**, 134–152.
586 J. A. Lewis, *J. Am. Ceram. Soc.*, 2000, **83**, 2341–2359.
587 Q. Zhang, F. Zhang, S. P. Medarametla, H. Li, C. Zhou and D. Lin, *Small*, 2016, **12**, 1702–1708.
588 D. X. Luong, A. K. Subramanian, G. A. L. Silva, J. Yoon, S. Cofer, K. Yang, P. S. Owuor, T. Wang, Z. Wang, J. Lou, P. M. Ajayan and J. M. Tour, *Adv. Mater.*, 2018, **30**, 1707416.
589 S. Lu, Q. Zhou, Y. Ouyang, Y. Guo, Q. Li and J. Wang, *Nat. Commun.*, 2018, **9**, 3405.
590 J. Carrasquilla and R. G. Melko, *Nat. Phys.*, 2017, **13**, 431.
591 R. Ramprasad, R. Batra, G. Pilania, A. Mannodi-Kanakkithodi and C. Kim, *npj Comput. Mater.*, 2017, **3**, 54.
592 B. Cao, L. A. Adutwum, A. O. Oliynyk, E. J. Luber, B. C. Olsen, A. Mar and J. M. Buriak, *ACS Nano*, 2018, **12**, 7434–7444.
593 K. Choudhary, B. DeCost and F. Tavazza, *Phys. Rev. Mater.*, 2018, **2**, 083801.
594 H. Gao, T. J. Struble, C. W. Coley, Y. Wang, W. H. Green and K. F. Jensen, *ACS Cent. Sci.*, 2018, **4**, 1465–1476.
595 C. Kim, G. Pilania and R. Ramprasad, *Chem. Mater.*, 2016, **28**, 1304–1311.
596 J. R. Kitchin, *Nat. Catal.*, 2018, **1**, 230–232.

597 E. Liotti, C. Arteta, A. Zisserman, A. Lui, V. Lempitsky and P. S. Grant, *Sci. Adv.*, 2018, **4**, eaar4004.
598 T. K. Patra, F. Zhang, D. S. Schulman, H. Chan, M. J. Cherukara, M. Terrones, S. Das, B. Narayanan and S. K. R. S. Sankaranarayanan, *ACS Nano*, 2018, **12**, 8006–8016.
599 F. Pedregosa, G. Varoquaux, A. Gramfort, V. Michel, B. Thirion, O. Grisel, M. Blondel, P. Prettenhofer, R. Weiss and V. Dubourg, *J. Mach. Learn. Res.*, 2011, **12**, 2825–2830.
600 A. Seko, T. Maekawa, K. Tsuda and I. Tanaka, *Phys. Rev. B: Condens. Matter Mater. Phys.*, 2014, **89**, 054303.
601 S. Yuan, Z. Jiao, N. Quddus, J. S. Kwon, II and C. V. Mashuga, *Ind. Eng. Chem. Res.*, 2019, **58**, 3531–3537.
602 Y. Zhang and C. Ling, *npj Comput. Mater.*, 2018, **4**, 25.
603 R. P. Joshi, J. Eickholt, L. Li, M. Fornari, V. Barone and J. E. Peralta, *ACS Appl. Mater. Interfaces*, 2019, **11**, 18494–18503.
604 A. Mansouri Tehrani, A. O. Oliynyk, M. Parry, Z. Rizvi, S. Couper, F. Lin, L. Miyagi, T. D. Sparks and J. Brgoch, *J. Am. Chem. Soc.*, 2018, **140**, 9844–9853.
605 A. E. Gongora, B. Xu, W. Perry, C. Okoye, P. Riley, K. G. Reyes, E. F. Morgan and K. A. Brown, *Sci. Adv.*, 2020, **6**, eaaz1708.
606 C. Zhan, W. Sun, Y. Xie, D.-e. Jiang and P. R. C. Kent, *ACS Appl. Mater. Interfaces*, 2019, **11**, 24885–24905.
607 Y. L. Zhong, Z. Tian, G. P. Simon and D. Li, *Mater. Today*, 2015, **18**, 73–78.
608 Y. Liu, P. Li, F. Wang, W. Fang, Z. Xu, W. Gao and C. Gao, *Carbon*, 2019, **155**, 462–468.
609 Y. Abate, D. Akinwande, S. Gamage, H. Wang, M. Snure, N. Poudel and S. B. Cronin, *Adv. Mater.*, 2018, **30**, 1704749.

